OPTIMUM DEPLOYMENT OF NONCONVENTIONAL WELLS

A DISSERTATION
SUBMITTED TO THE DEPARTMENT OF PETROLEUM ENGINEERING
AND THE COMMITTEE ON GRADUATE STUDIES
OF STANFORD UNIVERSITY
IN PARTIAL FULFILLMENT OF THE REQUIREMENTS
FOR THE DEGREE OF
DOCTOR OF PHILOSOPHY

Burak Yeten
June 2003

© Copyright by Burak Yeten 2003
All Rights Reserved

I certify that I have read this dissertation and that, in my opinion, it is fully adequate in scope and quality as a dissertation for the degree of Doctor of Philosophy.

Dr. Khalid Aziz
(Principal Co-Advisor)

I certify that I have read this dissertation and that, in my opinion, it is fully adequate in scope and quality as a dissertation for the degree of Doctor of Philosophy.

Dr. Louis J. Durlofsky
(Principal Co-Advisor)

I certify that I have read this dissertation and that, in my opinion, it is fully adequate in scope and quality as a dissertation for the degree of Doctor of Philosophy.

Dr. Jef K. Caers

Approved for the University Committee on Graduate Studies:

Abstract

Nonconventional wells (i.e., wells with an arbitrary trajectory or multiple branches) offer great potential for the recovery of petroleum resources. Wells of this type are underutilized in practice, however, in part because it is difficult to optimize their deployment. In this dissertation, we focus on the reservoir engineering aspects of the optimum deployment of nonconventional wells. The effects of uncertain geological and engineering parameters are included in this optimization. To maximize reservoir performance (recovery or net present value), we optimize the number of producers and injectors, their types (e.g., vertical, horizontal or multilateral), locations and trajectories, as well as their control strategy via smart (intelligent) completions.

We apply a genetic algorithm (GA) as our master engine for the optimization of well type, location and trajectory. This engine is accompanied by an artificial neural network (ANN) which acts as a proxy to the reservoir simulations (objective function evaluations), a hill climber, which searches the local neighborhood of the current solution, and a near wellbore upscaling, which allows the incorporation of near wellbore heterogeneity from detailed reservoir descriptions into coarse simulation models. In addition, we introduce an experimental design methodology (ED) to reduce the number of simulations required to quantify the effects of the multiple uncertain parameters during this optimization process. Within this framework we can account for the control of the wells through a "reactive" control strategy. Using such a strategy, downhole control devices can open or close depending on the fluids produced from different segments of the well.

We also developed an optimization tool based on a nonlinear conjugate gradient algorithm that enables decisions regarding the deployment of smart completion technology. This tool is independent of the well type, location and trajectory optimization. It allows us to implement a "defensive" control strategy; i.e., the control devices are opened or closed

based on a well control optimization. With this strategy, reservoirs can be screened for smart well technology. Reservoir uncertainty can also be accounted for within this framework.

We present single and multiple well deployment examples for different synthetic reservoir models. In these examples, well type, location and trajectory are optimized. The effects of uncertainty are included in several of the examples. We determine sensible single and multiple well deployment plans with the algorithms developed. We show that the objective function (cumulative oil produced or net present value of the project) is always increased relative to its value in the first generation of the optimization, in some cases by 30% or more. The optimal well type is found to vary depending on the reservoir model and objective function. We also show that the optimal type of well can differ depending on whether single or multiple realizations of the reservoir geology are considered.

We next screen various types of reservoirs and wells with our defensive control optimization and quantify the benefits of deploying this technology. Improvement in predicted performance using inflow control devices, which is as high as 65% in one case, is demonstrated for all of the examples considered. There is, however, significant variation in the level of improvement attainable using these devices, so sophisticated decision making techniques may be required when considering their use in practice.

Finally we apply all the tools we have developed to a portion of a giant oil field located in Saudi Arabia. We demonstrate the potential benefits of deploying optimized multilateral wells and smart completions. The complex geological features in this field illustrate the advantages of this technology in a practical setting.

Acknowledgements

I would like to express my gratitude and sincere appreciation to Dr. Khalid Aziz and Dr. Louis J. Durlofsky for their support, encouragement guidance and patience through the course of my Ph.D. study. Without their assistance, this work would not have been accomplished. I extend my appreciation to Dr. Jef K. Caers and Dr. Roland N. Horne for their useful insights, suggestions and guidance throughout my studies.

I am grateful to the Stanford University Petroleum Research Institute's Nonconventional Wells (SUPRI-HW) and Reservoir Simulation (SUPRI-B) Industrial Affiliates Program and to Saudi Aramco for financial support.

Also thanks to all the SUPRI-O folks for the "eye opener" brainstorming sessions over the past two years.

Last but not the least, I would like to thank to all my friends for their love and support. My gratitude is endless to my family, Selim, Selma and Burcin.

Contents

Abstract **iv**

Acknowledgements **vi**

1 Introduction **1**

1.1 General Background 1

1.2 Literature Survey 3

1.2.1 Optimization Techniques 3

1.2.2 Nonconventional Wells 4

1.2.3 Well Placement Optimization 5

1.2.4 Smart Wells 7

1.2.5 Well Control Optimization 9

1.2.6 Uncertainty around Reservoir Description 10

1.2.7 Assessment of Uncertainty for Field Developments 11

1.3 Statement of the Problem 12

1.3.1 Solution Approach 14

1.3.2 Concluding Remarks 14

2 Well Type, Location and Trajectory Optimization **16**

2.1 Formulation 16

2.2 Main Optimization Engine 23

2.3 General Description of GAs 23

2.3.1 Basic Terminology 24

2.3.2 Step-wise Procedure 28

2.4 Implementation of GA for the Optimization Problem 31

2.5 Features of the Optimization Engine 33
2.6 Enhancing the Efficiency of Optimization - Helper Tools 35
2.6.1 Near-well Upscaling 35
2.6.2 Artificial Neural Networks 38
2.6.3 Hill Climber 42
2.6.4 Overall Algorithm 43
2.6.5 “Optimized” Simulations 43
2.7 Sensitivities to GA and Helper Parameters 45
2.7.1 Robustness and Effectiveness of GA 45
2.7.2 Sensitivities with respect to Helper Algorithms and Ranking Weight 52
2.8 Applications on Synthetic Models 54
2.8.1 Case 1 - Optimum Well in a Gaussian Permeability Field 54
2.8.2 Case 2 - Optimum Well in a Layered Reservoir 61
2.8.3 Case 3 - Optimum Well in a Fluvial Reservoir 63
2.8.4 Case 4 - Multiple Wells in a Fluvial Reservoir 64
2.9 Assessment of Single Source of Uncertainty 68
2.9.1 Formulation 68
2.10 Concluding Remarks 73

3 Well Control Optimization **74**
3.1 Multi-Segment Wells 76
3.2 Methodology 77
3.3 Control Strategies 78
3.3.1 Reactive Control Strategy 78
3.3.2 Defensive Control Strategy 78
3.4 Optimization Algorithm for Defensive Control Strategy 79
3.4.1 Implementation 81
3.4.2 Optimizer and Links to Simulator 83
3.5 Applications on Synthetic Models 83
3.5.1 Case 1: Vertical Injection and Production Wells 83
3.5.2 Case 2: Multilateral Well in a Fluvial Reservoir 87
3.6 Assessment of Uncertainty 94

3.6.1 Application . . . 94
3.7 Comparison with Optimal Control Theory . . . 97
3.8 Concluding Remarks . . . 99

4 Optimization in a Practical Setting 101
4.1 Screening for Nonconventional Wells . . . 101
4.1.1 Comparison with Different Well Types . . . 107
4.2 Optimum Nonconventional Well in SA-6 Area . . . 111
4.3 Simulation Model . . . 113
4.4 Smart Well Type Location and Trajectory Optimization . . . 114
4.4.1 Optimization Runs - Fish Bone Type Smart Well . . . 117
4.4.2 Optimization Runs - Fork Type Smart Well . . . 122
4.5 Smart Well Control Optimization . . . 126
4.5.1 Conclusions . . . 127
4.6 Concluding Remarks . . . 128

5 Conclusions and Future Work 132
5.1 Conclusions . . . 132
5.2 Future Work . . . 133

Nomenclature 135

Bibliography 139

Appendix 152

A Assessment of Multiple Sources of Uncertainty 152
A.1 Experimental Design (ED) . . . 152
A.2 Integrating ED to Optimization Algorithm . . . 154
A.3 Application . . . 155
A.3.1 Validation of the Coarse Model . . . 156
A.3.2 Selection of Uncertain Parameters . . . 156
A.3.3 Optimization of the Field Development . . . 156

List of Tables

2.1 Correlation Coefficients between Fine and Coarse (s-k) Models 38
2.2 Test Matrix A 46
2.3 Test Matrix B 47
2.4 Test Matrix C 48
2.5 Test Matrix D 49
2.6 Average and Standard Deviations of PI Values, in STB/psi, of Optimum Wells for 20 Optimizations 51
2.7 Test Matrix 53
2.8 Average and Standard Deviations of PI Values, in STB/psi, and Number of Simulations Required 53
2.9 Case 1 - Reservoir and Rock Properties 55
2.10 Case 1 - Fluid Properties 56
2.11 Case 1b - Economic Parameters 58
2.12 Case 2 - Reservoir and Rock Properties 61
2.13 Case 4 - Reservoir and Rock Properties 66

3.1 Case 1 - Comparison of Different Instrumentation Strategies 85
3.2 Case 2 - Simulation Model Properties 88
3.3 Case 3 - Permeability Statistics 95
3.4 Case 3 - Comparison of Cumulative Oil Production 96

4.1 Properties of Simulation Layers 103
4.2 Rock Curves for Matrix Blocks 103
4.3 Rock Curves for Stratiform Super - K Layers 104
4.4 Rock Curves for Fracture Blocks 105

4.5 Fluid Properties 113
4.6 Fish Bone Type Smart Well Optimizations 117
4.7 Optimum Fish Bone Type Smart Wells 117
4.8 Optimized Fish Bone Type Smart Well Coordinates - Run #1 118
4.9 Optimized Fish Bone Type Smart Well Coordinates - Run #2 118
4.10 Optimized Fish Bone Type Smart Well Coordinates - Run #3 118
4.11 Optimum Fork Type Smart Wells 122
4.12 Optimized Fork Type Smart Well Coordinates - Run #1 122
4.13 Optimized Fork Type Smart Well Coordinates - Run #2 123
4.14 Optimized Fork Type Smart Well Coordinates - Run #3 123
4.15 Cumulative Oil Production (in MMSTB) for Optimum Fish Bone Type Smart Wells with Different Control Strategies 126
4.16 Cumulative Oil Production (in MMSTB) for Optimum Fork Type Smart Wells with Different Control Strategies 127

A.1 Placket-Burman Design 157
A.2 Statistics of the Factor Distributions 157

List of Figures

2.1 A Linear Well Trajectory 17
2.2 Basic Multilateral Well Types (TAML, 1999) 19
2.3 Well Trajectory Optimization Parameters 20
2.4 Crossover Operator 26
2.5 Mutation Operator 26
2.6 Schematic of GA Optimization Steps 29
2.7 Representation of the Parameters on a Chromosome String 31
2.8 Representation of a 2D Linear Trajectory on a Block Centered Grid 34
2.9 Representation of Near-well Permeability Heterogeneity via Skin Values on Coarser Models 38
2.10 Comparison of Cumulative Oil Production 39
2.11 Comparison of Water Cut 39
2.12 Comparison of Cumulative Gas Production 40
2.13 Schematic of the Artificial Neural Network 40
2.14 Schematic of Overall Optimization Algorithm 44
2.15 Case 1 - Histogram of the Horizontal Permeability 55
2.16 Case 1a - Progress of the Optimization 57
2.17 Case 1a - Optimum Horizontal Well 57
2.18 Case 1b - Progress of the Optimization 59
2.19 Case 1b - Optimum Well (Quad-Lateral) 60
2.20 Case 1b - Variation of Well Types with Generation 60
2.21 Case 2 - Progress of the Optimization 62
2.22 Case 2 - Optimum Well (Dual-Lateral) 62
2.23 Case 3 - Histogram of the Horizontal Permeability 64

2.24 Case 3 - Progress of the Optimization 65
2.25 Case 3 - Optimum Well for Single Realization (Tri-Lateral) 65
2.26 Case 4 - Progress of the Optimization 66
2.27 Case 4 - Best Development Plans at Various Generations 67
2.28 Assessment of Uncertainty during Well Type, Location and Trajectory Optimization 69
2.29 Case 3b - Progress of the Optimization 71
2.30 Case 3b - Optimum Well for Multiple Realizations (Quad-Lateral) 71
2.31 Case 3b - Performance of Optimum Well for Each Realization 72

3.1 An Example Completion of a Horizontal Smart Well 75
3.2 An Example Completion of a Multilateral Smart Well 75
3.3 A Sketch of Well Segments (GeoQuest, 2001b) 76
3.4 Optimization of Valve Settings in Time 82
3.5 Case 1 - Well Completions 84
3.6 Case 1 - Cumulative Oil Production Comparison 86
3.7 Case 1 - Water Cut Comparison 86
3.8 Case 2 - Top View of the Multilateral Well Configuration 89
3.9 Case 2 - Lateral Oil Production Rate, Base Case 90
3.10 Case 2 - Lateral Oil Production Rate, Controlled Case 91
3.11 Case 2 - Lateral Water Cut, Base Case 91
3.12 Case 2 - Lateral Water Cut, Controlled Case 92
3.13 Case 2 - Pressure along the Mainbore and Branches, Base Case 92
3.14 Case 2 - Pressure along the Mainbore and Branches, Controlled Case 93
3.15 Case 2 - Change of Device Settings in Time 93
3.16 Case 3 - Histogram of Horizontal Permeability Distribution 94
3.17 Case 3 - Geostatistical Realizations with the Fixed Multilateral Well 95
3.18 Permeability Distribution and Well Locations for Comparison Model (Brouwer and Jansen, 2002) 98
3.19 Comparison of Final Oil Saturation Maps 99
3.20 Comparison of Final Oil Saturation Maps 100

4.1 3D View of the Simulation Model 102

4.2 Orientation of Fractures on the Simulation Grid 106
4.3 Areal View of the Completions of the Tri-lateral Well 107
4.4 Production Profiles of Each Branch without Smart Completions 108
4.5 Water Cut Profiles of Each Branch without Smart Completions 108
4.6 Production Profiles of Each Branch with Optimized Valve Controls 109
4.7 Water Cut Profiles of Each Branch with Optimized Valve Controls 109
4.8 Closure Setting Profiles of Each Valve 110
4.9 Oil Production Profiles for Tri-lateral and Smart Tri-lateral Wells 110
4.10 Water Cut Profiles for Tri-lateral and Smart Tri-lateral Wells 111
4.11 Incremental Recoveries Obtained for Various Well and Completion Alternatives 112
4.12 Initial Oil Saturation Distribution 113
4.13 Well Templates Used for the Optimizations 114
4.14 Final Oil Saturation Distribution of Layer 6 for Base Case 2 116
4.15 Oil Saturation Color Legend 116
4.16 Comparison of Cumulative Oil Production for Optimized Fish Bone Type Smart Wells 119
4.17 Comparison of Field Water Cut for Optimized Fish Bone Type Smart Wells 120
4.18 Final Oil Saturation Distribution of Layer 6 for Run #1 120
4.19 Final Oil Saturation Distribution of Layer 6 for Run #2 121
4.20 Final Oil Saturation Distribution of Layer 6 for Run #3 121
4.21 Comparison of Cumulative Oil Production for Optimized Fork Type Smart Wells 123
4.22 Comparison of Field Water Cut for Optimized Fork Type Smart Wells . . . 124
4.23 Final Oil Saturation Distribution of Layer 6 for Run #1 124
4.24 Final Oil Saturation Distribution of Layer 6 for Run #2 125
4.25 Final Oil Saturation Distribution of Layer 6 for Run #3 125
4.26 Comparison of Cumulative Field Oil Production for Fish Bone Type Smart Wells Optimized in Run #1 128
4.27 Comparison of Cumulative Field Oil Production for Fish Bone Type Smart Wells Optimized in Run #2 129

4.28 Comparison of Cumulative Field Oil Production for Fish Bone Type Smart Wells Optimized in Run #3 129
4.29 Comparison of Cumulative Field Oil Production for Fork Type Smart Wells Optimized in Run #1 130
4.30 Comparison of Cumulative Field Oil Production for Fork Type Smart Wells Optimized in Run #2 130
4.31 Comparison of Cumulative Field Oil Production for Fork Type Smart Wells Optimized in Run #3 131
4.32 Comparison of Well Performances 131

A.1 Application of Experimental Design 155
A.2 Progress of Optimization 158
A.3 RS of the Optimized Development Plan 159
A.4 Optimized Development Plan 160

Chapter 1

Introduction

1.1 General Background

A conventional well is a vertical or a slightly deviated well. Horizontal, highly deviated and multilateral wells are generally referred to as nonconventional or advanced wells (NCWs). A nonconventional well may be as simple as a horizontal well or a vertical/horizontal wellbore with one sidetrack or as complex as a horizontal, extended reach well with multiple lateral and even sublateral branches.

The drilling of nonconventional wells has become standard practice during the past decade. A single NCW may be more cost effective than multiple vertical wells in terms of overall drilling and completion costs. In addition, NCWs can operate at low drawdown, hence reducing coning in many cases. NCWs are well suited for the efficient exploitation of complex reservoirs since they act to increase drainage area and are capable of reaching attic hydrocarbon reserves or reservoir compartments. Consequently, by drilling these wells, capital expenditures and operating costs can be reduced. These appealing advantages, which lead to more efficient reservoir management, are driving oil and gas producers to reconsider fields which previously had marginal economics, such as mature, tight, thin or heavy oil reservoirs. Compared to conventional wells, these wells provide for the same or better reservoir exposure but with fewer wells, hence improving production and injection strategies. With these advantages, slot utilization can be optimized for offshore developments (Bosworth *et al.*, 1998; Karakas and Ayan, 1991; Sadek *et al.*, 1998; Aubert, 1998; Vo and Madden, 1995; Chralez and Bréant, 1999; Hovda *et al.*, 1996; Taylor and Russel,

1997; Horn *et al.*, 1997; Wong *et al.*, 1997; Freeman *et al.*, 1998; Joshi, 1988; Boardman, 1997; Fernandez *et al.*, 1999; Sarma, 1994).

A "smart" (or intelligent) well is a nonconventional well with smart completions. Smart completions can be defined as completions with instrumentation (special sensors and valves) installed on the production tubing which allow continuous in-situ monitoring and adjustment of fluid flow rates and pressures. They provide the flexibility of controlling each branch or section of a multilateral well independently. In the case of a monobore well (such as a horizontal well), they transform the wellbore into a multi branch well, again providing the control flexibility for each segmented branch.

Smart wells comprise an important component of advanced well technology. Their benefits have been demonstrated in the industry especially for multiple reservoirs with commingled production. Their benefits for single reservoir production (non-commingled production) are also being explored. Because they are able to monitor and control the fluid flow rates and pressures, these completions can be effective for controlling the coning or cusping of the driving fluids and allocating the optimum production rate to each controlled branch. Hence, these technologies provide new ways to improve reservoir management (Bosworth *et al.*, 1998; Tubel and Hopmann, 1996; Robinson, 1997; Gai, 2001; Yeten and Jalali, 2001).

There are also some disadvantages associated with advanced well technology, especially with multilaterals. Due to the complex and rapidly progressing nature of this technology, the drilling and operation of these wells carries some risk, mainly mechanical failures or incorrect trajectory selection or landing. The uncertainty due to reservoir description further complicates the problem. In the case of a mechanical failure, well intervention might be required, which could be very costly, especially for offshore applications. Although drilling and completion of most of the advanced wells are achievable with today's technology, the risk element makes it very difficult to evaluate the economics of these projects. Due to the complexity of NCW technology, selecting the appropriate well for a particular setting is often difficult.

The main objectives of this study are to find the optimum design of well trajectories and control schedules with a given stochastic or deterministic reservoir model. The wells might be of any type (advanced or conventional). Having defined the location and the trajectory of the wells, the next step is transforming the wells into smart wells, i.e., introducing the

flow control and monitoring devices at appropriate locations. With this instrumentation completed the control schedule of the downhole control devices can be optimized.

We now proceed with presenting a survey of the current methodologies applied in the industry for well placement and control optimization.

1.2 Literature Survey

In this chapter, an overview of previous work regarding the optimum deployment of NCWs (including smart wells) in a field development context will be presented. Existing approaches to find the optimum well type, placement, trajectory and control strategy will be reviewed. Also, several optimization techniques will be briefly described. The motivation here is to identify the missing components in the current practice and to see how these gaps can be filled.

1.2.1 Optimization Techniques

Optimization is a mature field and many algorithms have been developed over the years. All optimization techniques seek the global optimum. In reality, depending on the problem, some of the optimization techniques perform better in terms of efficiency and robustness than others. There is generally a trade-off between speed, robustness and the probability of finding the global optimum (Reed and Marks II, 1999).

In general, optimization algorithms can be classified as deterministic or stochastic. Most deterministic optimization algorithms can be classified as evaluation-only methods or gradient based methods. Evaluation-only methods are simpler, since they do not require gradient calculations, but they are often slow and inefficient. The Hooke-Jeeves pattern search algorithm, polytope algorithm (also known as Nelder-Mead simplex search (Reed and Marks II, 1999) or downhill simplex method (Press *et al.*, 1999)) and Powell's conjugate direction method can be listed among the popular evaluation-only methods. Gradient based algorithms use the derivatives of the objective function to guide their search. For smooth, continuous objective functions, convergence to a global optimum with these methods can be quite fast. Gradient descent, best-step steepest descent (Cauchy's method), conjugate gradient descent, Newton's method, Gauss-Newton, Levenberg-Marquardt, and

so called quasi-Newton methods or variable metric methods are popular gradient based algorithms.

Deterministic algorithms always converge to the same optimum if they are started with the same initial guess. Depending on the starting point, this optimum might be local or global. Therefore it can be useful to start the algorithm with different initial points in an attempt to reach better solutions. The advantage of stochastic methods is that every state has a nonzero chance of occurrence so, if the procedure runs long enough, the global optimum will be visited eventually. The problem is that this may take a very long time and this guarantee is lost if the algorithm is terminated early (Reed and Marks II, 1999). As stochastic evaluation-only methods, both simulated annealing and genetic algorithms have the advantage of being relatively easy to implement in the sense that the algorithms are uncomplicated and there are no complex matrix manipulations. They need very little problem specific information and do not require gradients so they can be used on discontinuous functions or functions described empirically rather than analytically. Under certain conditions, they will tolerate a noisy evaluation function (Reed and Marks II, 1999).

Stochastic algorithms are widely used for various applications, such as history matching, parameter estimation, production optimization, etc., in the oil and gas industry (e.g., Sen *et al.* (1993); Martinez *et al.* (1994); Fujii and Horne (1994); Harding *et al.* (1996); Palke and Horne (1997); Mohaghegh *et al.* (1998); Stoisits *et al.* (1999); Montoya-O *et al.* (2000); Romero *et al.* (2000a); Fichter (2000); Romero *et al.* (2000b); Jikich and Popa (2000); Vazquez *et al.* (2001); Guyaguler *et al.* (2001). Bittencourt and Horne (1997), Santellani *et al.* (1998), Guyaguler *et al.* (2002), (Montes *et al.*, 2001) and Beckner and Song (1995) have applied genetic algorithms to well placement optimization.

1.2.2 Nonconventional Wells

Numerous studies have been published regarding the benefits of drilling nonconventional wells (Bosworth *et al.*, 1998; Karakas and Ayan, 1991; Sadek *et al.*, 1998; Aubert, 1998; Vo and Madden, 1995; Chralez and Bréant, 1999; Hovda *et al.*, 1996; Taylor and Russel, 1997; Horn *et al.*, 1997; Wong *et al.*, 1997; Freeman *et al.*, 1998; Joshi, 1988; Boardman, 1997; Fernandez *et al.*, 1999; Sarma, 1994). These studies stress the use of this technology to increase the drainage area by connecting different reservoir compartments (commingled production) with fewer well slots in offshore platforms and to postpone the breakthrough

of driving fluids. They also discuss the importance of nonconventional wells in terms of transforming marginal projects into profitable ones, especially for heavy oil and/or tight reservoirs. Although Bosworth *et al.* (1998), TAML (1999), Ehlig-Economodies *et al.* (1996), Gallivan *et al.* (1995), Vij *et al.* (1998) and Sugiyama *et al.* (1997) establish some criteria to determine the appropriate type of well for different reservoir geometries and heterogeneities, there is no study that deals with the systematic determination of the optimum type, placement and trajectory of these wells.

1.2.3 Well Placement Optimization

Beckner and Song (1995) define the optimal field development as the well scheduling and placement that maximizes the NPV. They treated the problem as a "travelling salesman problem", and therefore suggested the use of stochastic algorithms such as simulated annealing and genetic algorithms, which are known to be suitable for this kind of problem (Guyaguler, 2002). In their work they used a simulated annealing algorithm to identify optimum locations and the deployment schedule of 12 horizontal wells of fixed length and orientation. They used a reservoir simulator and an economics model for the objective function evaluations. They ran different cases and showed how the development plan can change with respect to different reservoir parameters and varying well costs. They also found non-uniform well spacing to be the optimum development strategy during primary depletion. Nesvold *et al.* (1996) coupled linear programming techniques with reservoir simulation to optimize a multifield production allocation and the development of the Ekofisk and outlying fields.

Bittencourt and Horne (1997) optimized the placement of multiple vertical and horizontal wells using a hybrid optimization algorithm that consisted of GA, polytope and Tabu search methods in conjunction with a numerical simulator. Pan and Horne (1998) investigated least squares and kriging interpolation algorithms to use as proxies to reservoir simulations for several cases, including field development optimization. They collected data for the interpolation algorithms by performing simulations on different levels of the unknowns. These levels of the unknowns were chosen by the Uniform Design Technique developed by Fang (1980). Pan and Horne (1998) state that their algorithm substantially reduces the number of simulations that is required to find the global optimum in the problems considered. They also found kriging superior to least squares for the proxy generation.

Guyaguler *et al.* (2002) applied a hybrid optimization algorithm that utilized a GA, a polytope method, kriging and artificial neural networks (used as proxies for the function evaluations), along with a reservoir simulator. They optimized up to four vertical injection well locations for a waterflood project to maximize the NPV. They found kriging to be a better proxy than neural networks during their optimizations.

Montes *et al.* (2001) optimized the placement of vertical wells using a GA without any hybridization. They performed sensitivities on the internal parameters of GA, such as mutation probability, population size and the use of elitism. They drew attention to issues like absolute convergence and robustness of the optimization engine. They concluded that the automated well placement optimization should complement geological and engineering judgement rather than replace it.

Centilmen *et al.* (1999) presented a neuro-simulation technique that forms a bridge between a reservoir simulator and a predictive artificial neural network. They selected several key well scenarios (all vertical) either randomly or by intuition. They numerically simulated these scenarios and then used them to train the network. Following the training step, they evaluated numerous well scenarios efficiently with little CPU cost. They stated that their approach is reasonably accurate and faster than conventional methods, and therefore it can effectively be used for field optimization.

Kabir *et al.* (2002) introduced an Experimental Design (ED) methodology to develop fields by considering uncertainty in both geological and engineering parameters. By using ED they were able to define the factors that had the largest effect on the recovery (using a two level Placket-Burman design (Plackett and Burman, 1946)). They then used these factors in a three level D-optimal or full factorial design. In this step they were able to capture both the linear and nonlinear effects of the factors and the interactions between them. They next generated a response surface with multivariate analysis by fitting a polynomial, which served as a proxy to the simulator. Using this overall methodology they were able to identify the importance of each engineering and geological input parameter. They concluded that major geological features, such as stratigraphy and fluid contacts, play a major role when compared to reservoir heterogeneity in terms of anisotropy and Dykstra-Parson's coefficient (Dykstra and Parsons, 1950).

Qiu *et al.* (2001) suggested the use of fracture orientation to find the optimum orientation for horizontal wells. They stated that a well should intersect as many fractures as

possible during the primary depletion stage, while for reservoirs under secondary recovery they claimed that the opposite is true, since the fractures carry the injected fluids to the producers. They used this information to estimate the direction or the orientation of the horizontal wells. Cayeux *et al.* (2001) discussed the use of a shared earth model with advanced three-dimensional visualization tools to select target locations and well types. They gave some field applications concerned with optimum well planning, some of which focus on the use of reservoir simulation. Seifert *et al.* (1996) studied the optimum placement of horizontal and highly deviated wells. They tried to maximize the intersection of the randomly proposed well trajectories with the productive units. They used template locations and well types to find the optimum orientation. Then they ranked these trajectories in terms of their values (number of productive bodies intersected) and risks associated with their deployment. Their method is not automatic and depends partially on subjective ranking.

1.2.4 Smart Wells

Wells instrumented with control and monitoring devices are called intelligent or smart wells. Robinson (1997) gave the following definition for intelligent wells: "Intelligent well in the generic sense is a term that can be applied to a well that has a pressure and temperature transducer in place to monitor reservoir conditions along with a sophisticated multilateral well configuration that provides isolation of the laterals and has flow controls and sensors to control the production process in real-time". He also gave a brief description of the components of intelligent wells and their possible applications. Hamer and Freeman (1999) stated that the next step in multilateral completions will be the development and deployment of intelligent completions. They drew attention to the capabilities of these completions in terms of continuous downhole monitoring and providing advanced warning of approaching fluid fronts as well as adjusting the physical characteristics of the completion without costly intervention. Bosworth *et al.* (1998) and Greenberg (1999) considered future applications of intelligent completions to be a natural part of multilateral well designs. Tubel and Hopmann (1996) provided a clear description of control devices and their operational principles. They stated that intelligent wells should be able to increase recovery by controlling the production rate. They claimed that this technology will be utilized in subsea wells, deep water completions, multilaterals and extended reach horizontal wells.

Gai (2001) listed the following objectives of the deployment of smart completion technology, which summarizes possible benefits of this technology:

- To be able to choke back or shut off water from each lateral independently;
- To be able to measure the contributions of each lateral individually via in situ measurement of flow rate and pressure;
- To be able to gather information on the performance of multilateral wells especially the interaction between the laterals;
- To provide data (via continuous monitoring) for reservoir management, particularly to assist in planning further wells;
- To optimize oil production, lifting costs and reserve recovery.

The modelling of these control devices in reservoir performance studies is very important in terms of making reliable estimations, which are needed to quantify the potential benefits of these completions. In their segmented well model, Holmes *et al.* (1998) showed how these control devices can be implemented and modelled within a commercial reservoir simulator (GeoQuest, 2001a,b). Valvatne (2000) and Valvatne *et al.* (2001) presented a semi-analytical method based on Green's function to model control devices for single phase problems. The reservoir modelling part of this development is based on the methodologies proposed by previous authors (Wolfsteiner *et al.*, 2000a; Durlofsky, 2000; Wolfsteiner *et al.*, 2000b). Valvatne used several realistic well configurations and showed the benefits of downhole control devices. He stressed that instead of performing detailed finite difference simulations, which require extensive data input, a semi-analytical method can be used. This method can, in many single phase flow problems, efficiently reproduce the finite difference simulation results with good accuracy.

Jalali *et al.* (1998) showed the impact of intelligent completions on a crossflow problem which occurs in the wellbore in a non-communicating two layer gas reservoir. They also studied an injectivity problem in a linear waterflood, again in a two layer non-communicating oil reservoir. The application strategy of intelligent completions in both of these problems was the same although the problems had different fluid characteristics. The control strategy applied in this study was simply opening and closing layers to flow when necessary. Some

other recent studies showed that this technology is also beneficial for horizontal wells with high frictional pressure drops (Yeten and Jalali, 2001; Sinha *et al.*, 2001). These studies demonstrated that by delaying the breakthrough of unwanted fluids to the well, substantial incremental recovery can be attained. Yeten and Jalali (2001) also showed that these completion techniques provide flexibility during field development. Jalali and Charron (1998) showed the applications of downhole monitoring devices in some North Sea reservoirs. They demonstrated that the inflow performance relationship can be deduced via downhole monitoring. Additional studies addressing field and conceptual applications of smart wells were presented by several authors (Greenberg, 1999; Jalali and Charron, 1998; Rester *et al.*, 1999; Gai *et al.*, 2000; Yu *et al.*, 2000; Lie and Wallace, 2000; Afilaka *et al.*, 2001; Nielsen *et al.*, 2001; Lucas *et al.*, 2001).

In this study we will use smart well completion technology to mitigate the detrimental effects of wellbore hydraulics and reservoir heterogeneity. We will screen different reservoirs with various well configurations for the possible deployment of this technology.

1.2.5 Well Control Optimization

A few authors have previously addressed the optimization of smart wells. Brouwer *et al.* (2001) presented a static optimization methodology that maximized sweep in a waterflood study. They considered fully penetrating smart horizontal injection and production wells. Their basic algorithm involved shutting in the segments of the well with the highest productivity index and adding the production from these segments to other well segments. By doing that they could balance the production along the well and attain a better sweep efficiency. Dolle *et al.* (2002) introduced a dynamic optimization algorithm that used optimal control theory. Using this approach they demonstrated improved sweep and recovery over their previous method (Brouwer *et al.*, 2001). Brouwer and Jansen (2002) investigated the effects of smart completions with different well targets and constraints in a water flooding project using optimal control theory. They found considerable scope for accelerating production and increasing recovery for wells operating with rate targets. Sudaryanto and Yortsos (2000) also applied optimal control theory for the optimization of sweep efficiency. They optimized fluid injection rates for two-dimensional problems with vertical wells.

Khargoria *et al.* (2002) studied the impact of valve placement, inflow configuration and mode of operation on production performance using a horizontal well on a synthetic bottom water drive model. They envisaged control in reactive and proactive modes. They defined reactive control as the surface production choking or zonal isolation of production through closing valves discretely or continuously. With proactive control they rely on the data which is supplied from the sensors (distributed electrical arrays) installed on the well. With this data, they showed that the proactive control strategy can be used to avoid the displacing phases invading the near-well region. They used simulated annealing and conjugate gradient optimization algorithms to determine the optimum location and control settings of the valves to maximize the cumulative oil production. They did not update the valve settings in time, and assumed that they would be actuated from initial production. They converged to the same optimum with both of the methods.

Gai (2001) introduced an optimization method for multi-zone or multilateral flow control completions. He used the inflow performance relationship (IPR) and valve performance relationship (VPR) information to optimize the valve settings. In the absence of a commercial package to optimize the performance of laterals, he proposed the use of a graphical representation of the performance curves. He concluded his study by stating that the hardware for smart completions has advanced substantially in the last five years, but work on the optimization of the performance of smart wells has not matched hardware advancements. He also claimed that the industry is using trial-and-error approaches for well control. This recent paper clearly challenges academia and the industry to put more effort on this subject. We intend to address this issue by developing efficient and robust tools.

1.2.6 Uncertainty around Reservoir Description

There have been some frustrations in the deployment of multilateral wells. Problems have mainly been due to the incorrect selection of location, orientation or the trajectory of the branches. One of the sources of this error is inadequate information about the engineering and geological reservoir data, or the incomplete assessment of uncertainty around these parameters.

Beliveau (1995) stressed the uncertainty in prior estimation of the productivity of horizontal wells. He presented a study that considered more than 1000 horizontal wells worldwide, and he concluded that permeability heterogeneity is the most important factor in

terms of incorrect prior productivity estimations. Similarly, Aziz *et al.* (1999) stressed the importance of these uncertainties in predicting the performance of horizontal wells. They quantified the uncertainty by performing numerical simulations and concluded that the greatest source of uncertainty is the reservoir description and the way reservoir heterogeneity is introduced into prediction tools.

Sarma (1994) also stressed the importance of understanding the extent and nature of the heterogeneity which might adversely affect the performance of horizontal wells. This situation is also implied by Isah *et al.* (1995), who stated that unexpected geology is the principal cause of disappointing horizontal wells. Antonsen *et al.* (1993) also stressed the effect of geological uncertainty in terms of horizontal well performance. They performed sensitivity studies with respect to thickness, depth, well length and permeability on cumulative recovery. Among these parameters permeability was the most sensitive parameter, in agreement with the conclusions reached by other investigators (Beliveau, 1995; Aziz *et al.*, 1999; Yamada and Hewett, 1995; Gharbi and Garrouch, 2001). Smith *et al.* (1995) concluded their work by stating that poor reservoir characterization results in a high level of uncertainty. Smith *et al.* (1995) and Corlay *et al.* (1997) also claimed that the drilling of nonconventional wells will provide additional information and reduce the uncertainty and risks associated with the deployment of this technology.

These studies indicate that it is vital for us to incorporate the effect of uncertainty during the optimization processes.

1.2.7 Assessment of Uncertainty for Field Developments

Dejean and Blanc (1999) classified the sources of uncertainty as uncontrolled uncertainties on the reservoir description parameters and controlled uncertainties on the reservoir development scheme parameters. They emphasized that in order to make accurate production forecasts and optimize the reservoir production scheme, these uncertainties should be described and the most influential ones among them should be identified. They proposed the integration of experimental design, response surface methodology and Monte-Carlo methods to optimize the production scheme. They applied their methodology to a field to assess the effects of the uncertainties on cumulative oil production in time. From the results they obtained, they were able to build confidence intervals on the maximum cumulative oil production over time and confidence areas for the optimal location of a new production

well. Friedmann and Chawathé (2001) and Kabir *et al.* (2002) used a similar methodology to that of Dejean and Blanc (1999) to assess the uncertainties for the field development process.

Guyaguler and Horne (2001) addressed the uncertainties associated with well placement optimization problems using the utility theory framework along with numerical simulations as the evaluation tool. They evaluated their methodology using 23 history matched realizations of a test model based on a real field. They stated that the utility framework offered a means to quantify the influence of the uncertainties in conjunction with the risk attitude of the decision maker. They used a hybrid genetic algorithm for the optimizations. They also formulated the well placement optimization problem as a random function to increase the computational efficiency. Each time a well configuration was to be evaluated, a history matched realization of the reservoir properties was selected randomly, and the objective function was evaluated using this realization.

Manceau *et al.* (2001) combined experimental design and joint modelling methods to quantify the impact of the principal reservoir uncertainties on the cumulative oil production and to optimize future field development in a risk analysis approach. Using the joint modelling method, they were able to model the production recovery as a function of both uncertain engineering parameters as well as discontinuous parameters such as geostatistical realizations and equiprobable history matched models. They estimated the new locations for three vertical wells with this combined method and concluded that this framework provided an appropriate methodology for decisions making in a risk prone environment.

We now give a brief description of our method of solution.

1.3 Statement of the Problem

As stated in the previous section, the selection of the correct well type, location and trajectory is very important. The capital investment required to drill a nonconventional well is usually very high. It is very costly to correct mistakes made during this selection process. Another important factor that determines the performance of these wells is the wellbore hydraulics. Wellbore hydraulics might be important when the frictional pressure losses in the wellbore are large. This can cause the coning or cusping of unwanted fluids to the well. The production from such wells may then have to be limited due to surface facility

constraints. The smart completions technology provides the necessary tools to address the problems caused by wellbore hydraulics and reservoir heterogeneity. Therefore implementing the correct design and the correct utilization of these completions may be as important as implementing the correct well type and trajectory.

In a field development context we try to find the optimum number of production and injection wells to be drilled, their type, location, trajectories and control strategies that will maximize profit, or some other objective.

Well type optimization can be thought of as determining the optimum number of junction points with some specified number of branches emanating from these junctions. Therefore, via this optimization, the well types might range from monobore wells (i.e., vertical, horizontal or slanted) to complex multilateral wells with multiple junctions having multiple branches. This and other optimization problems are mainly driven by economic considerations. Hence, the cost functions associated with drilling and completing these wells are necessary.

Optimization of well location and trajectory involves finding the optimum well heel and geometry, i.e., location of the junction points and the length and orientation of the mainbore and each branch. The primary objective here is to contact appropriate oil pockets or reservoir layers. The drillability of the well and the interference between laterals are issues for this problem. During the optimizations, this is the phase where most of the associated constraints, such as not allowing the well to incline upwards, or the avoidance of wells or laterals colliding with each other or with existing wells, appear.

The last phase of the nonconventional well optimization can be defined as the well control optimization, i.e., decision on deployment of smart well control technology and optimum operating schedule. `ECLIPSE` (GeoQuest, 2001a) offers ways of modelling these devices and a "reactive" control strategy (activating the devices in real time as the rate or type of the produced fluids change) can be implemented within the simulation data file. Therefore, a degree of smart well control can be included during the optimization of the well type, location and trajectory.

Another optimization process for the well control can be defined as a "defensive" control strategy, which can be applied during the decision making process for the deployment of this technology. In this case the activation of the devices is optimized to delay coning/cusping of unwanted fluids, which maximizes cumulative oil production and results in

higher NPV through an accelerated production scheme. This methodology, which will be explained in detail in the coming chapters, is appropriate for use as a screening tool rather than for actual operations.

Due to our inadequate and imperfect knowledge, many equiprobable reservoir descriptions can be generated. Therefore it is vital to assess the consequences of geological uncertainty within the optimization procedures.

1.3.1 Solution Approach

As indicated above, we want to find the optimum number of wells, their types, locations and trajectories as well as their suitability for smart completions. The problem of the optimum deployment of NCWs is solved via two independent optimization schemes. The first optimization engine will provide the optimum well type, location and trajectory, or simply optimum design of the well, with or without the reactive control implemented. The second procedure will provide the optimum defensive control strategy that can help with decision making on instrumenting the wells with smart completions.

We need optimization tools and reservoir simulators capable of modelling smart wells. These are our objective function evaluators. The well type, location and trajectory optimization problem will be solved by a stochastic search engine, namely a genetic algorithm. As discussed in Chapter 2, this algorithm gives us the possibility of integrating all the decision parameters of the problem. This optimization method requires many objective function evaluations. Depending on the complexity of the problem, the number of simulations needed can be on the order of thousands. The procedure must therefore be hybridized with “helper” algorithms and proxies to reduce the CPU cost.

The screening tool for the deployment of smart completions will be a gradient based algorithm, namely a nonlinear conjugate gradient method. This method along with its implementation will be explained in detail in Chapter 3.

1.3.2 Concluding Remarks

In this chapter we gave a general background of NCWs and also motivated the necessity of the optimization of their deployment.

The literature review leads to the following observations:

- Mostly stochastic search engines have been used to optimize well locations. We are not aware of any previous studies that address the combined determination of optimum well type, placement and trajectory.

- Optimization of smart well control is in its early stages. Different techniques have been proposed, though the area is very open to further exploration.

- The assessment of the effects of uncertainty to various geological and engineering parameters is vital for reliable decision making. Therefore the optimization framework must consider uncertainty.

The outline of this dissertation is as follows. In Chapter 2, the formulation and optimization of the well type, location and trajectory problem are presented. Sensitivities with respect to some of the algorithm parameters are presented, and guidelines for the selection of these parameters are established. The methodology to assess and quantify the effects of geological uncertainty is also described. Several synthetic examples are presented. Additional discussion involving the treatment of multiple sources of uncertainty is included in Appendix A. In Chapter 3, we describe the formulation for the optimization of well control. A methodology to assess the uncertainty for this screening tool is described. Again using several synthetic examples, the benefits that can be attained through the deployment of the smart completions technology are quantified. In Chapter 4, we apply all of our developments to a real field located in Saudi Arabia. Finally, we draw conclusions and give recommendations for future developments in Chapter 5.

Chapter 2

Well Type, Location and Trajectory Optimization

2.1 Formulation

In this study, the trajectory of a well and its laterals will be handled as independent lines in three-dimensional (3D) space. Any line connecting two points in 3D space can be viewed as a possible (lateral) trajectory. Here we will assume this to be a straight line. The parameters defining the well trajectory will be the starting point of the well or heel, H, and the ending point of the well or toe, T. In order to determine the production profile of a well, which will serve as the basis of computing revenues for the economic model (or just the "value" of the project), finite difference reservoir simulations will be performed. Since each point on a grid can either be represented by its map coordinates, x, y, z in real space, R, or by its directional indices, I, J and K in grid space, G, the parameters to be optimized become the coordinates or indices that define the heel, H, and the toe, T, of the mainbore and lateral(s) as shown in **Fig. 2.1**.

$$\begin{aligned} H = R : H(x, y, z) &\overset{c}{\leftrightarrow} G : H(I1, J1, K1) \\ T = R : T(x, y, z) &\overset{c}{\leftrightarrow} G : T(I2, J2, K2). \end{aligned} \tag{2.1}$$

Eq. 2.1 shows the transformation of the coordinates of a point from real to grid space or

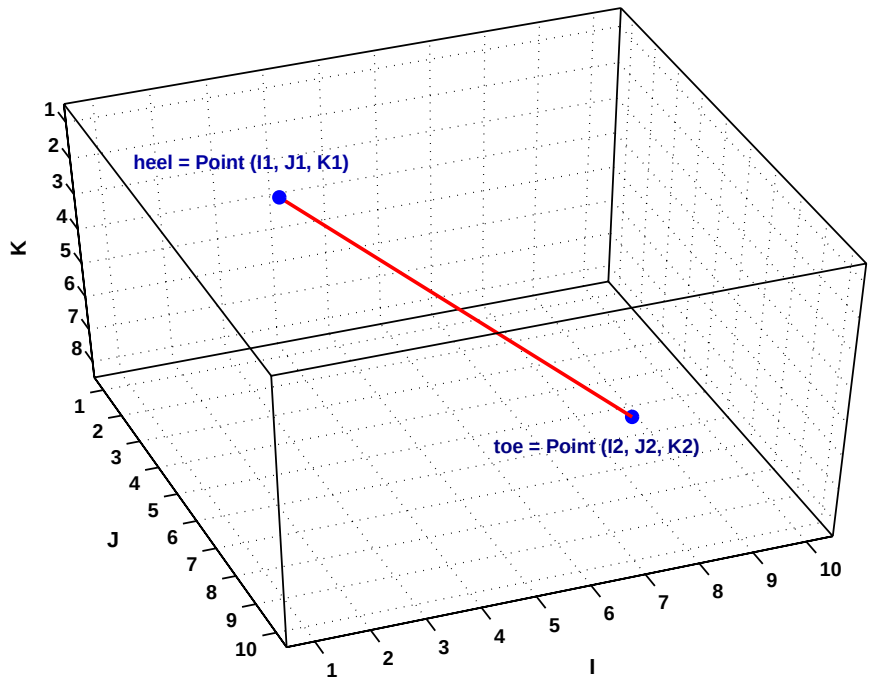

Figure 2.1: A Linear Well Trajectory

vice versa, via a mapping function, c, which is built by using the reservoir structure and grid information:

$$c : R \leftrightarrow G. \tag{2.2}$$

Now let us define the following vectors, **h** and **t**, which are the vector locations of the points H and T respectively:

$$\mathbf{h} = R : H \begin{pmatrix} h_x & h_y & h_z \end{pmatrix}^{\mathrm{T}}, \tag{2.3}$$

$$\mathbf{t} = R : T \begin{pmatrix} t_x & t_y & t_z \end{pmatrix}^{\mathrm{T}}. \tag{2.4}$$

Then the trajectory vector $\boldsymbol{\tau}$ can be defined using the parametric definition of a line passing through points **h** and **t** in 3D space:

$$R : \boldsymbol{\tau} = \mathbf{h} + m \cdot (\mathbf{t} - \mathbf{h}), \tag{2.5}$$

where m is a parameter between 0 and 1. This representation is useful for representing the junction points, which are defined as points on the mainbore from which laterals emanate. Specifically, rather than representing a lateral in terms of six parameters (x, y, z for both endpoints), we can define the lateral in terms of four parameters (m and x, y, z for the far endpoint). The real space vectors $\mathbf{h}$, $\mathbf{t}$ and $\boldsymbol{\tau}$ can be mapped to grid coordinates by the same mapping function given by Eq. 2.2. The length of the well l_w is given by:

$$l_w = |R : \boldsymbol{\tau}| = \sqrt{(h_x - t_x)^2 + (h_y - t_y)^2 + (h_z - t_z)^2}. \tag{2.6}$$

Previously defined parameters can be represented using the directional angles, $\alpha_x, \alpha_y, \alpha_z$. The relation between the various parameters are given by direction cosines:

$$\begin{aligned} \cos\alpha_x &= \frac{h_x - t_x}{l_w}, \\ \cos\alpha_y &= \frac{h_y - t_y}{l_w}, \\ \cos\alpha_z &= \frac{h_z - t_z}{l_w}. \end{aligned} \tag{2.7}$$

The following relation also holds:

$$\cos^2(\alpha_x) + \cos^2(\alpha_y) + \cos^2(\alpha_z) = 1. \tag{2.8}$$

Therefore choosing H, l_w, α_x and α_z as the unknowns, coordinates defining the trajectory can be found via Eqs. 2.7 and 2.8. We can optimize a linear trajectory of a well/branch by choosing different sets of parameters.

The optimization routine should be able to handle any kind of multilateral well trajectory. **Fig. 2.2** shows some basic types of currently available multilaterals. In order to be able to handle all different types of multilaterals, the parameters to be optimized must be selected carefully. Simply optimizing the heel and toe points (either in grid space or real space) for each of the laterals and the mainbore will not be appropriate since severe constraints will have to be applied in order to allow the different well types to evolve in the genetic algorithm. The constraints might be the maximum allowable length, or orientation in the horizontal and vertical directions of the wellbore. These severe constraints might conflict with the nature of the proposed optimization engine. The second set of parameters

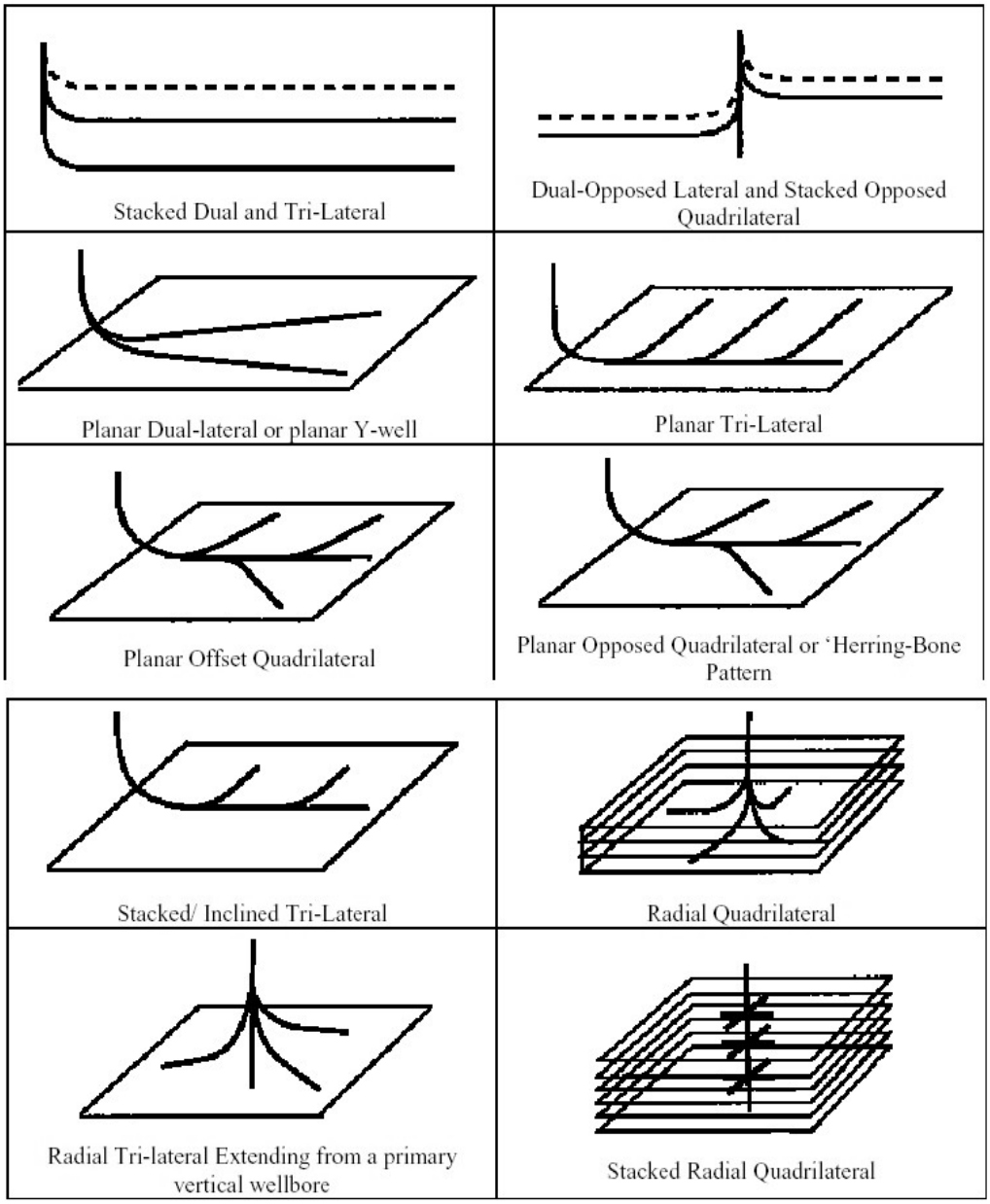

Figure 2.2: Basic Multilateral Well Types (TAML, 1999)

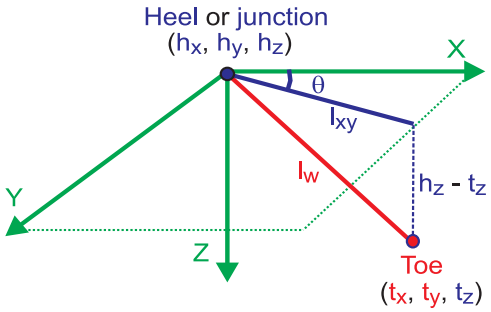

Figure 2.3: Well Trajectory Optimization Parameters

described in the previous paragraph (heel, angles and length of the well) are more appropriate for use in the algorithm, though they still require some manipulation. These parameters must be optimized for each lateral and the mainbore.

In hydrocarbon reservoirs, the thickness of the reservoir is usually much smaller than lateral extents. While gridding the reservoir simulation model, the grid sizes for the vertical direction (Δz) are therefore generally much smaller than the horizontal grid dimensions (Δx and Δy). This causes problems for the parameter set proposed previously. It is therefore more appropriate to define different parameters for vertical and horizontal dimensions, so that the contrast between these two coordinate axes will be properly taken into account. **Fig. 2.3** shows the new set of parameters for any kind of well (mainbore and laterals). In this figure, blue colored parameters are the parameters to be optimized and the red colored parameters are those that can be calculated from the optimized parameters.

As can be seen from Fig. 2.3, l_{xy} is specified as the projected length of the actual trajectory on the $x-y$ plane, t_z is the depth of the toe, as defined before (cf. Eq. 2.4), and the angle θ is the angle between l_{xy} and the x axis. Therefore, given H, l_{xy}, θ and t_z, T can be calculated using simple trigonometry. The set of parameters is identical for both the mainbore and its laterals, except that the heel point of a lateral is represented in terms of the junction point specified via parameter m, defined in Eq. 2.5.

Two related parameters within our formulation define the well type. The first parameter (N_{jun}) specifies the maximum number of junctions that the mainbore can have; the second parameter (N_{lat}) fixes the number of laterals that can emanate from any junction. Both parameters are specified by the user. The special case $N_{jun} \times N_{lat} = 0$ corresponds to a monobore well (which can be vertical, horizontal or slanted). This set of parameters and

some other secondary parameters, which are also user inputs, allow the algorithm to arrive at all of the multilateral configurations shown in Fig. 2.2.

The vector of parameters to be optimized, designated $\mathbf{p}$, is given by:

$$\mathbf{p} = \left(\begin{bmatrix} h_x \\ h_y \\ h_z \\ l_{xy} \\ \theta \\ t_z \end{bmatrix} \begin{bmatrix} J^1 \\ l^1_{xy} \\ \theta^1 \\ t^1_z \end{bmatrix} \cdots \begin{bmatrix} J^k \\ l^k_{xy} \\ \theta^k \\ t^k_z \end{bmatrix} \quad q \quad d_w \right)^T . \tag{2.9}$$

The first column of $\mathbf{p}$ represents the mainbore; subsequent columns correspond to the k laterals, well production targets and hole diameter. When a lateral shares a junction with another lateral ($N_{lat} > 0$), the J of subsequent lateral(s) is dropped from $\mathbf{p}$.

The number of producers and injectors can also be optimized, which allows us to find the optimum development plan. For multi-well optimization, Eq. 2.9 is extended to accommodate the unknowns required for each well. The wells become producers or injectors or they might appear or disappear from the development plan as determined by the parameter q. The case $q > 0$ represents a producer, $q < 0$ represents an injector, and finally $q = 0$ indicates that the well is shut-in (the well does not exist).

The optimization problem can now be represented by:

$$\underset{\text{constraints}}{\text{maximize}} \left\{ f\left(\mathbf{p}\right) \right\}, \tag{2.10}$$

where f is the objective function. Although our tool allows for both the minimization and maximization of f, we will concentrate on maximization problems. The objective function can involve any field or well parameter, but it is usually chosen to be either the cumulative oil production of the field or the net present value (NPV) of the project. In the latter case, f is defined as follows:

$$f = \sum_{n=1}^{Y} \left(\frac{1}{\left(1+i\right)^n} \begin{bmatrix} Q_o \\ Q_g \\ Q_w \end{bmatrix}^T_n \cdot \begin{bmatrix} C_o \\ C_g \\ C_w \end{bmatrix}_n \right) - C_d, \tag{2.11}$$

where Q_p is the field production of phase p during the discounting period n, C_p is the profit or loss associated with this production, and subscripts o, g and w designate oil, gas and water. The production vector, **Q**, is obtained from the reservoir simulator. The quantity i is the annual interest rate (APR), Y is the total number of discount periods and C_d is the cost of drilling and completing all the open wells (for which $q \neq 0$). This cost can vary very significantly depending on the field location and conditions, and is an important user defined function.

For purposes of this study, we represent C_d for a single well as follows:

$$C_d = \sum_{k=0}^{N_{lat}} \left[A \cdot d_w \cdot \ln\left(l_w\right) \cdot l_w \cdot (2-\alpha)\right]_k + \sum_{k=1}^{N_{jun}} C_{jun}. \tag{2.12}$$

This is an approximate formula, though it is based on cost figures obtained for a real onshore field (Bowling, 2002). In Eq. 2.12, $k = 0$ represents the mainbore, $k > 0$ represents the laterals, d_w is the diameter of the mainbore (in ft) and C_{jun} is the cost of milling the junction. The parameter A is a constant which contains conversion factors and represents the specific costs related to the field location and conditions. The parameter α accounts for the inclination of the well and is given by:

$$\alpha = \frac{h_z - t_z}{l_w}. \tag{2.13}$$

The contrast between the cost of drilling a vertical well and a horizontal well is captured by the term $(2-\alpha)$ in Eq. 2.12. For vertical wells, $\alpha = 1$, while for horizontal wells $\alpha = 0$, which means that a horizontal well will be twice as expensive as a vertical well on a per unit length basis.

There are some constraints which can be implemented either by the user or internally by the code. Any violation of these constraints penalizes the solution. The penalty assigned to each individual is checked before the objective function is evaluated. If one of the following conditions occurs, the individual is penalized and the simulation is not performed:

1. Toe point calculated from the parameters (H, θ, l_{xy} and t_z) is out of the grid range or out of the toe search space, which can be specified by the user.

2. Mainbore or any of its laterals' trajectories intersects (i.e., shares a grid block) with either each other or with already existing wells within the simulation model.

3. Mainbore or any of its laterals have zero length. This happens when the heel and toe points coincide.

2.2 Main Optimization Engine

Genetic algorithms (GAs) are the main optimization engine used for this problem. The major reasons for choosing GA are as follows:

- They are not "greedy" algorithms, so the solutions are not likely to be trapped in the first local optimum found.
- They do not require any gradients, which are not readily available from commercial reservoir simulators.
- They search from a set of points rather than a single point, which broadens the exploration of the search space.
- All of the unknowns in this problem can be expressed as integers, i.e., discrete variables. A GA is, in fact, designed for discrete variable optimization problems.
- They are easy to hybridize with other optimization or search algorithms.
- They are appropriate for parallel computing, which speeds up the optimization performance.

2.3 General Description of GAs

GAs were suggested by the concepts of evolution and natural selection by Holland (1975), and since then they have been intensively studied in theory and simulation. GAs are search algorithms based on the mechanics of natural selection and natural genetics. They combine the survival of the fittest among string structures (constructed with a special coding of the parameter set) with a structured yet randomized information exchange to form a search algorithm. In every generation, a new set of artificial entities (strings) is created using bits and pieces of the fittest of the old; an occasional new part is tried for good measure. Although GAs perform a stochastic search, this search is no simple random walk. They

efficiently exploit historical information to speculate on new search points with expected improved performance.

Unlike many other methods, GAs use probabilistic transition rules to guide their search. They use random choice as a tool to guide the search toward regions of the search space with likely improvement. As a class of adaptive search techniques, GAs are useful for global function optimization (Xu and Vukovich, 1994).

2.3.1 Basic Terminology

A GA uses a specific terminology which is basically inherited from biology and genetics. Below is a list of some terms which will be used extensively within this dissertation:

Individual An individual is a potential solution to the optimization problem. That is, it stores the optimized parameters coded in a special string format (alphabet), which are also called genes or chromosomes. The alphabet can have any base, but a common format is binary coding. For example the heel point of (5, 8, 3), in grid space - $G : H$, can be transformed into genes by simply converting each parameter of the heel ($I1$ = 5, $J1$ = 8, $K1$ = 3) into binary digits. The length of the string can be determined from the search space dimensions (grid dimensions in this case). That is, if the grid has dimensions of 25×25×15, one needs 5 digits in the binary alphabet to represent $I1$ and $J1$ and a 4 digit binary to represent $K1$. For $I1$, for example, we have:

$$\{11111\} = 1 \times 2^4 + 1 \times 2^3 + 1 \times 2^2 + 1 \times 2^1 + 1 \times 2^0 = 31$$

The binaries that represents the heel are:

$$(\{00101\}, \{01000\}, \{0011\}) = \{00101010000011\}$$

Note that the binary to decimal conversion applies from right to left of the string.

Allele Each of the bits within an individual string, also called genes.

Population Set of *individuals*, or possible solutions to the optimization problem.

Generation Iteration level within the optimization.

Evolving Progressing to the next *generation*.

Fitness "Goodness" of the optimized parameters, return value of the objective function.

Evaluation Objective or *fitness* function.

Fittest Best *individual* within a generation.

Elitism Carrying the *fittest* individual to the next generation.

Parents An individual couple randomly selected according to their fitness and mated for reproduction.

Children Resulting individuals after the reproduction.

Crossover Reproduction operator. Crossover randomly selects one or more indices on the strings of two individuals (*parents*) and swaps the content of the strings after this index, as shown in **Fig. 2.4**, to produce *children*. The random number drawn for this operation should be less than the crossover probability, p_c, defined a priori, otherwise crossover is not performed.

Mutation Reproduction operator. Mutation visits all the *alleles* of an individual and flips the bit provided that the random number drawn for each allele is less than the mutation probability, p_m, defined by the user, as shown in **Fig. 2.5**. It is applied for each child after the crossover operation.

Gray codes A Gray code is a function $G(i)$ of the integers i and has the following potentially useful property: The binary representation of $G(i)$ and $G(i+1)$ differ in exactly one bit. An example of a Gray code is the following sequence: 0000, 0001, 0011, 0010, 0110, 0111, 0101, 0100, 1100, 1101, 1111, 1110, 1010, 1011, 1001 and 1000, for $i = 0, \ldots, 15$ (Press *et al.*, 1999). Note that the sequence would look like the following if i was directly mapped to binary space: 0000, 0001, 0010, 0011, 0100, 0101, 0110, 0111, 1000, 1001, 1010, 1011, 1100, 1101, 1110, 1111. For example, in order to go from 7 to 8 (i.e., from 0111 to 1000) all four bits have to be changed, but with the Gray coding changing one bit is enough (0100 to 1100). Goldberg (1989)

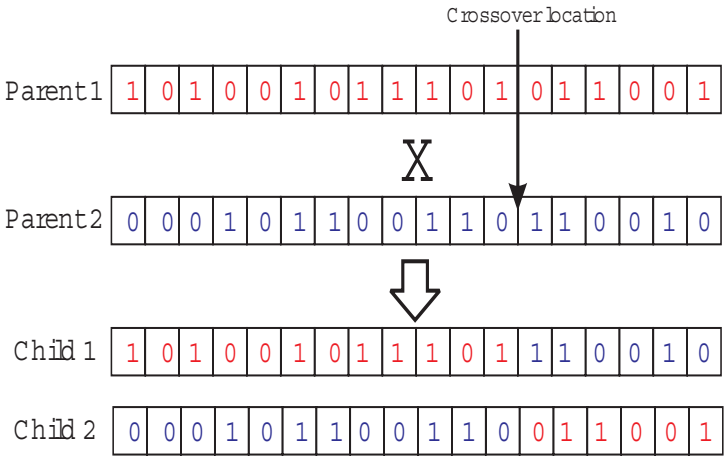

Figure 2.4: Crossover Operator

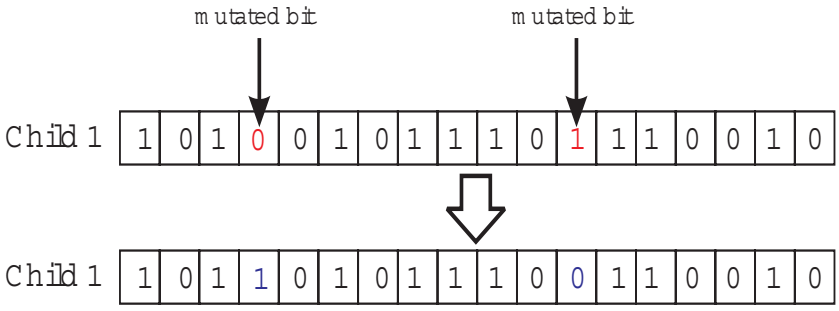

Figure 2.5: Mutation Operator

refers to this as the "adjacency property". A Gray code representation acts to force the mutation operator to act more locally.

Rejuvenation Means that the best solutions encountered during the overall optimization process are brought back to life at some generation levels (genesis). Also referred to as ancestors by Fichter (2000). This process is open to argument since it disturbs the actual genetic information by replacing the population with some outsiders. But experience shows that a better solution is often found after this operation.

Age This is one of the convergence criteria. It can only be implemented with elitism. If the solution does not improve more than a predefined tolerance, for a predefined number of generations (ages), then the algorithm is deemed to be converged to this solution.

The reproduction probabilities, p_c and p_m, can have a significant impact on the performance of GA. The population size, N, is another important parameter. Though all of these parameters are problem dependent, N is typically set to be of a size about equal to the length of the chromosome (i.e., the number of bits on the parameter string), p_m is taken to be approximately $1/N$, and p_c is set to a value between 0.6 and 1 (Guyaguler, 2002).

Generally, for a given problem, a standard genetic or evolutionary algorithm consists of the following (Xu and Vukovich, 1994):

1. A genetic or chromosomal representation of a solution to the problem.
2. A means of generating an initial population of solutions.
3. An evaluation function.
4. A function which ranks or selects the "good" or fittest solutions.
5. Genetic operators that change the composition of an individual during reproduction.
6. Algorithm parameters such as population size, mutation and crossover probabilities.

There are some more complex features and operators of GAs. In this study the most basic reproduction operators, with some additional features of the GA such as rejuvenation and elitism, are applied. Having given some basic features and terminology of GA, it is now appropriate to introduce a brief flowchart of the GA optimization routine.

2.3.2 Step-wise Procedure

The basic steps of a typical GA engine are:

1. Code the unknowns in a defined alphabet (form of an individual).
2. Generate an initial distribution of individuals (potential set of solutions - population) randomly or intuitively.
3. Evaluate the fitness of the individuals.
4. Exit if the specified convergence criteria are met.
5. Rank the individuals according to their fitness.
6. Assign a selection probability to each individual with respect to its rank within the population.
7. Select the individuals randomly, with the fittest individuals selected with the highest probability (analogous to natural selection - survival of the fittest).
8. Mate the fittest individuals randomly for reproduction.
9. Apply reproduction operators:
   (a) crossover
   (b) mutation.
10. Populate a new generation with the reproduced children.
11. Go to step 3.

The above flowchart can be visualized as shown in **Fig. 2.6**. This sketch shows the optimization of two points (heel and toe).

We now describe the overall procedure in more detail. In the first step, a set of chromosome strings (or *individuals*) is generated randomly or intuitively to form the *population*. The size of the population (number of individuals) is specified as a user input. Then in step 2, the coded information (binary alphabet is used in this case) is transformed into the heel and toe points, which are the parameters to be optimized. Red subscripts in Fig. 2.6

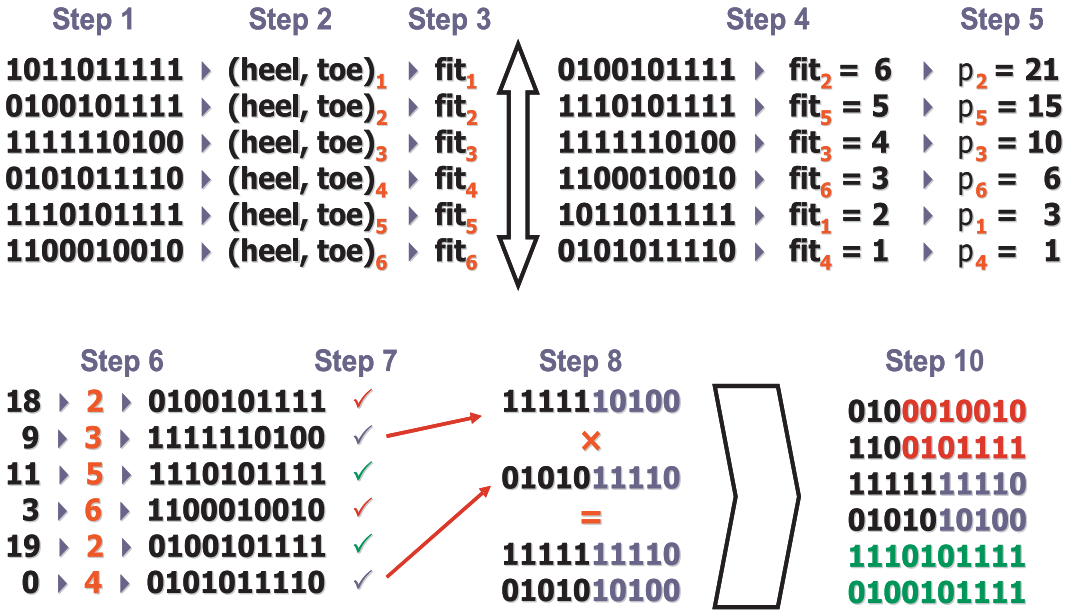

Figure 2.6: Schematic of GA Optimization Steps

indicate the identification (ID) of each individual. Having these points generated, a linear trajectory is created for every individual and these trajectories are then transformed into completion data, so the objective function evaluator (reservoir simulator, for example) can be run for each individual. In step 3, the objective function for each of the individuals (fitness) is evaluated.

The next step sorts the individuals with respect to their corresponding fitness values. For example, Individual #2 has the highest fitness, so it is the best solution within this population, and Individual #5 is the second best solution. Then their fitness values are set to their ranks in the reverse order within the population. Step 5 assigns a probability value according to each individual's fitness within the population. There are numerous ways of determining these probability values (Goldberg, 1989). In Fig. 2.6, these values were simply given by the rank of an individual itself plus all the ranks of the individuals which are below this individual:

$$\begin{aligned} p_i^l &= \left(\sum_{j=1}^{i} (f)_j \right)^{\omega} \\ p_i^u &= \left(\sum_{j=i}^{N} (f)_j \right)^{\omega}, \end{aligned} \tag{2.14}$$

where p_i^l and p_i^u are the lower and upper boundaries of probability of the selection interval of individual i, f is the fitness of the individual, N is the size of the population and ω is a weighting factor (the larger the ω, the more probability is given to the fitter individuals). Then a random number is drawn from a uniform distribution with minimum of 0 and maximum of the highest probability value assigned to the best individual. The probabilities set for the upper threshold of selection are shown in step 5 (with $\omega = 1$). In the actual implementation of the algorithm the probabilities are scaled between 0 and 1. For example, in order for Individual #5 to be selected, the drawn number should be within [10,15). Similarly, the only possibility for the least fit individual (Individual #4) to be selected is that the drawn number should be 0. As one can see, the better the individual's fitness, the higher its probability of selection. In step 6, N random numbers are drawn and these numbers determine which individuals will proceed to the reproduction step. This part of the cycle simulates the "natural selection" process. Within this process some of the individuals might be selected more than once, and some of them might not be selected at all.

The idea here is to use more of the genetic information from the fittest individuals, so that better (*fitter*) offspring (*children*) might be expected after reproduction. Step 7 mates the selected individuals randomly, and in step 8 the reproduction operators (*crossover* and *mutation*) are applied to the mated couples of individuals. The resulting children now form a new population for the next generation. The parents and the unselected individuals simply vanish (die). A fresh population *evolves*; that is, children (new individuals) are now carried to step 3. The cycle continues until a convergence criterion is met or the maximum number of generations, which can be specified, is reached.

A GA can never be guaranteed to find the global optimum. But the best solution found can always be expected to be a "good" solution. Theoretically the global solution will be found if an infinite number of generations were allowed to evolve and very large population sizes were used. However, this is not achievable in practice.

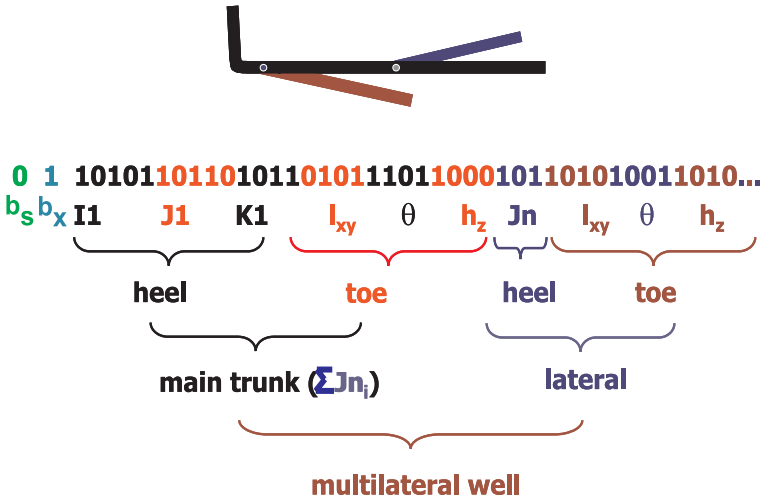

Figure 2.7: Representation of the Parameters on a Chromosome String

2.4 Implementation of GA for the Optimization Problem

We now describe the specific GA engine used in this study. The parameters to be optimized are first encoded in a predefined alphabet. **Fig. 2.7** illustrates the representation of the unknowns in a binary alphabet. Each group of bits, or *genes*, represents an unknown. In this study we use a rank-based selection criterion; i.e., the probability of selection increases with an individual's rank (quantified by the objective function) in the population (see Eq. 2.14).

The length of the chromosome will in general vary with the number of unknowns, as can be seen from Fig. 2.7. Since we want to consider a number of different well types and different numbers of wells during the course of the optimization, we need to have the ability to represent all possible well combinations on a chromosome. It is possible to use chromosomes of different lengths. Were we to do this, however, the population might be dominated by individuals occurring in early generations. For example, a population containing all monobore wells could never evolve into multilaterals in later generations. Similarly, a development scheme containing one producer and one injector could never become a more complex scheme.

In order to avoid this problem, we use a chromosome of fixed length. The length of the chromosome is determined from the predefined maximum number of wells (N_w), maximum number of junctions per well (N_{jun}) and laterals per junction (N_{lat}) parameters.

Individuals having less than these maximum numbers of wells or junctions and laterals will still be represented by chromosomes of the prescribed length (which is the maximum length required to represent the most complex well combination possible). Depending on the value of particular bits on the chromosome string the wells might be opened or closed (defined by status bits, b_s) or become injectors or producers (defined by sex bits, b_x). The value of the status and sex bits are directly reflected to q as shown below:

$$
\begin{aligned}
& q \leftarrow q \times b_s \times b_x, \\
& \text{where} \\
& b_s = \begin{cases} 1 & \text{open} \\ 0 & \text{shut} \end{cases} \\
& \text{and} \\
& b_x = \begin{cases} 1 & \text{producer} \\ -1 & \text{injector} \end{cases}
\end{aligned}
\tag{2.15}
$$

The status and sex bits define the well as an open production or injection well. The type bits define its type (i.e., monobore or a multilateral). Type bits specify the location of the junction (J^k) on the mainbore from which N_{lat} laterals emanate. If J^k (see Fig. 2.7) is greater than zero, then all the information that follows on the chromosome defines the lateral (i.e., specifies l_{xy}, θ and t_z for the lateral). If $J^k = 0$, all the information regarding the laterals of this junction is ignored. Note that N_{lat} is a predefined parameter and is the same for every junction point. Therefore the well type optimization is performed only by determining the N_{jun} parameter. As the optimization proceeds and mutation and crossover occur, these bits might take different values resulting in different combinations of producers and injectors with various configurations. This representation of information on the chromosome has the advantage that an initial population of single monobore wells can evolve into various types of complex multilateral producers or injectors, with multiple junctions and multiple laterals per junction.

The convergence criteria applied in this study is based on the improvement of the solution. If the solution has not improved for a predefined number of generations (i.e., if the solution *ages* for some number of generations), within a predefined tolerance, then this solution is deemed to be the optimum. The optimization also stops when the number of

generations reaches a predefined value, or the current generation is populated with identical individuals (*inbreed* situation).

2.5 Features of the Optimization Engine

The optimization engine interfaces with Schlumberger GeoQuest's commercial reservoir simulator, namely ECLIPSE (GeoQuest, 2001a), and ChevronTexaco's CHEARS (ChevronTexaco, 2001). When a new set of wells is proposed as a possible set of optimum solutions (individuals within the population), these wells are written to the data file of the reservoir simulator and the simulator is run for each of the individuals so their fitness can be evaluated. Choosing a reservoir simulator with extensive capabilities as the objective function evaluator allows us to implement many types of production and economic constraints, such as environmental and regulatory obligations or surface facility limitations. This can usually be accomplished with the existing keywords of the simulator. Although the simulation runs are expensive, the advantage is that we can access all of the features of a well-established reservoir simulator like ECLIPSE or CHEARS. The developed GA code can fully communicate with these simulators, and any summary keywords can be read from their output. Necessary SCHEDULE [1] data can be written automatically, including segmentation of the well for the Multi-Segment Wells option (valid for ECLIPSE), which provides the flexibility to handle well control optimization problems by using downhole control devices (i.e., transforming the proposed well into a smart well).

The well trajectories in finite difference reservoir simulators should be represented as completions at the centers of the grid blocks. This requires the representation of the well in a staircase manner as shown in **Fig. 2.8**. This figure shows the mapping of the trajectory defined in real space, $R : \boldsymbol{\tau}$ - blue lines, to the trajectory defined in grid space $G : \boldsymbol{\tau}$ - green full circles connected by red lines, by using the mapping function, c, defined in Section 2.1. The implemented trajectory (red lines) is clearly longer than the actual one (blue line). This situation can be corrected by using the correct well index (WI) which could be obtained by an approach such as that developed by Wolfsteiner *et al.* (2003). This approach requires some additional calculations and was not applied here. Instead, a simpler correction was

[1] The SCHEDULE section in a reservoir simulator data file specifies the operations to be simulated (production and injection controls and constraints) and the times at which output reports are required (GeoQuest, 2001a).

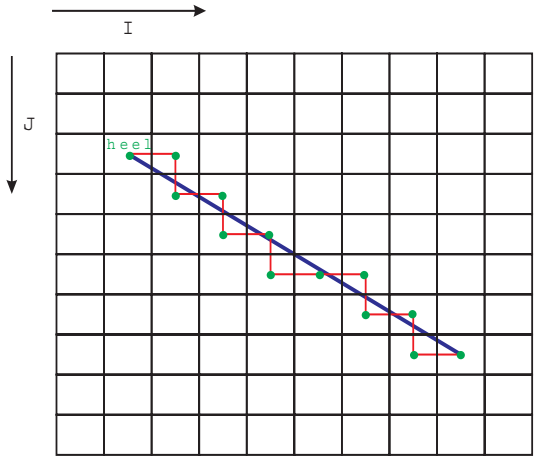

Figure 2.8: Representation of a 2D Linear Trajectory on a Block Centered Grid

used, based on a suggestion given in the Technical Description of ECLIPSE (GeoQuest, 2001b). This correction simply reduces the productivity index (PI) of each connection by a factor, ζ, via the WPIMULT keyword of ECLIPSE (GeoQuest, 2001a). A similar correction was also implemented for CHEARS via the WELLCOMP keyword. This factor is calculated by simply dividing the length of the actual trajectory by the length of the stair-step trajectory:

$$\zeta = \frac{l_w}{l_g}, \tag{2.16}$$

where l_w is the length of the well as defined before (cf. Eq. 2.6) and l_g is the length of the stair-step trajectory:

$$l_g = \sum_{k=1}^{N_{comp}-1} \Delta_k. \tag{2.17}$$

In Eq. 2.17 the parameter Δ can be defined as either Δx, Δy or Δz of the grid, depending on the direction of the penetration of the particular line segment defining the implemented trajectory. The parameter N_{comp} is the number of the completions defining the trajectory in the grid space.

Within the developed code, any combination of well trajectories (vertical, horizontal,

slanted or multilateral), wellbore diameters and production rates can be optimized simultaneously. For multilateral well location and trajectory optimization, the location of the mainbore and the trajectories of the laterals emanating from this mainbore are optimized. If a multilateral is being considered within the optimizer, the mainbore is not perforated, which is the usual practice in the industry. The code allows for a side track from an existing well. In this case the mainbore is not optimized since its location and trajectory are already known. The trajectories of the wells can be optimized at specified regions of the reservoir, i.e., each well might have its own search space. Wells might be constrained with respect to their dip, which implies that the wells might be forced to be horizontal with some specified dipping tolerance.

The percentage of the unperforated section to the actual length of the lateral is a user input. This parameter is used to define the fractional length of the lateral starting from its junction point on the mainbore to its heel, which is not perforated. The reason this portion of the lateral is unperforated is to give the drillers enough room to hit the desired target.

The parameter to be maximized or minimized can be anything which can be recognized by the reservoir simulator. `ECLIPSE` conventions are used to choose the objective function. For example, one can choose to maximize the cumulative recovery of the field (`FOPT`), or the well (`WOPT`), or one can choose to minimize the water cut of the field, well or group (`FWCT`, `WWCT`, `GWCT`). Apart from the `ECLIPSE` summary keywords (see `ECLIPSE` Reference Manual (GeoQuest, 2001a) for details), two additional keywords are also introduced: PI and NPV. Selection of PI will perform the optimization to maximize the single phase (oil) PI of the well. This keyword is not valid for `CHEARS`. Selection of NPV will invoke an economic model (see Eq. 2.11) to maximize the net present value.

2.6 Enhancing the Efficiency of Optimization - Helper Tools

2.6.1 Near-well Upscaling

In addition to accelerating the optimization procedure through the use of proxies that efficiently estimate simulation results (as described below), it is also useful to accelerate the run times of the individual simulations. Very large and complex models can not be used for the purpose of NCW optimization due to the expensive reservoir simulations that are

required for objective function evaluations. This issue can be addressed by coarsening (or upscaling) the detailed geologic description.

Here we will present a procedure especially designed for upscaling in the vicinity of NCWs. Our upscaling procedure combines standard grid block upscaling (i.e., the calculation of equivalent grid block permeability from the fine grid model) with the calculation of an effective near-well skin. The near-well skin accounts approximately for the effect of fine scale heterogeneity on the flow that occurs in the near-well region. The upscaling technique is related to earlier semi-analytical and finite difference approaches in which highly variable permeability fields were represented in terms of an effective near-well skin s and a constant background effective permeability $\mathbf{k}^*$. We assume that detailed, heterogeneous permeability realizations, generated geostatistically, are available. For each particular realization, we compute s and $\mathbf{k}^*$ for use in the finite difference simulator as follows (Wolfsteiner *et al.*, 2000a; Durlofsky, 2000; Wolfsteiner *et al.*, 2000b; Yeten *et al.*, 2000).

The skin s accounts for near-well heterogeneity and varies with position along the well. The skin designated for the portion of a well in grid block i is designated s_i. This skin is a function of the local near-well permeability, designated $k_{a,i}$, the background permeability $\mathbf{k}^*$ and the effective radius of the region over which the near-well permeability is computed, r_a. The skin for each well segment is then computed as:

$$s_i = \left(\frac{k_s^*}{k_{a,i}} - 1 \right) \ln \frac{r_a}{r_w}, \tag{2.18}$$

where r_w is the wellbore radius and k_s^* is the geometric average of the diagonal components of $\mathbf{k}^*$. This representation derives from the standard definition of skin (Hawkins, 1956), with appropriate modification to account for the heterogeneous permeability field.

The effective permeability $\mathbf{k}^*$ can be computed either numerically via steady state single phase flow calculations over the entire domain or through the use of approximate analytical expressions (Ababou, 1990). In either case this computation represents a minor overhead relative to solving the full two or three phase fine grid problem. The local near-well permeability is a weighted average of k in the near-well region a. It is computed by integrating over the region a, which is an elliptic cylinder of size and shape as determined from the correlation structure of the permeability field and the direction of penetration of

the well (Wolfsteiner *et al.*, 2000a):

$$k^{\omega}_{a,i} = \frac{1}{\Gamma_a} \int_a \frac{k^{\omega}(\mathbf{x})}{r^n} d\mathbf{x}, \tag{2.19}$$

where $\Gamma_a = \int r^{-n} d\mathbf{x}$ is a normalizing factor. The quantity ω is the permeability weighting exponent. Values of $\omega = -1, 0, 1$ correspond to a harmonic, geometric (i.e., logarithmic) and arithmetic averaging respectively and n is a spatial weighting parameter. In this work we take $\omega = 0$ and $n = 2$, which corresponds to a generalized geometric weighting.

The skin for well segment i as computed from Eqs. 2.18 and 2.19 is then input directly into the finite difference simulator. We refer to the methodology as s-$\mathbf{k}^*$ (Durlofsky, 2000) if the background permeability is constant (i.e., all the grid blocks are populated with k^*_x, k^*_y and k^*_z). The methodology is called s-k when the grid blocks are populated with the upscaled permeability values (i.e., the coarse model is heterogeneous). In this case k^*_s in Eq. 2.18 is replaced with the geometric average of the diagonal components of the upscaled permeability of the completion block i. The representation of fine grid heterogeneity in the near wellbore region on the coarsened model (s-k methodology) is depicted in **Fig. 2.9**.

Validation of s-k Approximation

The general level of accuracy of the s-$\mathbf{k}^*$ permeability model was established in several studies through extensive comparisons with detailed single and two phase flow finite difference calculations (Wolfsteiner *et al.*, 2000a; Yeten *et al.*, 2000). We also tested the s-k version of this method (defined above) for several well trajectories in a heterogeneous geostatistical permeability field as will be shown in this section.

Here we will present 10 monobore wells, which are randomly generated. We compare the performance of these wells on both fine and coarse grids with the s-k approximation. We used a reservoir model, which will be discussed below (see Section 2.8.1 for details) for this purpose. **Fig. 2.10** compares the performance of the wells in terms of cumulative oil production. **Figs. 2.11** and **2.12** compare the performances with respect to water cut and cumulative gas production, respectively. The blue lines on these figures are the unit slope lines, i.e., perfect correlation. **Table 2.1** presents both the Pearson and rank correlation coefficients, R and R_{rank}, calculated for these attributes using the simulation results for the

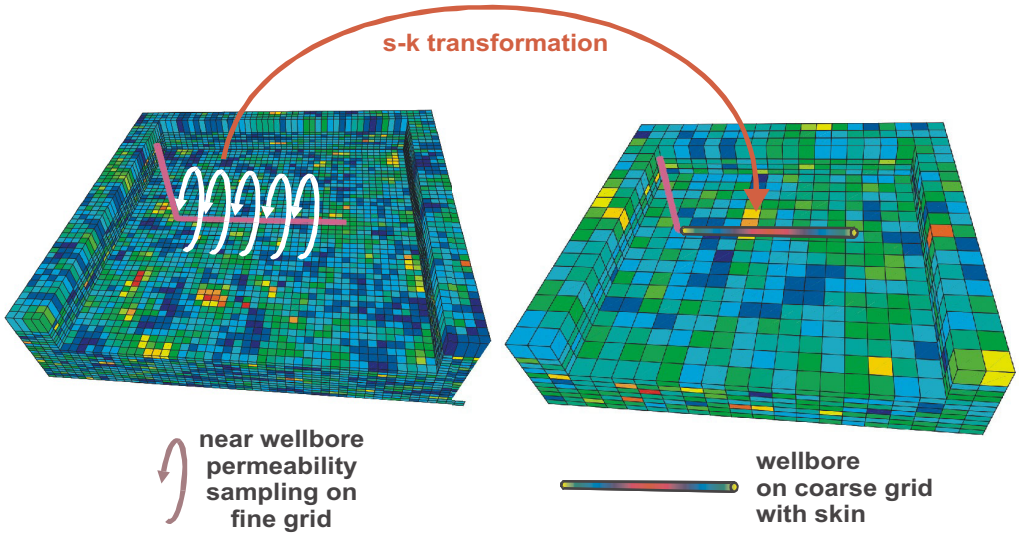

Figure 2.9: Representation of Near-well Permeability Heterogeneity via Skin Values on Coarser Models

Table 2.1: Correlation Coefficients between Fine and Coarse (s-k) Models

Attribute	R	R_{rank}
Cumulative Oil Production	0.9038	0.9758
Water Cut	0.9759	0.9879
Cumulative Gas Production	0.9917	0.9515

10 wells.

Rank correlations are 0.95 or greater for all quantities. For purposes of our GA optimization procedure, this level of agreement between the fine scale solution and our approximate representation is fully acceptable.

2.6.2 Artificial Neural Networks

In this study, we use a feed-forward artificial neural network (ANN) as a proxy to the objective function f (i.e., the ANN is used instead of the simulation to estimate f). ANNs are nonlinear mapping systems that possess a structure that is loosely based on the operation of the nervous systems of humans and animals (Reed and Marks II, 1999). In general

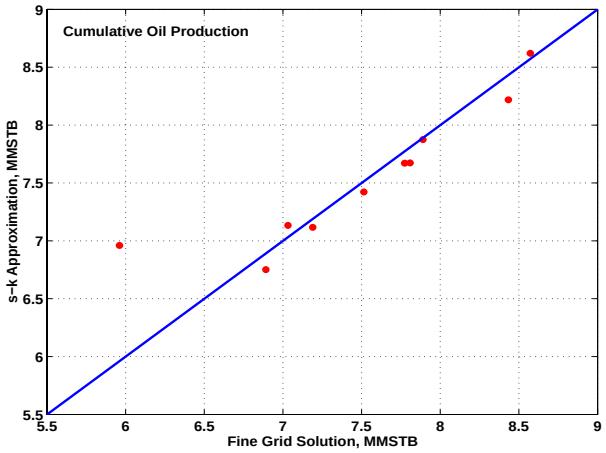

Figure 2.10: Comparison of Cumulative Oil Production

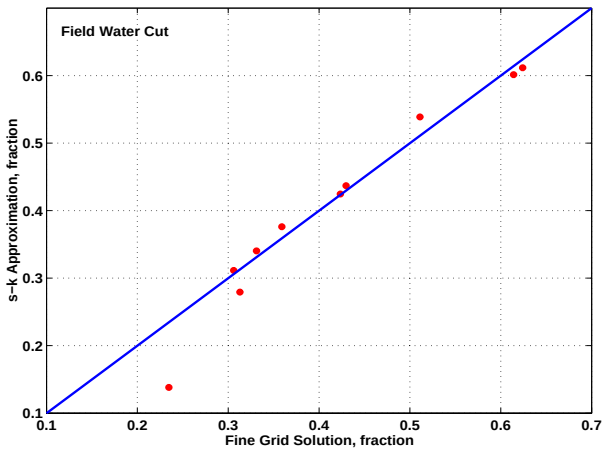

Figure 2.11: Comparison of Water Cut

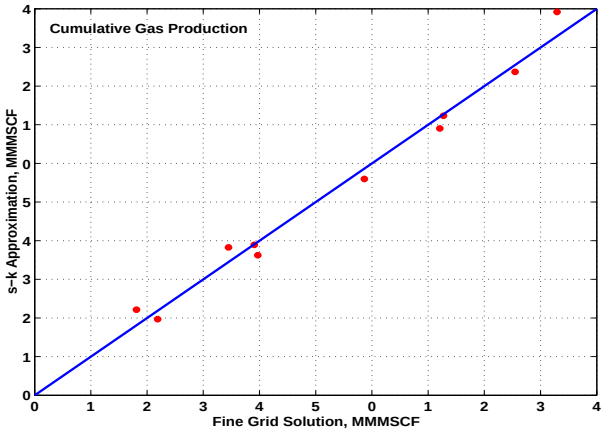

Figure 2.12: Comparison of Cumulative Gas Production

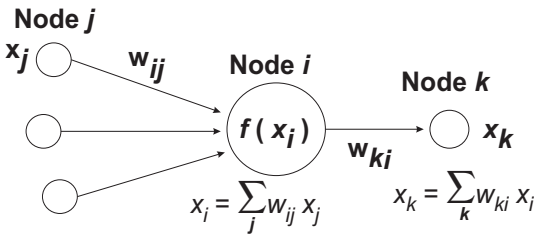

Figure 2.13: Schematic of the Artificial Neural Network

terms, an ANN consists of a large number of simple processors linked by weighted connections. Each unit receives inputs from many other nodes and generates a single scalar output that depends only on locally available information, either stored internally or arriving via weighted connections. The output is distributed and acts as an input to other processing nodes (Reed and Marks II, 1999). The power of the system emerges from the combinations of multiple units in a network.

In an ANN, the state of every node is determined by the signals it receives from the other nodes. The connection from any node j to another node i has a weight w_{ij}, as shown in **Fig. 2.13**. Each node adds all incoming signals and assigns a simple nonlinear function (usually the sigmoid function) to the sum (Harris and Stocker, 1998). The "training" of the network is essentially the optimization of the connection weights, determined such that the error between the output of the network and observed data is minimized.

We use an ANN with a single hidden layer. The optimal number of nodes in the hidden layer varies with the size of the optimization problem via (Masters, 1993):

$$N_{hidden} \geq \sqrt{N_{input} \cdot N_{output}}\,, \tag{2.20}$$

where N_{input} and N_{output} are the number of input and output nodes. The input nodes specify the heel and toe coordinates of each perforated well segment along with the other unknowns such as q and d_w. The number of input nodes are the number of possible well segments. Therefore, during a well type optimization or for a multiwell development optimization, the input nodes might include non-existing wells or laterals. This information will be specially coded for ANN, so that it will neglect this information for the training and testing processes. In applying the ANN, we have found it useful to quantify the effects of near-well heterogeneity via an overall effective skin s, computed along the lines described above. The output nodes provide the estimate of the objective function.

During the optimization, as we perform actual reservoir simulations, we store the parameter vector and the corresponding fitness in separate data sets, which we designate as training and testing data sets. One out of five simulation results is put into the testing data set, while the other four are placed in the training data set. When these data sets are populated with sufficient data, we train the network; i.e., optimize the connection weights. This optimization is itself accomplished using a GA in conjunction with a nonlinear conjugate gradient algorithm.

Once the network is trained, we test the network with the testing data set (which was not used in the training). The estimates from the network are compared to the observed values and the correlation coefficient, R, between the two is computed. If R is greater than a predefined threshold, typically 0.75-0.85 (a user input), we take the trained network to be reliable. If R is below this value, we do not use the ANN as a proxy in this generation.

The ANN used in this study cannot extrapolate accurately beyond the limits of its training. Because our aim is to continually improve the fitness of the population, we need to avoid situations where the ANN underestimates the fitness of a highly fit individual. For this reason, whenever the network estimate exceeds a predefined value (this value will vary from generation to generation) which is close to the current maximum, we perform an actual reservoir simulation instead of relying on the ANN estimate.

We repeat the training and testing cycle for each generation as new data are introduced.

As the GA solution progresses, the fitness of the solutions within the population increases. The ANN training therefore involves increasing numbers of fit individuals as the optimization proceeds. As a result of this, we generally observe more reliable results from the ANN in the later generations than in the earlier generations.

2.6.3 Hill Climber

Another of the helper tools applied here is an evaluation-only search method, referred to as a hill climber (HC), which is a heuristic adaptation of the Hooke-Jeeves pattern search algorithm (Reed and Marks II, 1999).

Hooke-Jeeves Pattern search algorithm takes small steps along each coordinate direction separately, varying one parameter at a time and checking if the objective function is improved. If a step in one direction increases the objective function, then a step in the opposite direction should decrease it. After N steps, each of the N coordinate directions will have been tested. This method usually accelerates convergence by remembering previous steps and attempting new steps in the same direction. An exploratory move consists of a step in each of the N coordinate directions ending up at the new base point after N steps. A pattern move consists of a step along the line from the previous base point to the new one. This becomes a temporary base point for a new exploratory move. If the exploratory move results in a higher objective function than the previous base point, it becomes the new base point. If this exploratory search fails, then the step size is reduced. The search is halted when the step size becomes sufficiently small (Reed and Marks II, 1999).

The hill climber used here perturbs the heel point of the mainbore, H, by one grid block in each direction. The well orientation is assumed to remain unperturbed, so T for the mainbore and all of the laterals can be easily evaluated. The combination of successful directions (i.e., those that improve f) is then determined and the search in this direction is started. The search continues in this direction as long as f increases. Therefore only a single pattern move step of the Hooke-Jeeves pattern search algorithm is applied. A final step is taken in the steepest individual direction (x, y or z), with the search again continuing as long as f continues to increase. In the case of optimization for multiple wells, one of the wells is randomly chosen by the hill climber and the climber works only on this well for that generation.

2.6.4 Overall Algorithm

A schematic of the overall optimization procedure is shown in **Fig. 2.14**. The relationship between the GA and the helper algorithms, and the basic way in which the optimization proceeds, is depicted in this figure.

In Fig 2.14 the blue arrows show the paths that GA takes during the course of the optimization. Each step is denoted by a full blue circle. In step 1 an initial population is formed. Then in step 2 the fitness of each individual is evaluated. The entire fitness evaluation process is encapsulated within the black circle in this figure. The evaluation is performed either using a reservoir simulator (green line emanating from step 2) or by the ANN (red line emanating from step 2), given that the trained network has met the reliability criteria as described above. If the fitness evaluation is performed by a reservoir simulation, then the information regarding this individual is fed to the ANN (green line connecting simulator and ANN icons) and added to its training or testing data set. At this point the skin transformer (s-k approximaton) is also applied. The s-k approximation can be used to provide skin values for the proposed well trajectories on coarse models. It can also provide an average skin, or permeability information evaluated for the well branches, to the ANN. In step 3 hill climbing is performed on some specified number of individuals. These individuals are those with the better fitness values. Note that the arrows emanating from the hill climber icon indicate that the climbing can be performed either by the reservoir simulator or by the ANN. Having completed this local search step, the rank based selection, reproduction and population update are performed to complete the current generation.

2.6.5 "Optimized" Simulations

The computational requirements of the optimization directly scale with the size of the simulation model. It was observed that around 99% of the optimization CPU time was spent in objective function evaluations (i.e., the reservoir simulations).

Assuming that a commercial reservoir simulator is the main engine for the objective function evaluations, the following improvements will speed up the optimizations:

1. Using `RESTART` runs. Initialization of the simulations takes some time. Since the initial state does not change, it can be determined once and used for all runs.

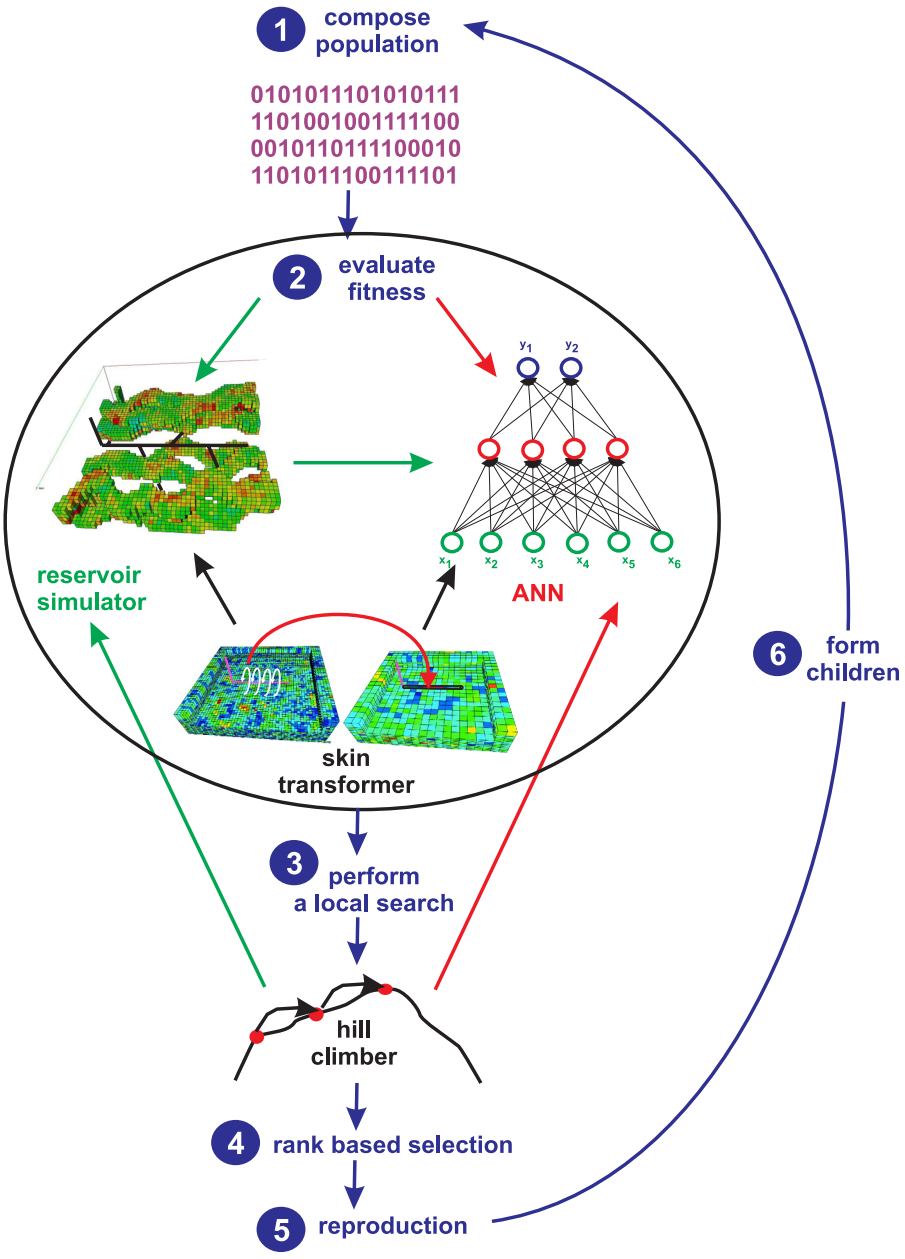

Figure 2.14: Schematic of Overall Optimization Algorithm

2. The use of keywords that deal with economic limits allow us to end poorly performing simulations early.

3. Understanding the model is very important. For example if the solutions tend to reach (pseudo) steady-state after some time for a primary depletion case, there is no need to run the simulations for the full duration. Simply calculating the productivity index (PI) at the time the simulation reaches the (pseudo) steady-state will suffice.

As mentioned above, the selection criteria within the GA are based on the ranking principle, so the suggestions offered here are assumed to preserve the ranking. This should be verified by performing a number of runs a priori.

2.7 Sensitivities to GA and Helper Parameters

2.7.1 Robustness and Effectiveness of GA

The crossover reproduction operator allows us to explore a broader search space, increasing the diversity of individuals within the population for the next generation. On the other hand, the mutation operator adds diversity and allows for the exploration of the local solutions. Therefore these operators are the heart of the GA. The probabilities assigned initially for these operators govern the robustness and quality of the optimization engine.

In order to test the robustness and effectiveness of the optimization algorithm and also to determine the effects of some of the GA parameters on the quality of the optimizations, a single phase heterogeneous simulation model was built. The model had $30 \times 30 \times 20$ grid blocks. The permeability distribution was obtained from an unconditioned sequential Gaussian simulation (Deutsch and Journel, 1998) with a mean of 20.3 and a standard deviation of 46.6 md. The objective function was to maximize PI after 300 days of primary production by finding an optimum monobore well. None of the helper algorithms were used, since the intention was to determine the effects of GA parameters such as population size, crossover and mutation probabilities, as well as Gray coding and rejuvenation. The unknowns were coded on a binary chromosome. Four major test matrices were generated, with each having seventeen subcases. Twenty different random number seeds were used for each of the subcases. Therefore $4 \times 17 \times 20 = 1360$ optimizations were performed.

Table 2.2: Test Matrix A

Case ID	N	p_c	p_m	Gray Coding	Rejuvenate
A.0	25	0.6	0.04	No	Never
A.1	25	0.8	0.04	No	Never
A.2	25	1	0.04	No	Never
A.3	25	0.6	0.001	No	Never
A.4	25	0.6	0.1	No	Never
A.5	25	0.8	0.001	No	Never
A.6	25	0.8	0.1	No	Never
A.7	25	1	0.001	No	Never
A.8	25	1	0.1	No	Never
A.9	50	0.6	0.04	No	Never
A.10	50	0.8	0.04	No	Never
A.11	50	1	0.04	No	Never
A.12	50	0.6	0.001	No	Never
A.13	50	0.6	0.1	No	Never
A.14	50	0.8	0.001	No	Never
A.15	50	0.8	0.1	No	Never
A.16	50	1	0.001	No	Never
A.17	50	1	0.1	No	Never

The optimizations were ended either at the 60^{th} generation or when the entire population had identical individuals. Test matrices are given in **Table 2.2 - Table 2.5**.

The outcomes of optimizations using 20 random number seed realizations for each case are given in **Table 2.6**. In this table μ represents the mean and σ represents the standard deviation of the PI values obtained for the optimum well. Mean values reflect the effectiveness of the optimization algorithm; the higher the mean the more effective the algorithm. The standard deviation provides an indication of the robustness of the algorithm; the lower the standard deviation, the more robust the algorithm. Based on these considerations, we define the parameter, κ, as:

$$\kappa = \mu - \sigma, \tag{2.21}$$

in order to determine the optimum settings for the algorithm. The particular combination

Table 2.3: Test Matrix B

Case ID	N	p_c	p_m	Gray Coding	Rejuvenate
B.0	25	0.6	0.04	Yes	Never
B.1	25	0.8	0.04	Yes	Never
B.2	25	1	0.04	Yes	Never
B.3	25	0.6	0.001	Yes	Never
B.4	25	0.6	0.1	Yes	Never
B.5	25	0.8	0.001	Yes	Never
B.6	25	0.8	0.1	Yes	Never
B.7	25	1	0.001	Yes	Never
B.8	25	1	0.1	Yes	Never
B.9	50	0.6	0.04	Yes	Never
B.10	50	0.8	0.04	Yes	Never
B.11	50	1	0.04	Yes	Never
B.12	50	0.6	0.001	Yes	Never
B.13	50	0.6	0.1	Yes	Never
B.14	50	0.8	0.001	Yes	Never
B.15	50	0.8	0.1	Yes	Never
B.16	50	1	0.001	Yes	Never
B.17	50	1	0.1	Yes	Never

Table 2.4: Test Matrix C

Case ID	N	p_c	p_m	Gray Coding	Rejuvenate
C.0	25	0.6	0.04	No	at every 10 generations
C.1	25	0.8	0.04	No	at every 10 generations
C.2	25	1	0.04	No	at every 10 generations
C.3	25	0.6	0.001	No	at every 10 generations
C.4	25	0.6	0.1	No	at every 10 generations
C.5	25	0.8	0.001	No	at every 10 generations
C.6	25	0.8	0.1	No	at every 10 generations
C.7	25	1	0.001	No	at every 10 generations
C.8	25	1	0.1	No	at every 10 generations
C.9	50	0.6	0.04	No	at every 10 generations
C.10	50	0.8	0.04	No	at every 10 generations
C.11	50	1	0.04	No	at every 10 generations
C.12	50	0.6	0.001	No	at every 10 generations
C.13	50	0.6	0.1	No	at every 10 generations
C.14	50	0.8	0.001	No	at every 10 generations
C.15	50	0.8	0.1	No	at every 10 generations
C.16	50	1	0.001	No	at every 10 generations
C.17	50	1	0.1	No	at every 10 generations

Table 2.5: Test Matrix D

Case ID	N	p_c	p_m	Gray Coding	Rejuvenate
D.0	25	0.6	0.04	No	at every 5 generations
D.1	25	0.8	0.04	No	at every 5 generations
D.2	25	1	0.04	No	at every 5 generations
D.3	25	0.6	0.001	No	at every 5 generations
D.4	25	0.6	0.1	No	at every 5 generations
D.5	25	0.8	0.001	No	at every 5 generations
D.6	25	0.8	0.1	No	at every 5 generations
D.7	25	1	0.001	No	at every 5 generations
D.8	25	1	0.1	No	at every 5 generations
D.9	50	0.6	0.04	No	at every 5 generations
D.10	50	0.8	0.04	No	at every 5 generations
D.11	50	1	0.04	No	at every 5 generations
D.12	50	0.6	0.001	No	at every 5 generations
D.13	50	0.6	0.1	No	at every 5 generations
D.14	50	0.8	0.001	No	at every 5 generations
D.15	50	0.8	0.1	No	at every 5 generations
D.16	50	1	0.001	No	at every 5 generations
D.17	50	1	0.1	No	at every 5 generations

of the parameters that maximizes κ can be considered as the optimum set. Note that this sensitivity analysis ignores the efficiency of the algorithm, i.e., the number of objective function evaluations is not taken into account.

The maximum values of μ and κ for each case are highlighted with red on Table 2.6. The minimum σ (most robust) encountered in these optimizations are highlighted with blue, and they consistently coincide with the maximum κ and μ cases. As seen from this table, three of the four optimum settings are achieved in sub case # 11 (Cases A, B and C). The optimum settings for Case D belong to its subcase # 10.

Some of the rows of Table 2.6 are highlighted with gray. In all of these cases, the optimizations ended prematurely, because all the individuals were identical prior to the 60^{th} generation. The algorithm internally assumes convergence when this inbreed condition occurs. The common parameter for these cases is that they have a low mutation probability ($p_m = 0.001$). Due to this low probability, the algorithm can not bring additional diversity to the population and after some generations all the individuals become identical, ending the optimization with a premature convergence. The converged well has a poor PI especially when the population size is low (note that $N = 25$ for subcases #3, 5 and 7, where κ is the lowest).

From Table 2.6, some conclusions with respect to specific parameters can also be drawn:

- The only difference between Cases A and B is the introduction of Gray coding to the optimization (cf. Tables 2.2 and 2.3). Comparing these cases, it can be clearly seen that the Gray coding does not provide any benefits to the optimizations. The average PI values for Case A are almost always higher than those of Case B. It is hard to draw any solid conclusions in terms of their effects on the robustness of the algorithm.

- Using higher population size almost always results in a higher κ value regardless of the case.

- Rejuvenation is found to be beneficial. Cases C and D usually have higher κ values than those of the corresponding entries of Cases A and B. It is difficult, however, to draw firm conclusions about the frequency of rejuvenation (comparing entries of Cases C and D).

- High crossover probabilities ($0.8 - 1.0$) enhance the quality of optimizations.

Table 2.6: Average and Standard Deviations of PI Values, in STB/psi, of Optimum Wells for 20 Optimizations

	Case A			Case B			Case C			Case D		
ID	μ	σ	κ	μ	σ	κ	μ	σ	κ	μ	σ	κ
0	23.1	0.8	22.3	22.8	1.5	21.3	23.2	1.0	22.2	23.3	1.2	22.1
1	23.4	1.0	22.4	22.8	1.3	21.5	23.7	0.7	23.0	23.0	1.3	21.7
2	23.7	1.3	22.4	22.4	1.1	21.3	23.8	1.1	22.7	23.7	0.9	22.8
3	17.5	3.1	14.4	15.1	2.9	12.2	18.2	2.6	15.6	18.9	3.3	15.6
4	21.4	1.4	20.0	21.8	1.3	20.5	21.6	1.4	20.2	21.9	1.5	20.4
5	18.8	2.5	16.3	15.3	2.8	12.5	19.4	2.5	16.9	20.4	2.5	17.9
6	21.7	1.3	20.4	21.5	1.4	20.1	21.6	0.9	20.7	22.0	1.1	20.9
7	18.5	2.9	15.6	16.7	3.2	13.5	19.0	2.8	16.2	20.3	2.8	17.5
8	22.0	1.5	20.5	21.2	1.1	20.1	22.0	1.3	20.7	22.3	0.8	21.5
9	23.4	1.0	22.4	23.0	0.9	22.1	23.5	1.0	22.5	23.8	1.0	22.8
10	23.6	0.7	22.9	22.9	1.0	21.9	23.4	1.1	22.3	23.9	0.7	23.2
11	23.7	0.7	23.0	23.0	0.6	22.4	23.9	0.6	23.3	23.7	0.9	22.8
12	20.3	2.5	17.8	18.7	3.0	15.7	21.1	2.3	18.8	21.9	2.3	19.6
13	22.8	1.2	21.6	22.1	1.0	21.1	22.3	1.3	21.0	22.5	1.1	21.4
14	20.9	2.3	18.6	18.6	2.2	16.4	21.3	2.5	18.8	21.7	2.5	19.2
15	21.7	1.4	20.3	21.6	1.0	20.6	22.7	1.0	21.7	22.2	1.0	21.2
16	21.5	1.8	19.7	18.9	2.5	16.4	22.0	1.8	20.2	22.2	1.8	20.4
17	22.4	1.1	21.3	21.8	0.9	20.9	22.4	1.1	21.3	22.1	1.0	21.1

- Using a high (0.1) or very low (0.001) mutation probability has a detrimental effect on the quality of optimizations.

- These observations are consistent with the typical values proposed by Guyaguler (2002) for population size, crossover and mutation probabilities.

2.7.2 Sensitivities with respect to Helper Algorithms and Ranking Weight

In this section, we present the sensitivities with respect to rank weighting factor, ω (see Eq. 2.14) and the deployment of the hill climber and ANN. To assess the effects of these factors on the quality and efficiency of the optimization engine, a single phase heterogeneous simulation model was built. The model had $50 \times 50 \times 30$ grid blocks representing a channel reservoir. The optimizations were based on finding the optimum multilateral well that maximizes the PI at the end of 300 days. The type of the well was not fixed and was also a decision parameter. The maximum number of junction points was specified as 3. Only one lateral was allowed to emanate from each of these junctions. A population size of 72 was used in all of the optimizations. Crossover and mutation probabilities were set to 1.0 and 0.01389, respectively. The optimizations were ended either at the 40^{th} generation or when the solution aged for 10 generations. Elitism was used. The rejuvenation operator was not deployed. The unknowns were coded on a binary chromosome.

Three major test cases were prepared with each having two subcases. Fifty different random number seeds were used for each of the subcases. The test matrix is given in **Table 2.7**.

The outcomes of optimizations using 50 random number seed realizations for each case are given in **Table 2.8**. In this table μ again represents the mean and σ represents the standard deviation of the PI values obtained for the optimum well. The following conclusions can be drawn from this analysis:

- Regardless of the case, the use of ANN reduced the number of simulations required considerably, by more than half in some cases.

- The mean values of PI for Cases A and C are slightly less than that of the cases which did not use ANN (mostly due to premature convergence). This indicates that there is

Table 2.7: Test Matrix

Case ID	ω	Hill Climber	ANN
Case A.1	2	on	on
Case A.2	2	on	off
Case B.1	1	on	on
Case B.2	1	on	off
Case C.1	2	off	on
Case C.2	2	off	off

Table 2.8: Average and Standard Deviations of PI Values, in STB/psi, and Number of Simulations Required

Case ID	PI		Number of Simulations	
	μ	σ	μ	σ
Case A.1	42.7	5.4	362.5	90.1
Case A.2	43.2	5.7	819.7	275.8
Case B.1	40.3	6.3	315.8	70.0
Case B.2	39.4	6.0	525.3	108.8
Case C.1	39.8	7.3	321.5	91.8
Case C.2	41.0	5.1	797.7	293.6

a chance of missing the optimum while using ANN.

- Taking $\omega = 2$ means that the selection will favor more fit individuals for reproduction. This is found beneficial as we compare the entries for Cases A and B.

- The hill climber is found to be very effective. With very little overhead, the PI values were considerably increased (see entries for Cases A and C).

2.8 Applications on Synthetic Models

In this section we present the application of our optimization methodology to several reservoir models. We consider four basic cases along with several subcases. In all of the examples elitism and an aging criteria of ten generations were used. No well control strategy was implemented, and all the wells were assumed to be infinitely conductive. Rejuvenation at every ten generations was used for Cases 1, 2 and 4. All calculations used the ANN and hill climber algorithms. The near-well upscaling was used in some of the calculations, as indicated below. A binary alphabet was used in all of the cases unless otherwise specified. Crossover probabilities were set to 1, and mutation probabilities were set to the reciprocal of the population size in all of the optimizations. The parameter ω was set to 2 in all of the cases.

2.8.1 Case 1 - Optimum Well in a Gaussian Permeability Field

This case involves a dual-drive reservoir. We introduce a gas cap of large pore volume at the top of the reservoir and an aquifer at the bottom. The bubble point pressure of the system, which corresponds to the pressure at the bottom of the gas cap (5000 ft), is 4000 psi. The permeability field was generated using an unconditioned sequential Gaussian simulation (Deutsch and Journel, 1998) on a $50 \times 50 \times 21$ simulation grid. Dimensionless correlation lengths of 0.5, 0.5 and 0.05 were used in the x, y and z directions, respectively (correlation length was nondimensionalized by the system length in the corresponding direction). The ratio of vertical to horizontal permeability for each grid block was set to 0.1. The histogram and the statistics of the horizontal permeability component are shown in **Fig. 2.15**. The reservoir geometry and rock properties are given in **Table 2.9** and the fluid properties are presented in **Table 2.10**.

We upscaled this reservoir model to $20 \times 20 \times 11$ using the near-well upscaling procedure described above (s-k). The validation of this approximation for this model is given in Table 2.1. Although this upscaling ratio was small, the coarsened model ran almost 100 times faster than the fine model, due to some convergence problems encountered in simulations of the fine model. Two main economic constraints were implemented for this optimization. Specifically, the well was shut in if the water cut exceeded 95% and the production rate of the well was cut back by 10% whenever the production gas oil ratio (GOR)

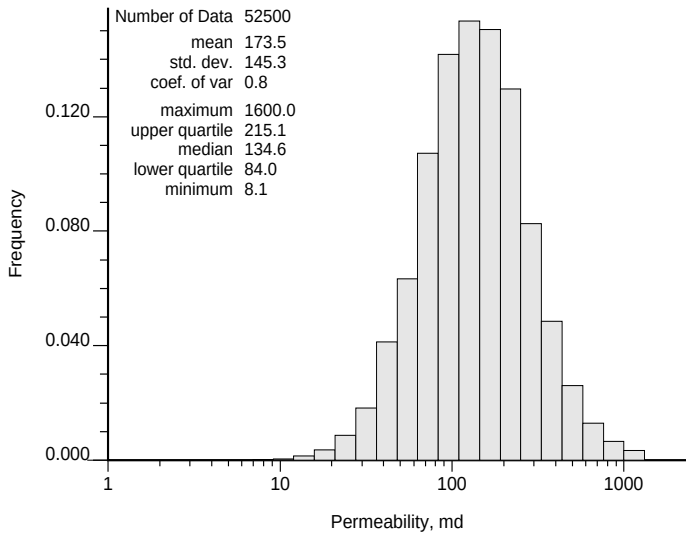

Figure 2.15: Case 1 - Histogram of the Horizontal Permeability

Table 2.9: Case 1 - Reservoir and Rock Properties

drainage area	5000 $\times$ 5000 ft^2
oil thickness	200 ft
ϕ	0.20
gas cap PV	0.4 MMft^3
R_s	1.0 MSCF/STB
c	3.0$\times 10^{-6}$ psi^{-1} at P_{bub}
k_{ro}	0.8 at $S_{wc} = 0.2$ and $S_{gr} = 0.05$
k_{rw}	0.4 at $S_{or} = 0.3$
k_{rg}	0.9 at $S_{wc} = 0.2$
k_h^*	153.0 md
k_v^*	11.0 md

Table 2.10: Case 1 - Fluid Properties

	γ at 14.7 psi	μ, cp at P_{bub}	$B, V/V$ at P_{bub}
oil	0.85	0.42	1.55
water	1.0	0.30	1.02
gas	0.71	0.02	0.71

exceeded 10 MSCF/STB.

Case 1a - Optimum Horizontal Well

Our first calculations are the determination of the optimum location, trajectory and target production rate (subject to a bottom hole pressure constraint) of a horizontal well. The objective function was to maximize the cumulative oil recovery at the end of five years subject to the constraints described above. A population size of 24 was used for this optimization and the solution was obtained in 231 simulations. **Fig. 2.16** shows the progress of the optimization in terms of the fitness of the best individual (best fitness) and the average fitness of the population. The average fitness is seen to increase steeply in the earlier generations and to then flatten in the later ones. This observation, which is very common in GA optimizations, clearly shows the evolution of the solutions toward a maximum. The fitness of the most fit individual (i.e., production from the best well) increases from the first generation to the last by almost 30% (from 10.3 MMSTB to 13.3 MMSTB). This represents a significant improvement and demonstrates the benefit of the GA optimization for problems of this type.

The optimal horizontal well is shown in **Fig. 2.17**. The optimum target liquid rate was found to be 10 MSTB/d. Note that the well is oriented diagonally in the reservoir and is located toward the middle of the reservoir, away from the gas cap and aquifer. This location and trajectory seem reasonable, as the optimal horizontal well would probably be expected to maximize reservoir exposure while being placed so as to avoid the production of gas and water.

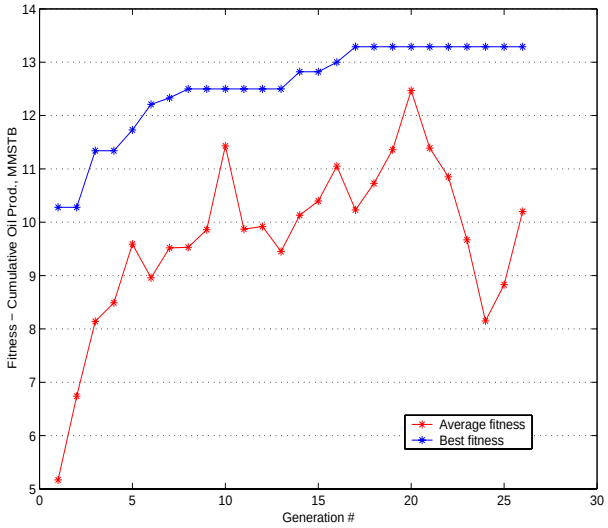

Figure 2.16: Case 1a - Progress of the Optimization

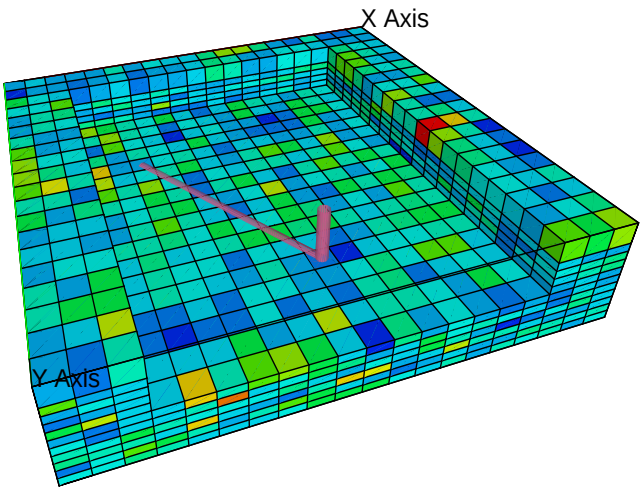

Figure 2.17: Case 1a - Optimum Horizontal Well

Table 2.11: Case 1b - Economic Parameters

Profit	Cost		
oil	water	gas	junction
$/bbl	$/bbl	$/MSCF	MM$
15	1	0.5	0.6

Case 1b - Optimum Well Type and Location

We consider the same reservoir but now determine the optimum well without restricting ourselves to wells that are purely horizontal. We specify $N_{jun} = 4$ and $N_{lat} = 1$. The optimization can therefore consider multilateral wells with up to four laterals, emanating from four independent junctions, as well as monobore wells, within the same population. The objective in this case is to maximize NPV. We use the economic figures shown in **Table 2.11**, which are used in the cost evaluations in Eqs. 2.11 and 2.12.

A population size of 88 was used for this optimization and the solution was obtained in 1027 simulations. The progress of the optimization is shown in **Fig. 2.18**. As in Case 1a, a target liquid rate of 10 MSTB/d was found to be the optimum. The NPV of the best well improves by about 34% from the first to the last generation, representing an increase of about $48 million. The optimum well in this case is a quad-lateral, as shown in **Fig. 2.19**. The well is again seen to contact a large reservoir area while avoiding proximity to the gas cap and aquifer. The evolution of the well types is presented in **Fig. 2.20**, where we show the number of each type of well (i.e., monobore, mono-lateral, dual-lateral, tri-lateral and quad-lateral) in each generation. We start with equal numbers of each well type. Toward the end of the optimization, the quad-lateral wells, which are optimal for this case, dominate the population.

The effect of rejuvenation at every 10^{th} generation is also evident in the figure. For example, at the 10^{th} generation, rejuvenated wells are mostly tri-laterals, since this is the optimal well type at this stage of the optimization. By the 20^{th} generation, however, we see that the quad-laterals are predominant, since they performed the best between the 10^{th} and 20^{th} generations. We emphasize that, due to our specialized representation of the different well types on the chromosomes, tri-laterals can evolve into quad-laterals during

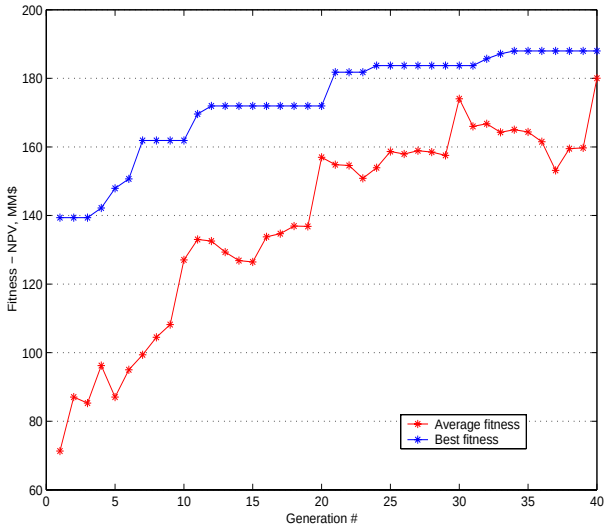

Figure 2.18: Case 1b - Progress of the Optimization

the reproduction operations and vice versa.

The “invalid” well type shown in the figure indicates wells that did not honor the constraints. In later generations, the number of invalid wells is quite high (almost half of the population) due to the fact that complex well trajectories (tri- and quad-laterals) are more likely to violate the constraints. This is largely because it is more difficult to fit these complex wells into the simulation grid. In addition, the probability of laterals intersecting each other increases with the number of laterals. Invalid wells are identified efficiently by the algorithm and do not cause a degradation in the performance of the optimization, given that high population sizes are used.

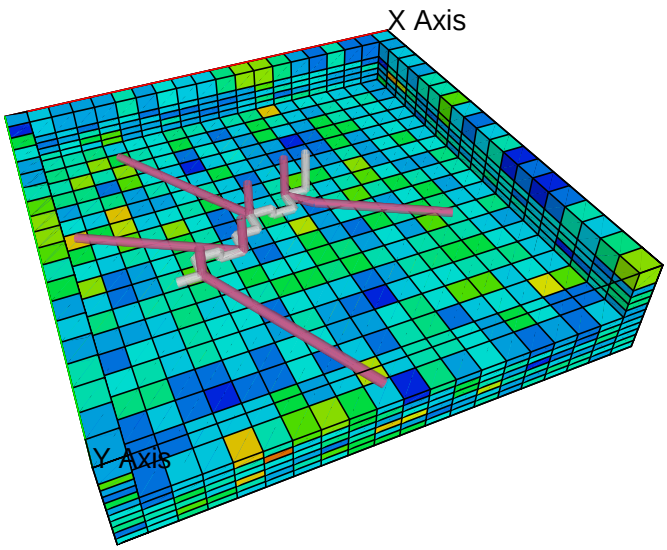

Figure 2.19: Case 1b - Optimum Well (Quad-Lateral)

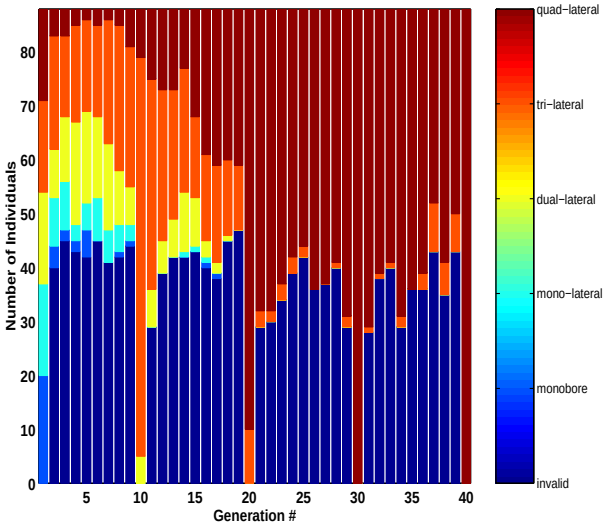

Figure 2.20: Case 1b - Variation of Well Types with Generation

Table 2.12: Case 2 - Reservoir and Rock Properties

drainage area	4000×4000 ft^2
oil thickness	200 ft
ϕ	0.20
c	3.0×10^{-5} psi^{-1} at 5000 psi
k_{ro}	0.8 at $S_{wc} = 0.2$
k_{rw}	0.4 at $S_{or} = 0.3$
$k_h^* = k_v^*$	layers 1-3: 100 md
$k_h^* = 10 \times k_v^*$	layers 4 & 8: 5 md
$k_h^* = k_v^*$	layers 5-7: 300 md
$k_h^* = k_v^*$	layers 9-10: 75 md

2.8.2 Case 2 - Optimum Well in a Layered Reservoir

This case involves production from a layered reservoir in which pre-existing injection and production wells operate. The reservoir does not contain a gas cap or aquifer and the fluid system is oil-water. The model properties are given in **Table 2.12**. The fluid properties for oil and water are as given earlier in Table 2.10. The permeability distribution for each of the layers was generated independently by unconditioned sequential Gaussian simulation (Deutsch and Journel, 1998) on a $40 \times 40 \times 10$ simulation grid. Average horizontal and vertical permeabilities for each layer, designated k_h^* and k_v^*, are shown in Table 2.12.

The initial reservoir pressure is 4000 psi at the top of the reservoir. The reservoir contains two fully penetrating vertical water injectors and an oil producer. The injectors have a target injection pressure of 4100 psi and the producer has a target liquid rate of 2 MSTB/d subject to a bottomhole pressure constraint. Our goal is to maximize the cumulative oil production by introducing a new production well. The N_{jun} and N_{lat} parameters were again specified to be 4 and 1. The production rate was fixed to be 4 MSTB/d for the new well.

A population size of 84 was used for this case and the solution was obtained in 679 simulations. **Fig. 2.21** shows the progress of the optimization. The cumulative field oil production increases by about 23% during the course of the optimization. The optimum well is a dual-lateral, shown in **Fig. 2.22**. The optimal well is located away from the existing wells with the laterals penetrating the first three layers of the model.

It is interesting to note that the optimized well avoids the highest permeability region of

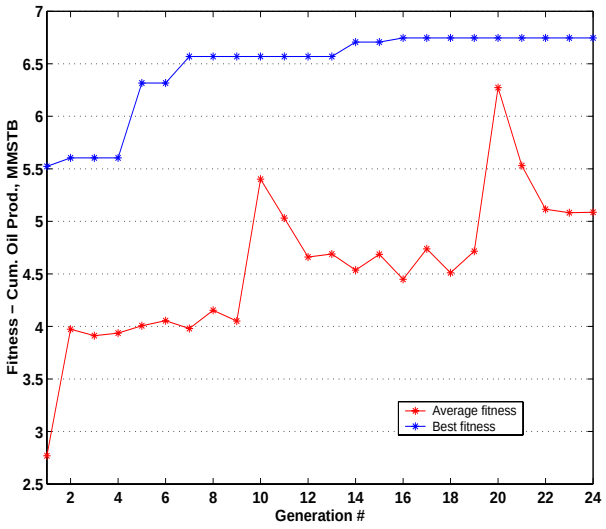

Figure 2.21: Case 2 - Progress of the Optimization

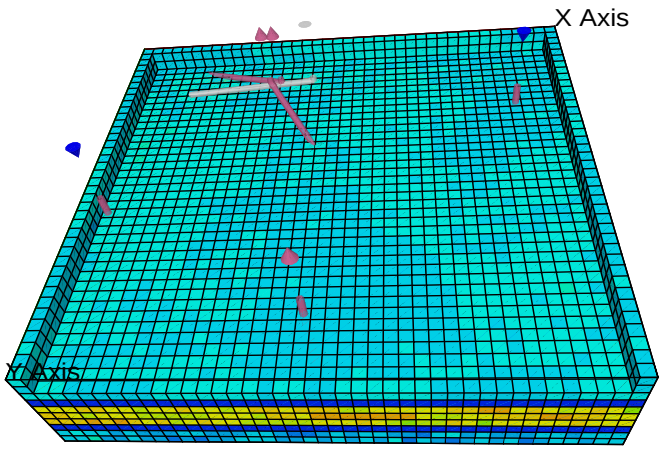

Figure 2.22: Case 2 - Optimum Well (Dual-Lateral)

the reservoir (layers 5-7, cf. Table 2.12). This is because the existing injectors and producer communicate through the high permeable layers and therefore already recover most of the oil from this region of the reservoir. The optimized well instead targets the less permeable region at the top of the reservoir, which is separated from the highest permeability layers by a low permeability layer. This case provides a good example of the performance of the GA optimization in the presence of existing wells. In such cases, the location and type of the optimal well may be somewhat nonintuitive.

2.8.3 Case 3 - Optimum Well in a Fluvial Reservoir

This case involves single phase flow (primary depletion) in a sealed, fluvial channel reservoir. The simulation model has a volume of $5000 \times 5000 \times 50$ ft^3 on a $50 \times 50 \times 5$ grid. The vertical to horizontal permeability ratio was again set to be 0.1. We used `fluvsim` (Deutsch and Tran, 2002) to simulate ten unconditioned realizations of this channel reservoir. The permeability distributions of the channel and background mudstone facies were populated independently using Gaussian sequential simulation (Deutsch and Journel, 1998). The volume ratio of channel sand to mudstone is 30%. The histogram and the statistics of the horizontal permeability for the ten realizations are shown in **Fig. 2.23**. Porosity was set to be constant at 0.2.

In this example a single realization is considered. The well produces under bottomhole pressure control, with the target pressure calculated with respect to the depth of the heel of the mainbore. For this reservoir we aim to maximize the NPV at the end of the first year of production by optimizing the well type, location and wellbore diameter. We allow for 14 different casing sizes, with outer diameter ranging from $4\frac{1}{2}$ to 20 inches. The bore sizes of the laterals are determined directly from the mainbore diameter. We use the same cost/profit figures shown in Table 2.11, except the junction cost is now taken to be \$150,000. The N_{jun} and N_{lat} parameters were again specified to be 4 and 1.

A population size of 40 was used for this case and the solution was obtained in 357 simulations. **Fig. 2.24** shows the progress of the optimization. The optimum well in this case is a tri-lateral well, shown in **Fig. 2.25**. This plot excludes the background mudstone for clarity. The laterals emanate from a short, slightly slanted mainbore and are oriented such that they penetrate a number of different sand channels. The production is not very sensitive to the wellbore diameter, so small wellbore sizes are found to be optimum ($5\frac{1}{2}$

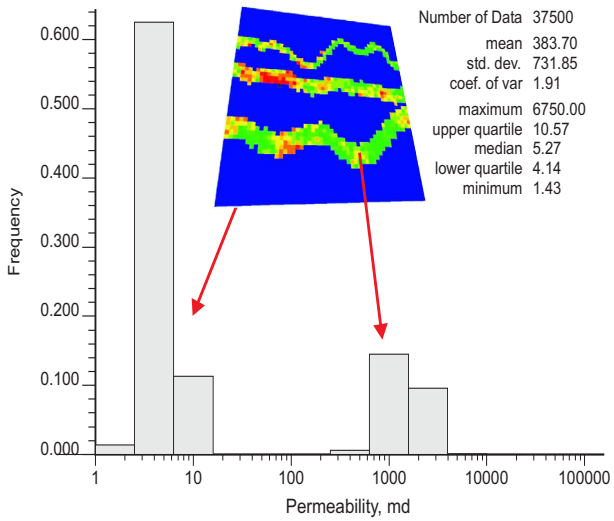

Figure 2.23: Case 3 - Histogram of the Horizontal Permeability

inches for the mainbore and $4\frac{1}{2}$ inches for the laterals).

2.8.4 Case 4 - Multiple Wells in a Fluvial Reservoir

In this example a single realization of the channel reservoir considered in the previous case is used. The model is a two phase oil-water system. The reservoir and rock properties for this model are given in **Table 2.13**.

The objective function is to maximize NPV by determining the optimum number of producers (up to 3 wells) and whether to deploy a water injector or not. The wells can have a maximum of 3 junctions. In this case we are optimizing the number of wells and their type, location and trajectory. The production rate was also considered as a decision parameter during the optimizations. A decimal alphabet was used during the construction of chromosomes. The cost of milling a junction was set to be $100,000 and a barrel of oil was assumed to bring a net profit of $20. The water handling cost was set to $1/bbl.

We used a population size of 80 for this case. The solution was obtained in 977 simulations. The progress of the optimization process is presented in **Fig. 2.26**. The best development plans at various generations are shown in **Fig. 2.27**. The black lines on this plot show the producers and the blue line shows the injector. The wells are not necessarily horizontal or located on the layers as shown. They are drawn on the top layer to give a clearer view. It

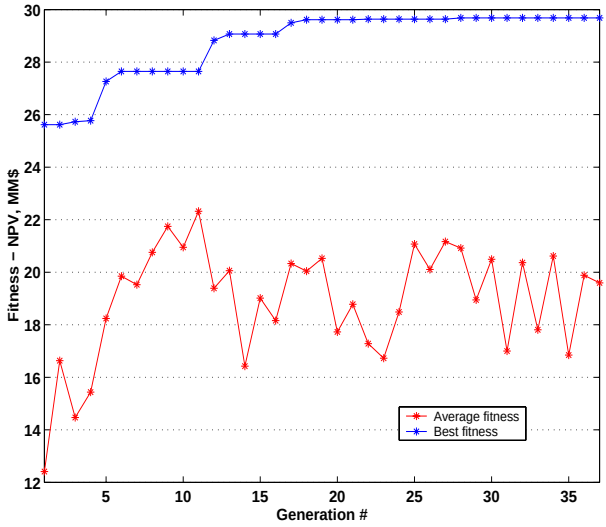

Figure 2.24: Case 3 - Progress of the Optimization

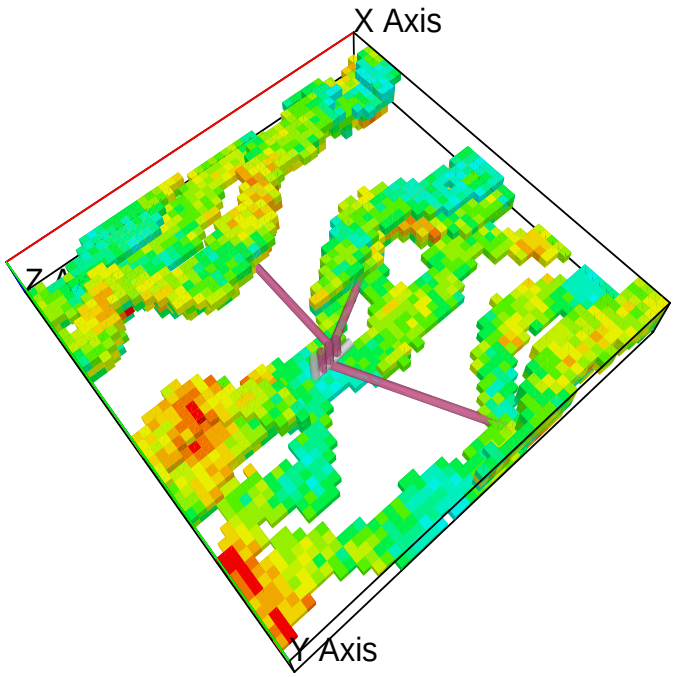

Figure 2.25: Case 3 - Optimum Well for Single Realization (Tri-Lateral)

Table 2.13: Case 4 - Reservoir and Rock Properties

drainage area	25000 $\times$ 25000 ft^2
pay thickness	50 ft
ϕ	0.12
c	3.0$\times 10^{-5}$ psi^{-1} at 5000 psi
k_{ro}	0.8 at $S_{wc} = 0.2$
k_{rw}	0.4 at $S_{or} = 0.3$
k_v/k_h	0.1

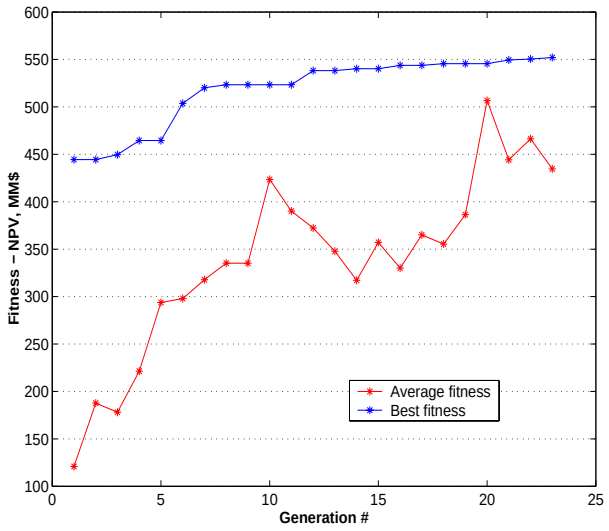

Figure 2.26: Case 4 - Progress of the Optimization

is worth noting how effectively the optimization procedure considers different well types. For example, in the first generation there are no injectors. Two producers exist, with one being a dual-lateral. In the consecutive generations an injector and three producers have been placed (one of them is a vertical well at Generation 4). The optimized development plan (Generation 23) involves three producers and a water injector, all monobore wells.

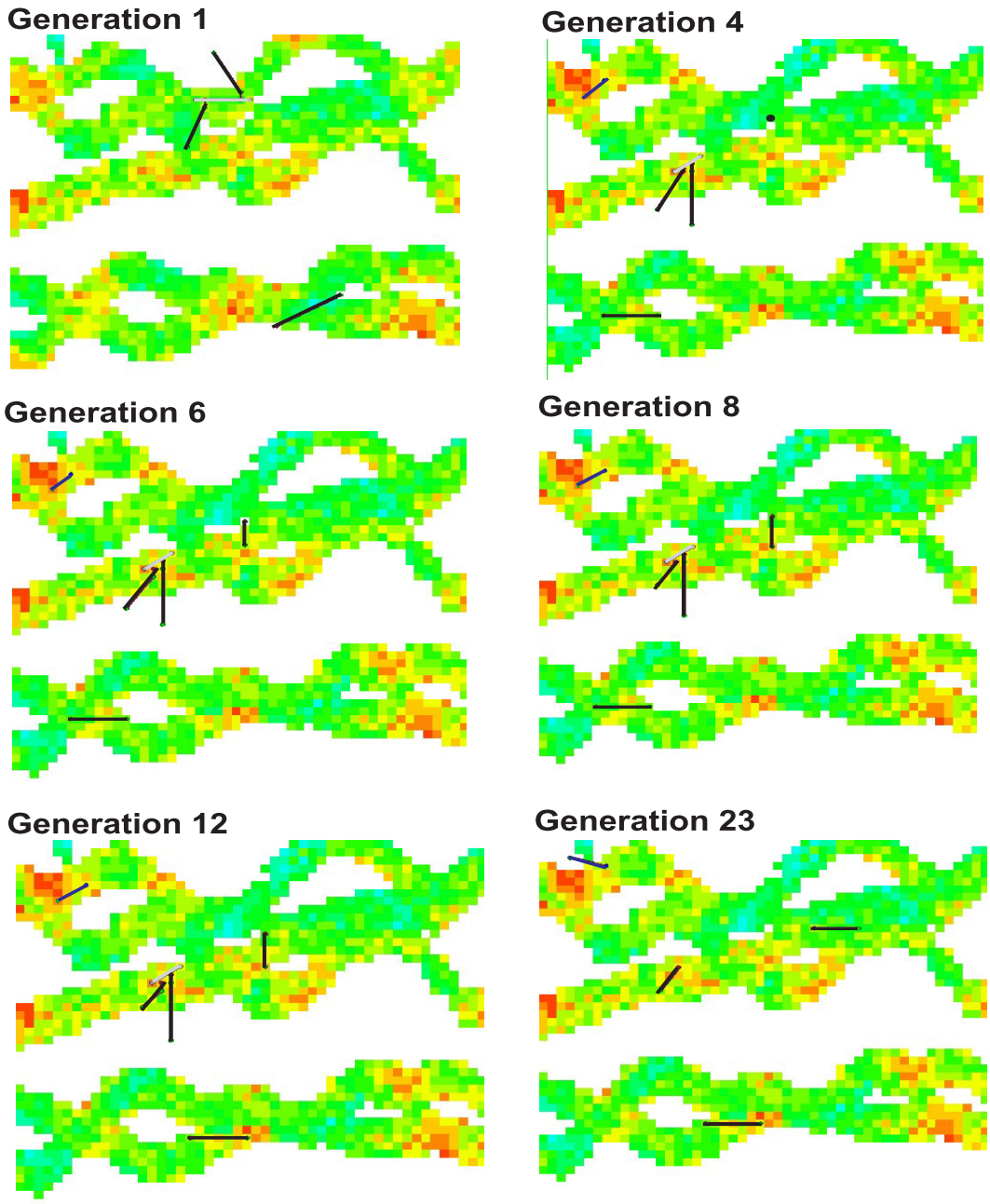

Figure 2.27: Case 4 - Best Development Plans at Various Generations

2.9 Assessment of Single Source of Uncertainty

Due to our inadequate knowledge of the subsurface, no reservoir description is certain. As discussed previously, this is one of the key reasons behind the disappointing performance of some nonconventional wells. These uncertainties must be quantified or resolved so that development decisions can be made. The uncertainty that we will consider might be related to any geological and/or reservoir parameters:

1. Rock properties; porosity, permeability.

2. Total pore volume; thickness, net-to-gross ratio (NTG), structure.

3. Boundaries; strength of the aquifer, compressibility of the gas cap.

4. Faults; number, location and connectivity.

5. Rock-fluid properties; relative permeability curves, residual saturations.

6. Gas-oil, water-oil contact depths.

The above list can easily be extended to account for uncertainties in other engineering and geological parameters that affect the reservoir performance.

2.9.1 Formulation

Our goal here is to optimize the well type, location and trajectory for a reservoir of uncertain geological description. There are several ways to approach this problem. One approach, shown in **Fig. 2.28**, depicts the following methodology: Whenever an individual is considered within a population, the development plan it represents will be applied to all the available realizations. That is, this development plan will be evaluated on each realization by performing a reservoir simulation. Once all simulations for an individual have been completed, the corresponding fitness can be set to the expected value of the outcomes (simulation results); i.e., the average over all realizations.

Assume we are trying to determine a development plan that maximizes a simulation output, f. We define f_{ij} as the value of this quantity for individual i in realization j. The

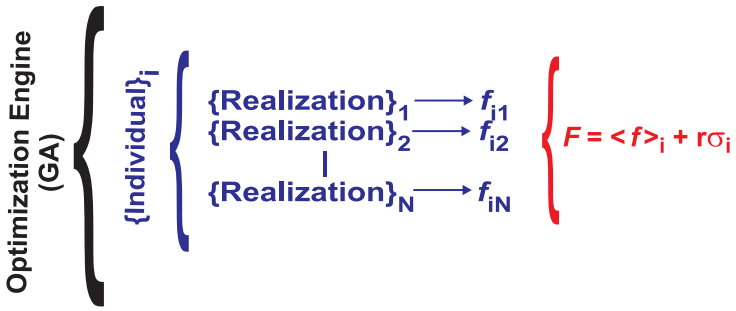

Figure 2.28: Assessment of Uncertainty during Well Type, Location and Trajectory Optimization

expected fitness value for individual i is as follows:

$$\langle f \rangle_i = \frac{\sum_{j=1}^{n} (f)_{ij}}{n}, \tag{2.22}$$

where n is the number of realizations. We can also calculate the standard deviation σ of the outcomes of f_{ij} via:

$$\sigma_i = \sqrt{\frac{1}{n} \sum_{j=1}^{n} (f_{ij} - \langle f \rangle_i)}. \tag{2.23}$$

The standard deviation is used here to quantify the uncertainty. By using this information we can define risk attitudes. The fitness function for individual i is now defined as

$$F_i = \langle \mathbf{f} \rangle_i + r \cdot \sigma_i, \tag{2.24}$$

where r is the risk attitude such that a positive r indicates a risk prone attitude (risk seeker), while a negative r indicates a risk averse nature (a decision making process that seeks to minimize risk). The case of $r = 0$ indicates risk neutrality (a decision maker that only relies on the expected value of the outcomes). The objective function can also be computed by introducing utility functions (Paté-Cornell, 1996) (or so called u-curves (Howard, 1998)) as shown by Guyaguler and Horne (2001). Eq. 2.24 can be replaced by any utility function that a decision maker can supply.

Application - Optimum Well with Multiple Permeability Realizations

This example is the extension of Case 3, described in Section 2.8.3. We now perform the optimization using all ten realizations. The goal now is to include the effects of reservoir uncertainty and to maximize the expected NPV with a risk averse attitude. For this purpose we set the risk coefficient, r, to -1. The ANN was trained to estimate Eq. 2.24 directly with the cost function C_d in Eq. 2.10 excluded (this term was evaluated directly). **Fig. 2.29** shows the progress of the optimization. The optimum well is a quad-lateral, as shown in **Fig. 2.30** (the reservoir here corresponds to one of the realizations). The optimal well has four laterals emanating from a slightly slanted mainbore; the heel of the well is located in the middle layer. Three of the laterals dip downwards while the fourth lateral is oriented horizontally in the middle layer. The optimum wellbore sizes are again found to be $5\frac{1}{2}$ inches for the mainbore and $4\frac{1}{2}$ inches for the laterals.

It is important to note that the optimum well in this case will not in general correspond to the optimum well for any of the ten realizations considered individually. This is because the optimization considers all ten realizations together. The optimal well can be expected to perform reasonably well for all of the realizations, since poorly performing realizations penalize the objective function F both in the average $\langle f \rangle$ and in σ. This is verified in **Fig. 2.31**, which shows the NPV of the optimal well for each of the ten realizations. These NPVs clearly vary from realization to realization, reflecting the heterogeneity of the reservoir. The standard deviation in NPV for the optimal well is the minimum observed during the entire optimization process. Unlike monobore wells, quad-lateral wells are able to penetrate multiple channels, which results in consistently high NPVs with relatively small variation between realizations. The variation in NPV across realizations with simpler wells (e.g., horizontal) is significantly larger. In fact, many of the monobore and mono-lateral wells that occurred in early generations had negative NPVs, which resulted in their extinction in later generations.

It is also worth noting that the optimized well was a quad-lateral when the risk coefficient, r was set to 0, i.e., a risk neutral attitude. For a risk prone decision maker, with $r = 1$, the optimum well was a tri-lateral. This illustrates that the optimum type of well may depend on the risk attitude.

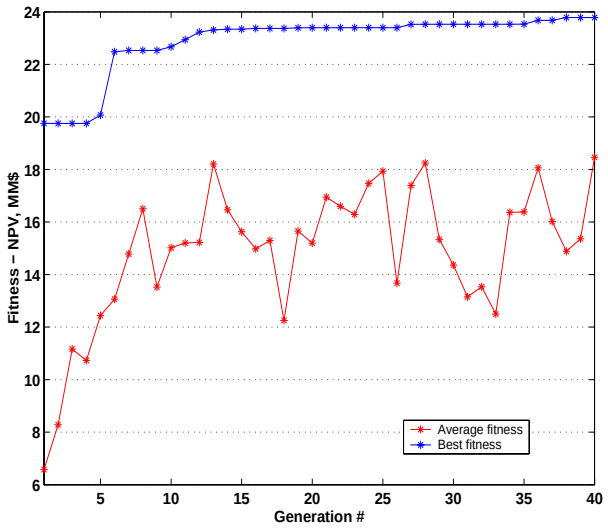

Figure 2.29: Case 3b - Progress of the Optimization

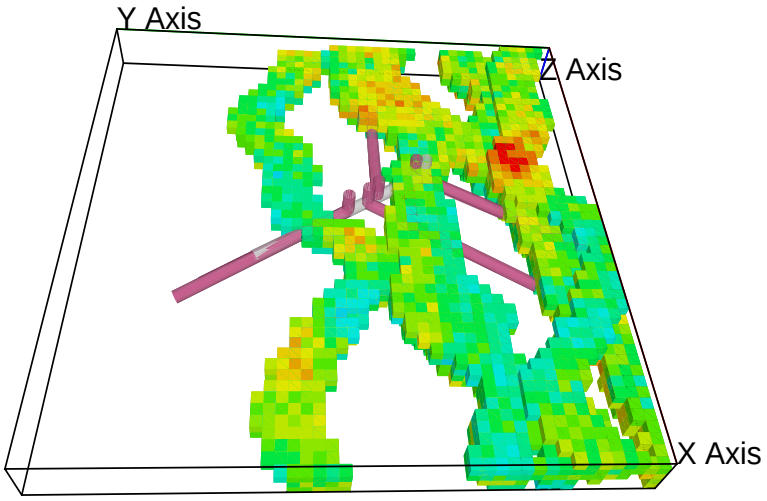

Figure 2.30: Case 3b - Optimum Well for Multiple Realizations (Quad-Lateral)

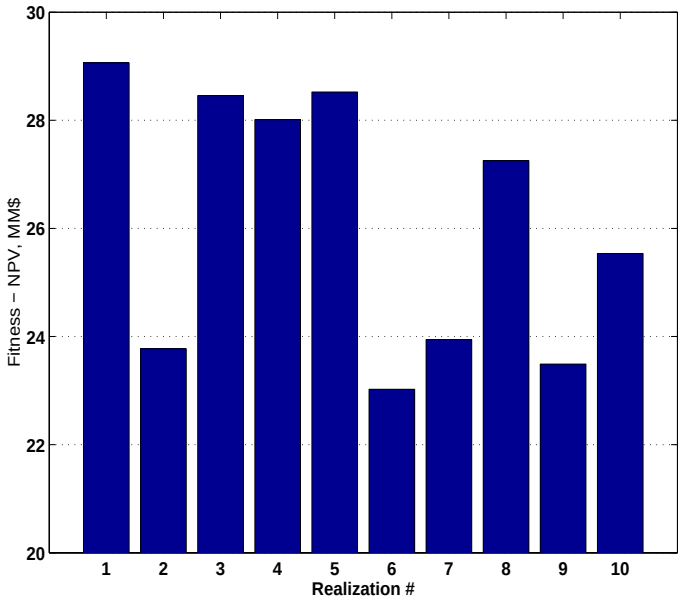

Figure 2.31: Case 3b - Performance of Optimum Well for Each Realization

2.10 Concluding Remarks

In this chapter we presented the development and implementation of an optimization algorithm that maximized the value (either through NPV or cumulative oil production) of a reservoir by determining the optimum number, type, location and trajectories of NCWs. Hybridization of the main search engine with various helper tools was shown. Sensitivities with respect to GA parameters as well as various levels of use of the helper tools were presented. Uncertainty around reservoir description was accounted for during the optimizations. Several synthetic examples were presented. A brief methodology as well as an example application to assess multiple sources of uncertainty (including geological and engineering parameters) is given in Appendix A.

In the next chapter, we will switch to the smart well control optimization problem, and screen several reservoirs and well types for the deployment of this technology. In Chapter 4, we will apply the full optimization framework to a field problem.

Chapter 3

Well Control Optimization

The smart well technology allows for well control optimization via the use of downhole flow control devices (valves) and flow and pressure sensors. With these tools it becomes possible to control or mitigate the detrimental effects of adverse reservoir conditions and or wellbore hydraulics on the performance of a well. Therefore it is appropriate to optimize well performance within the context of smart well technology.

Well control optimization, in this study, can be understood as the implementation of an optimum operating strategy for a smart well. A typical smart well with control and monitoring devices divides the wellbore into a number of independent branches or segments. **Figs. 3.1** and **3.2** present sketches of a smart horizontal well and a multilateral well with three downhole control devices. The main objective is to develop a production schedule and corresponding control settings that will maximize the output of the reservoir or optimize the operation with respect to some other criterion.

We choose ECLIPSE (GeoQuest, 2001a) as our objective function evaluator for our optimization algorithm. Specific features of ECLIPSE that make it suitable for our purposes will be presented in the following sections. The Multi-Segment Wells Option of ECLIPSE allows us to model smart completions. Therefore it will be useful to give a brief description of this option. More detailed information can be found elsewhere (Holmes *et al.*, 1998; GeoQuest, 2001b).

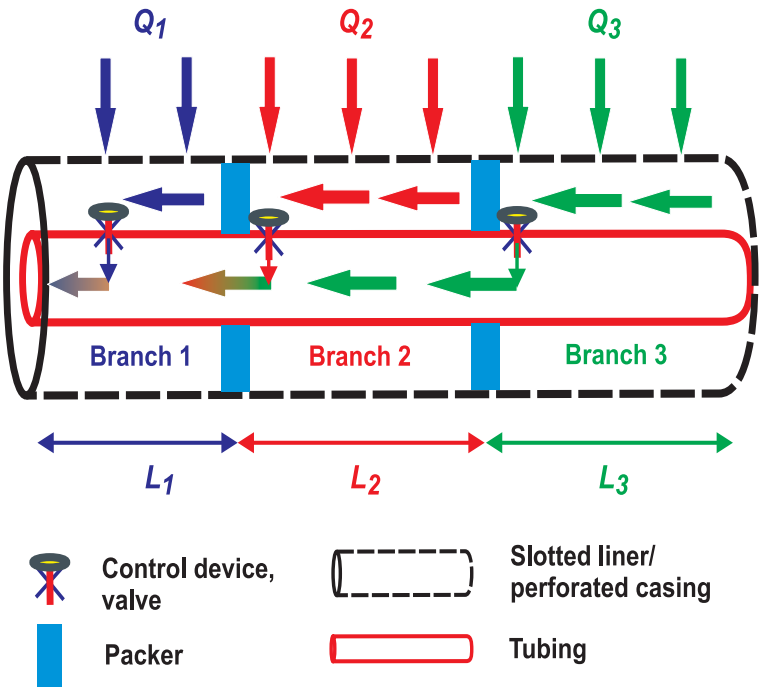

Figure 3.1: An Example Completion of a Horizontal Smart Well

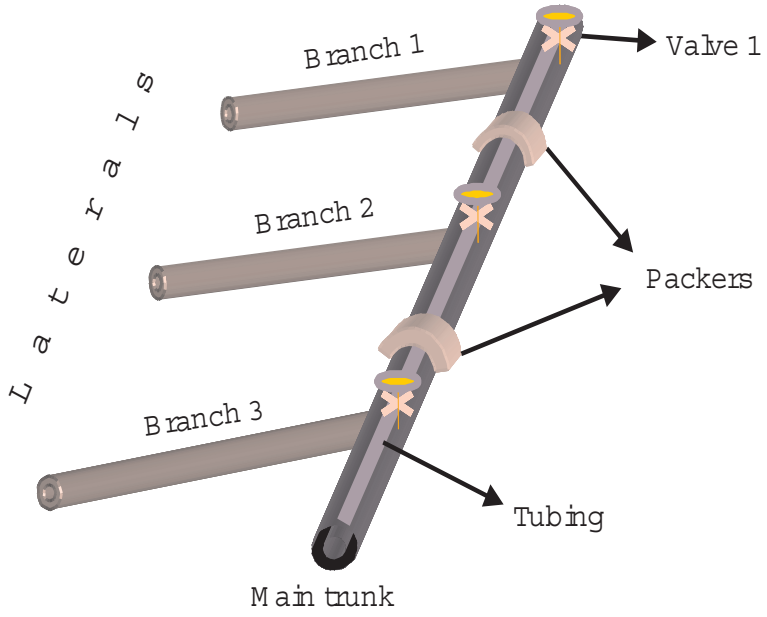

Figure 3.2: An Example Completion of a Multilateral Smart Well

3.1 Multi-Segment Wells

ECLIPSE (GeoQuest, 2001a) models wellbore flow via a fully implicit, strongly coupled well model in which the wellbore is divided into segments (Holmes *et al.*, 1998; GeoQuest, 2001a). This Multi-Segment Wells Option uses the drift flux model for the representation of multiphase flow in the wellbore, which enables the phases to flow with different velocities in the well.

A multi-segment well can be considered as a collection of segments arranged in a gathering tree topology. A monobore well consists of a series of segments arranged in sequence along the wellbore. A multilateral well is comprised of a series of segments along its mainbore, and each lateral branch consists of a series of one or more segments, which connect at one end to a segment of the main stem. It is also possible for lateral branches to have sub-branches, which allows for the modelling of inflow control devices as part of network segments. Each segment consists of a node and a flow path to the node of its parent segment. A node of a segment is positioned at the end that is furthest away from the wellhead as shown in **Fig. 3.3**. Each node lies at a specified depth, and has a nodal pressure, which is determined by the well model calculation. Each segment has a specific length, diameter, roughness, area and volume. The volume is used for wellbore storage calculations, while the other attributes are used in the friction and acceleration pressure loss calculations. Also associated with the flow path of each segment are the flow rates of each flowing phase, which are determined by the well model calculation (GeoQuest, 2001b).

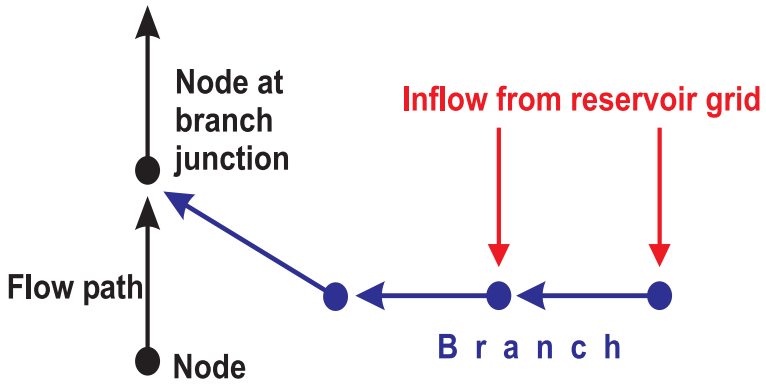

Figure 3.3: A Sketch of Well Segments (GeoQuest, 2001b)

3.2 Methodology

There are several ways of representing the opening or closing of downhole inflow control devices using the multi-segment well model in ECLIPSE. A convenient way of modelling the control devices is to represent the corresponding well segments as a sub-critical valve. This imposes an additional pressure drop in the segment due to flow through a constriction with a specified cross-sectional area. The simulator then calculates the total pressure drop (ΔP_t) across the inflow control device through the use of a model of sub-critical homogeneous flow in a pipe containing a constriction. This pressure drop is given by summing the frictional pressure losses and the pressure losses due to the control device (GeoQuest, 2001a):

$$\Delta P_t = \Delta P_c + \Delta P_f, \tag{3.1}$$

where the effect of the constriction, ΔP_c, is calculated via

$$\Delta P_c = C_u \frac{\rho v_c^2}{2C_v^2}, \tag{3.2}$$

and the pressure loss due to friction, ΔP_f, is calculated by the standard expression for homogeneous flow through a pipe (GeoQuest, 2001a):

$$\Delta P_f = 2C_u f \frac{l}{d} \rho_m v_p^2. \tag{3.3}$$

In the above equations ρ_m represents the density of the fluid mixture in the segment, $C_u = 2.159 \times 10^{-4}$ is a unit conversion factor (all units are given in the Nomenclature), C_v is a dimensionless valve coefficient, v_c and v_p are mixture velocities (flow rate divided by area) through the choke and pipe, respectively, f is the Fanning friction factor, and l and d represent the length and diameter of the pipe segment. The valve setting (i.e., degree of opening) of the inflow control device is specified in terms of the area of the constriction A_c. This area enters Eq. 3.2 via its effect on v_c; i.e., $v_c = q_c/A_c$, where q_c is the flow rate through the constriction.

3.3 Control Strategies

We now introduce two types of control strategies: "reactive" and "defensive" control.

3.3.1 Reactive Control Strategy

Reactive control refers to taking immediate actions via the control devices as the reservoir conditions and type and amount of fluid production change. ECLIPSE allows us to implement such a control strategy without introducing any complicated optimization procedures. Via an ECLIPSE keyword, namely WSEGMULT, within the Multi-Segment Wells Option, additional frictional pressure multipliers on the segments where the control devices are placed can be imposed. Increasing or decreasing these additional frictional pressure drops changes the magnitude of the back pressure and hence lets us model the opening or closing of the device. The additional pressure drop imposed is a function of the amount of water and gas produced through the valve segment and is defined by (GeoQuest, 2001a):

$$P_f^m = \max\left[A + B\left(WOR\right)^C + D\left(\frac{GOR}{GOR_{\min}}\right)^E, 1.0\right], \tag{3.4}$$

where P_f^m in Eq. 3.4 is the frictional multiplier and WOR and GOR are the water-oil and gas-oil ratios at the valve segment. GOR_{min} acts like a scaling factor, since GOR values are usually large in magnitude. The parameters of Eq. 3.4 can be chosen by performing several test runs or can be determined with an optimization algorithm.

Since ECLIPSE sets the control devices via Eq. 3.4, reactive control can be directly used during the optimization of well type, location and trajectory (described in Chapter 2) once the parameters of Eq. 3.4 are defined.

3.3.2 Defensive Control Strategy

Defensive control strategy refers to a kind of control that minimizes the detrimental effects of driving fluids appearing at wells. The detrimental effects can be due to reservoir heterogeneity or pressure drops in the production strings. By determining the optimum settings of the devices at early production times, these effects can be mitigated or avoided. With this strategy it is possible to delay the breakthrough of water or gas and accelerate production

by taking appropriate precautions. The details of the implementation will be discussed in the following section.

Smart wells technology offers continuous monitoring of pressures at appropriate locations. With data acquired from these gauges, it is possible to update the reservoir models as production progresses in time. The defensive control strategy considered here assumes that the reservoir model (and all of its realizations) are fixed during the optimization process. Therefore this methodology might not be appropriate for real world applications, since some uncertainties will be resolved as new data are collected and the model will be updated. This final model is, however, not known to us at the start of the optimization. For this reason, we consider the defensive control strategy as a screening tool which will help to determine if the well is a suitable candidate for smart well technology. The tool developed here is therefore most appropriate for use during the design phase.

3.4 Optimization Algorithm for Defensive Control Strategy

In our optimization, we want to avoid methods that require extensive reformulation of the flow simulator. This is because we wish to use the detailed well modelling and other capabilities implemented in ECLIPSE. Thus, the optimization portion of the overall algorithm must be external to the simulator.

The nature of the problem suggests a gradient based optimization algorithm. A valve can either be incrementally opened or incrementally closed, so there are only two directions in which any valve setting can move. The gradient information basically provides this direction. The current well control optimization engine is built on a nonlinear conjugate gradient (CG) algorithm adapted from Press *et al.* (1999). A brief description of the nonlinear CG is presented below. Further details of this algorithm can be found elsewhere (Reed and Marks II, 1999; Press *et al.*, 1999; Gill *et al.*, 1999; Shewuck, 1994).

Conjugate gradient methods can be used to find the minimum point of a quadratic function. Nonlinear CG methods can be applied to minimize any continuous function $f(\mathbf{x})$ for which the gradient, $\mathbf{f}'$, can be calculated. In a nonlinear CG method, the residual, $\mathbf{r}$, or the direction of steepest descent, is set to the negative of the gradient (Shewuck, 1994):

$$\mathbf{r}^k = -\mathbf{f}'\left(\mathbf{x}^k\right). \tag{3.5}$$

Here is an outline of the nonlinear CG algorithm used in this work (Shewuck, 1994):

$$\begin{aligned}
&\mathbf{d}^0 = \mathbf{r}^0 = -\mathbf{f}'\left(\mathbf{x}^0\right)\\
&\text{Find } \alpha^k \text{ that minimizes } f\left(\mathbf{x}^k + \alpha^k \mathbf{d}^k\right)\\
&\mathbf{x}^{k+1} = \mathbf{x}^k + \alpha^k \mathbf{d}^k\\
&\mathbf{r}^{k+1} = -\mathbf{f}'\left(\mathbf{x}^{k+1}\right)\\
&\mathbf{d}^{k+1} = \mathbf{r}^{k+1} + \beta^{k+1}\mathbf{d}^k\\
&\text{where}\\
&\beta^{k+1} = \max\left\{\frac{\left(\mathbf{r}^{k+1}\right)^T\left(\mathbf{r}^{k+1}-\mathbf{r}^k\right)}{\left(\mathbf{r}^k\right)^T\mathbf{r}^k}, 0\right\}.
\end{aligned} \tag{3.6}$$

In these equations the subscript k indicates the iteration level; $k = 0$ refers to the initial guess. The search directions, $\mathbf{d}^k$, are computed by the Gram-Schmidt conjugation of the residuals. The value of the step size α^k that minimizes $f\left(\mathbf{x}^k + \alpha^k \mathbf{d}^k\right)$ is found by ensuring that the gradient is orthogonal to the search direction. The Gram-Schmidt constant, β^k, is calculated in Eq. 3.6 using the Polak-Ribiérie method. An alternate approach is to use the Fletcher-Reeves method (Shewuck, 1994; Press *et al.*, 1999).

The algorithm is deemed to be converged when the norm of the residual falls below a specified value, which is typically taken to be a small fraction of the initial residual. The convergence criteria can thus be specified as:

$$\left\|\mathbf{r}^k\right\| < \varepsilon \left\|\mathbf{r}^0\right\|, \tag{3.7}$$

where ε is the fractional convergence tolerance, here taken to be 0.01.

Our optimization problem is defined as:

$$\underset{0\le x_i\le 1}{\text{maximize}}\ f\left(\mathbf{x}\right), \tag{3.8}$$

where f is the objective function (e.g., the recovery factor or net present value), $\mathbf{x}$ is the vector that holds the valve settings and x_i is a component of $\mathbf{x}$. These valve settings vary continuously between 0 (valve fully closed) and 1 (valve fully open) and are given by A_c/A_{max}, where A_{max} is the maximum constriction area (valve fully open). The gradient

vector, $\mathbf{f}'$, is calculated numerically using a forward finite difference approximation:

$$\mathbf{f}' = \frac{\partial f}{\partial \mathbf{x}} = \frac{f(\mathbf{x}+h) - f(\mathbf{x})}{h}. \tag{3.9}$$

We use a step size, h, of 0.05 in this study. The $\mathbf{f}'$ computed by Eq. 3.9 can sometimes be a very large positive or negative number. This might cause the next proposed setting to be too large or too small or even negative, which is of course unphysical. To avoid this situation the objective function is also scaled between 0 and 1. If we specify the recovery factor as our objective function there is no need for this scaling, as the recovery factor is already in the range $0 \leq f \leq 1$. When the valve settings approach the upper limit (i.e., $x_i \rightarrow 1$), we replace Eq. 3.9 with a backward difference approximation to avoid the unphysical situation of $x_i + h > 1$.

3.4.1 Implementation

We implement the optimization algorithm such that the performance of the reservoir for a particular set of valve settings can be determined via forward simulations. This is accomplished by dividing the entire simulation period into n optimization steps (these steps are distinct from the simulator time steps). We first optimize the valve settings for the first period ($t = 0$ to $t = t_1$). This optimization is performed such that the settings for this period will be the optimum for the entire simulation. Once this optimization is completed, we proceed to the next optimization period ($t = t_1$ to $t = t_2$) by restarting the simulation from the end of the previous optimized step. This is repeated for each optimization step. Using this approach we ensure that the settings determined for the earlier steps will not have detrimental effects at later times. For example, were we to optimize only over the optimization step and not over the entire simulation period, we might introduce a situation in which valve settings are optimal for $t = 0$ to $t = t_1$ but severe water coning appears for $t = t_1$ to $t = t_2$. Our approach avoids this limitation. It is also worth noting that we assume valve settings to have an infinite resolution, i.e., they can be continuously opened or closed.

For control devices with discrete settings, this optimization algorithm might not be suitable, since the decision parameters are not continuous parameters and gradient evaluation may be difficult. Therefore a discrete parameter optimization engine such as GA might be more appropriate for such cases.

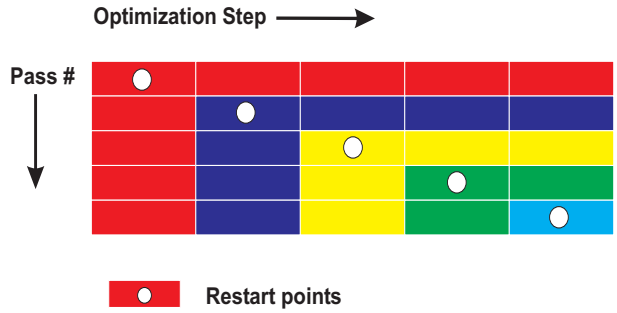

Figure 3.4: Optimization of Valve Settings in Time

The optimization procedure used in this work can be specified as follows:

1. Divide the simulation period into n time periods at which the settings will be updated to optimize the objective function.

2. For each period i, optimize the device settings such that they maximize or minimize the objective function for the remaining simulation period (i.e., solve Eq. 3.8).

3. Restart the simulation from the end of the previous period.

4. Repeat steps 2 and 3 until the entire simulation period is covered.

The overall process is depicted in **Fig. 3.4**. In this figure each color represents an optimized valve setting for the specific time period. The circles on this figure represent the restart points which coincide with the end of an optimization period. The optimization process clearly becomes more computationally expensive as more periods are considered. For the cases presented below, $O(100)$ simulations were required for the optimizations. The exact number of simulations is quite case specific, and could be reduced through the use of proxy functions such as artificial neural networks and response surfaces, though this was not investigated here.

We note finally that several variants of this procedure could be implemented. The method cannot be expected to achieve the global maximum or minimum unless multiple passes of the algorithm are introduced. This is because settings at the early periods are optimized under the assumption that they will persist for the remainder of the simulation, which is not the case. This is probably not a significant concern in practice, however, as the valve settings at early times have the most impact on oil recovery. This in turn suggests

that the optimal settings at early times are not substantially affected by changes at later times. There may be cases, however, for which modifications to the above algorithm will be required.

3.4.2 Optimizer and Links to Simulator

The optimizer, as indicated above, drives `ECLIPSE` for objective function evaluations. An interface establishes communication between the optimization routines and the simulator. Although the examples presented here are based on the maximization of the recovery factor and cumulative oil production, different objective functions, such as the net present value of the project, the minimization of water cut or the gas-oil ratio of individual wells, well groups or the entire field can easily be implemented. Multiple valves installed on different wells and their associated production rates/bottomhole pressures or injection rates/injection pressures can also be optimized along with the valve settings.

3.5 Applications on Synthetic Models

In this section we deploy the tools developed in this chapter to screen different reservoirs (by using a defensive control strategy) for deployment of smart well technology.

3.5.1 Case 1: Vertical Injection and Production Wells

In this case we consider a quarter of a five-spot pattern and a layer-cake reservoir. We chose this simple case to illustrate the impact of downhole inflow control in a system that does not involve complex well trajectories. There are three 20 ft thick producing units which are separated by 1 ft thick shale barriers. The reservoir dimensions are $3000 \times 3000 \times 62$ ft^3. The porosity was taken to be constant with a value of 0.14. The layers are of homogeneous permeability of 50 md, 250 md and 500 md, from top to bottom. The shale barriers are impermeable. The ratio of the vertical to horizontal permeability in each layer was taken to be 0.1. The displacement is unfavorable, with an endpoint mobility ratio of 6.7. The well completions are shown in **Fig. 3.5**; both of the wells are instrumented with control devices. In this figure the arrows show the valves directing the flow in and out of the wellbore. The valves in a sense transform the simple vertical wells into wells with three branches, with

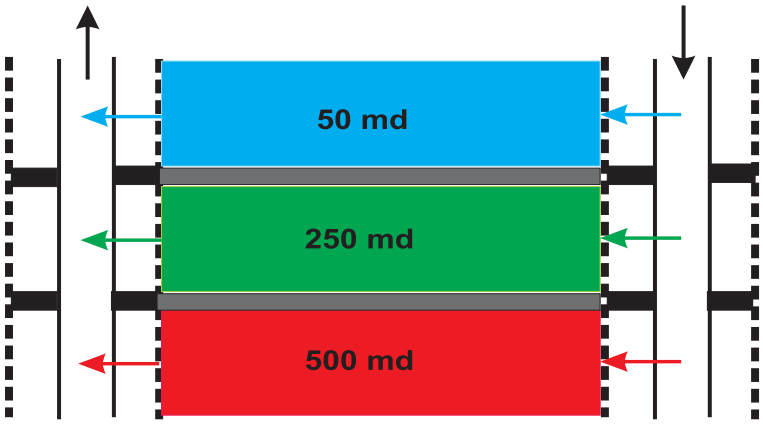

Figure 3.5: Case 1 - Well Completions

each "branch" separated by production packers (solid black rectangles in Fig. 3.5). Each well is completed with 7-inch casing and 3.5-inch tubing in the controlled case; for the uncontrolled case the wells were completed only with 7-inch casing in the pay zone.

Water was injected at a bottomhole pressure target of 6500 psi and subject to the maximum injection rate of 12 MSTB/d. Production was specified to occur at a target bottomhole pressure of 1500 psi, subject to a maximum liquid rate of 6 MSTB/d. In both the controlled and uncontrolled cases, we reduced the current liquid production rate by 40% when the water cut exceeded 70%. A constraint of this magnitude was necessary, since it was impossible to adequately control water production via smaller production cuts or higher water cut thresholds. A minimum oil production rate of 100 STB/d was also imposed as an economic constraint. The simulations were performed for 1200 days. The valve settings were optimized in $n = 10$ optimization periods; i.e., they were updated every 120 days.

We first simulated this case without any instrumentation on either of the wells; this comprises the base case. We then considered three combinations of well instrumentation. The first case (Case 1a) refers to the case where only the producer was instrumented. In Case 1b only the injector was instrumented, while in Case 1c both of the wells were instrumented. The optimization algorithm was applied to Cases 1a, 1b and 1c, with the objective specified to be the maximization of oil recovery. **Table 3.1** compares the cumulative oil produced for each of these cases with the base case. This table shows that it is the optimum allocation of water injection to each layer that ensures the optimum overall production. Interestingly, when we instrumented both the injection and production wells and optimized their control

Table 3.1: Case 1 - Comparison of Different Instrumentation Strategies

Well Instrumentation	Cumulative Oil Production (MMSTB)	Additional Recovery (%)
None (Base Case)	1.73	0.0
Producer (Case 1a)	2.19	26.6
Injector (Case 1b)	2.40	38.7
Both (Case 1c)	2.33	34.7

schedules (Case 1c), we did not achieve a greater recovery than in the case where only the injector was instrumented. The reason for this is that the constrictions on the producer tubing, required for the downhole instrumentation, generated enough of a pressure drop (even when the valves were fully open) to limit production. Because the improvements offered by downhole control of the producer were not enough to offset this effect, the optimal scenario here entailed instrumenting only the injection well.

We now consider the production curves for the base case and Case 1b. **Fig. 3.6** compares the cumulative oil production in time for these two cases. As is evident from the figure, the producer in the base case stopped flowing at about 700 days. This is due to the economic constraint, which was triggered by the rate cuts that resulted from the high water cut. In the optimized case, although the producer was subjected to several rate cuts, the oil production rate remained above the economic limit throughout the simulation. **Fig. 3.7** compares the water cut for both cases. With the optimal injection allocation, breakthrough was delayed by 90 days. Optimization of the device settings improved the recovery for Case 1b by about 39% over the base case.

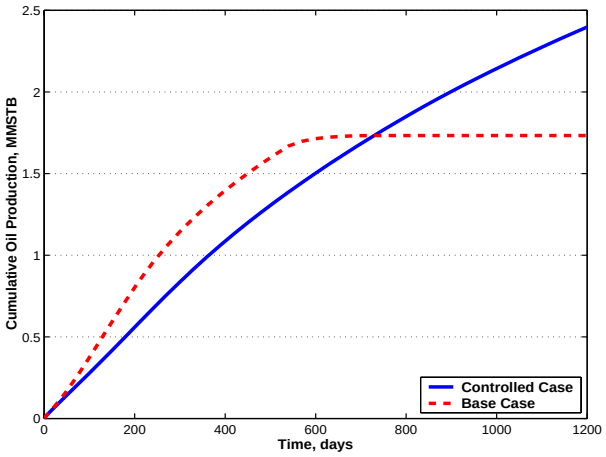

Figure 3.6: Case 1 - Cumulative Oil Production Comparison

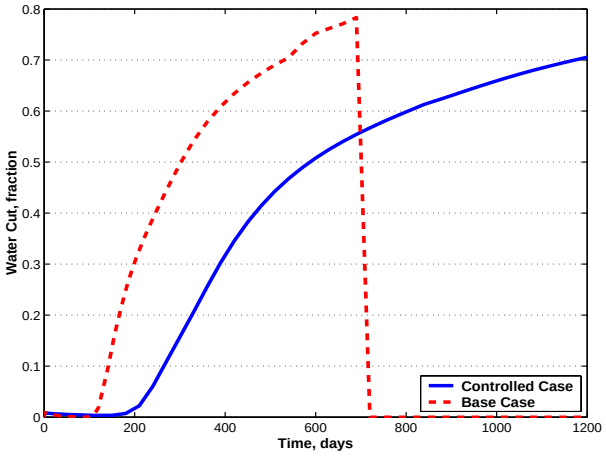

Figure 3.7: Case 1 - Water Cut Comparison

3.5.2 Case 2: Multilateral Well in a Fluvial Reservoir

We now apply our optimization procedure to a more complex problem involving three phase flow in a highly heterogeneous North Sea type fluvial reservoir. The simulation model is three-dimensional ($5000 \times 5000 \times 100$ ft^3) and contains both a gas cap and an aquifer. The model contains $50 \times 50 \times 6$ grid blocks. Other model parameters are given in **Table 3.2**. We generated an unconditional realization of the reservoir description consisting of two facies, channel sand and mudstone, using the `fluvsim` software (Deutsch and Tran, 2002). The permeability within each facies was populated independently and unconditionally by sequential Gaussian simulation (Deutsch and Journel, 1998). The vertical to horizontal permeability was again taken to be 0.1. The top layer of the model represents the gas cap; an analytical aquifer was introduced to maintain pressure support at the bottom of the reservoir.

We introduced a herringbone-pattern multilateral well with four laterals, located to intersect the channels. In order to minimize the interference between branches, the junctions were located equidistant along the mainbore with the laterals alternating in direction, as shown in **Fig. 3.8**. The background in this figure illustrates the permeability distribution, with red indicating high permeability and blue low permeability. The solid white circle in the figure indicates the heel of the well; the solid yellow circles on the mainbore depict the locations of the valves that control each lateral. The well was completed in the fifth layer of the model, 15 ft above the water-oil contact. The mainbore was not perforated. Each lateral is approximately 2150 ft long.

Initial production was specified at a total liquid rate of 10 MSTB/d and the producing GOR was specified not to exceed 5 MSCF/STB. If this GOR constraint was violated, the surface rate of the well was cut back by 10%. There was also a constraint on water production; specifically, the well was shut in when the water cut exceeded 80%. A minimum bottomhole pressure of 1500 psi was imposed for lift considerations, although this BHP was not reached during any of the simulations due to the presence of the gas cap and aquifer. The simulation proceeded for 900 days, with valve settings updated every 180 days ($n = 5$).

We first ran this simulation model with no instrumentation on the well (base case). In the base case the mainbore and laterals were completed as open holes with 7 inch and 5

Table 3.2: Case 2 - Simulation Model Properties

drainage area	5000×5000 ft^2
oil thickness	50 ft
gas cap thickness	50 ft
ϕ	0.20
gas cap PV	0.625 MMft^3
R_s	1.0 MSCF/STB
c at p_{bub}	3.0×10^{-6} psi^{-1}
k_{ro}	0.8 at $S_{wc} = 0.20$
	0.8 at $S_{gr} = 0.05$
k_{rw}	0.4 at $S_{or} = 0.30$
k_{rg}	0.9 at $S_{wc} = 0.20$
γ at 14.7 psi	
oil	0.85
water	1.0
gas	0.71
μ, cp at p_{bub}	
oil	0.42
water	0.30
gas	0.02
B, V/V at p_{bub}	
oil	1.55
water	1.02
gas	0.71

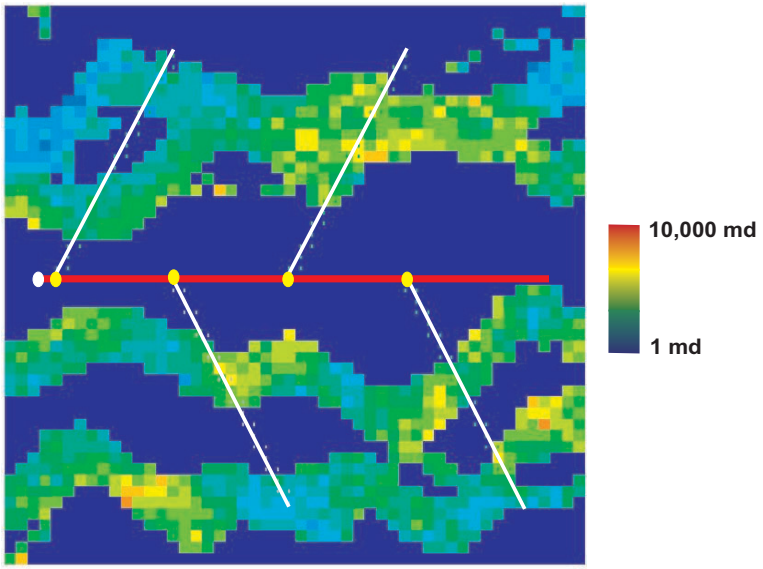

Figure 3.8: Case 2 - Top View of the Multilateral Well Configuration

inch diameters, respectively. The effects of wellbore friction were included in all simulations, with roughness taken to be 4×10^{-2} ft for both the mainbore and laterals. Next, we transformed the multilateral well into a smart well. The mainbore was completed with a 7 inch casing and a 3.5 inch tubing of roughness 4×10^{-4} ft. Lateral completions were the same as in the base case. We introduced four control devices on the tubing of the mainbore, close to each of the junctions, so that each of the laterals could be controlled independently. We then applied our optimization algorithm to maximize the cumulative oil production. We demonstrate the benefits of the control devices and their optimum operation in time through comparisons between the base and instrumented cases.

Figs. 3.9 and **3.10** show the oil production rate for each branch for the base and optimized cases respectively. Note how the highly unbalanced production profile evident in Fig. 3.9 has been effectively redistributed with our optimization algorithm, as shown in Fig. 3.10. In the uncontrolled case the well was shut in at about 600 days because of the water cut constraint. In the instrumented case, as a result of the optimum production allocation, the well produced for all 900 days of the simulation. This resulted in an increase in production of about 47% over the base case. Analogous behavior is observed in the water cut curves, presented in **Figs. 3.11** and **3.12** for the base and optimized cases respectively.

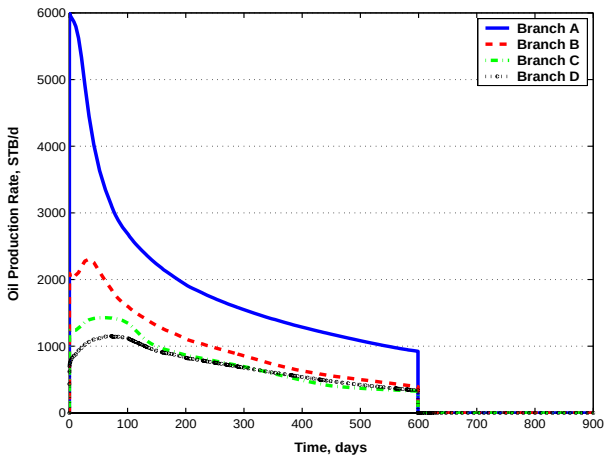

Figure 3.9: Case 2 - Lateral Oil Production Rate, Base Case

The unbalanced production for the base case may be due in part to the pressure drops along the laterals and the mainbore. These pressure drops caused the laterals that are closer to the heel to have lower pressure (and therefore higher drawdown), resulting in the production of more total fluid. The pressure drops along the mainbore and the laterals can be seen from **Fig. 3.13** and **Fig. 3.14** for the base and optimized cases, respectively. The discontinuities in the pressure between the mainbore and the laterals seen in Fig. 3.14 are due to the backpressure created by the valves. These plots show the conditions at 180 days. The pressure drops along the laterals can be seen to be about the same in the optimized case (see Fig 3.13).

The pressure drops across the valves as a function of time are presented in **Fig. 3.15**. These pressure drops are for the most part determined by the valve settings, which are in turn obtained from the optimization algorithm. The sharp changes in the pressure drop, at every 180 days, resulted from changes in the valve settings. The smaller variations are due to the evolving reservoir pressure and fluid compositions. From the figure, we see that the valve near Branch A was always partially closed, resulting in a pressure drop across the valve of over 100 psi. The valve near Branch D, by contrast, was kept almost fully open.

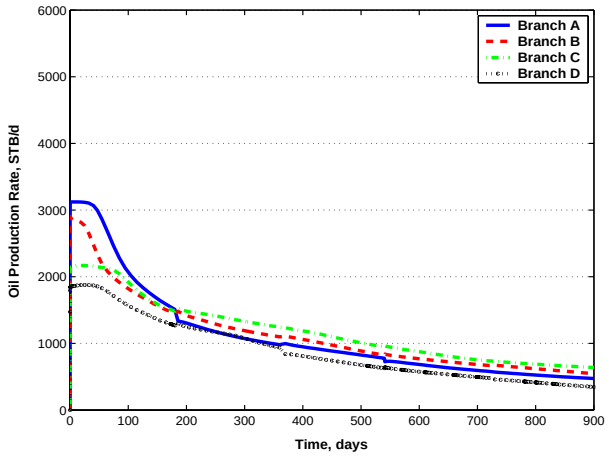

Figure 3.10: Case 2 - Lateral Oil Production Rate, Controlled Case

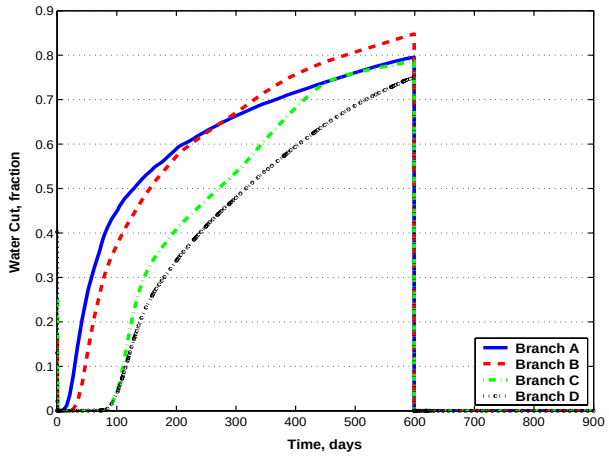

Figure 3.11: Case 2 - Lateral Water Cut, Base Case

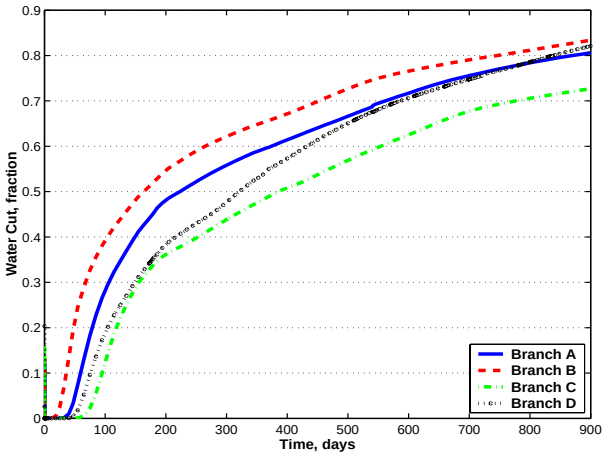

Figure 3.12: Case 2 - Lateral Water Cut, Controlled Case

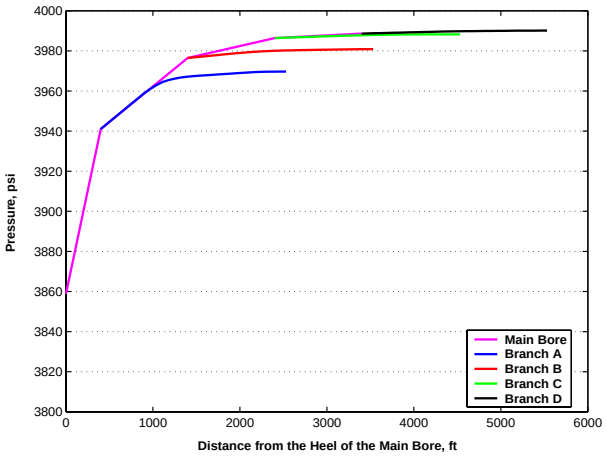

Figure 3.13: Case 2 - Pressure along the Mainbore and Branches, Base Case

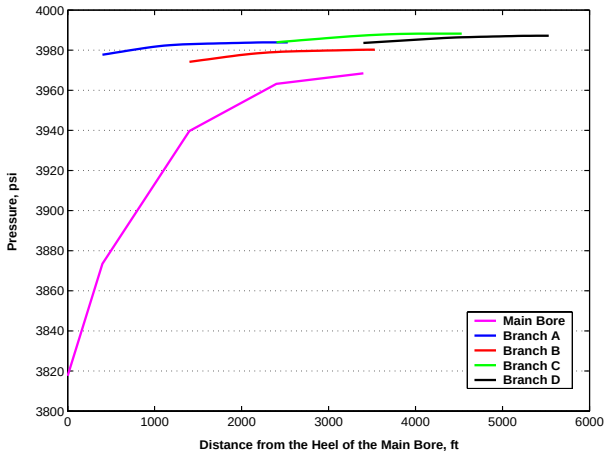

Figure 3.14: Case 2 - Pressure along the Mainbore and Branches, Controlled Case

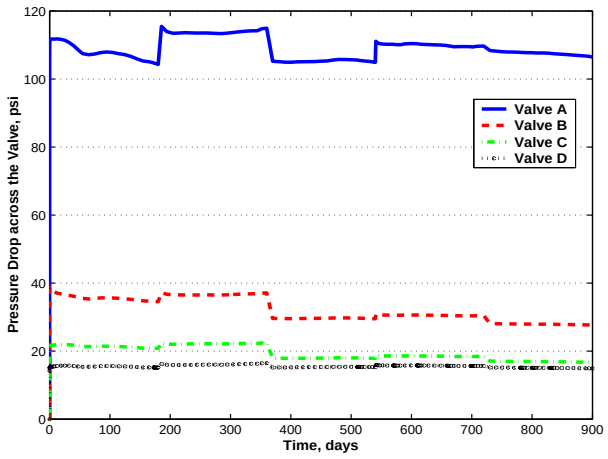

Figure 3.15: Case 2 - Change of Device Settings in Time

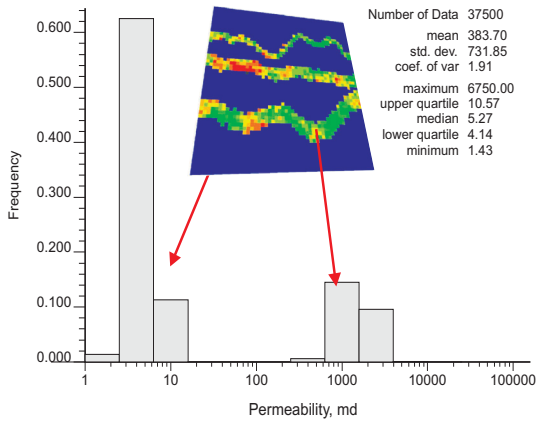

Figure 3.16: Case 3 - Histogram of Horizontal Permeability Distribution

3.6 Assessment of Uncertainty

The methodology implemented to assess the uncertainty around reservoir description is straightforward. We optimize the valve settings for each realization independently and then base our decisions on the outcomes of these optimizations.

3.6.1 Application

We now introduce four additional unconditional realizations of the channelized permeability field considered in Case 2, presented in Section 3.5.2. We use the same simulation model, well and production constraints as used in Case 2. **Fig. 3.16** shows the histogram and global statistics of the five permeability realizations. **Table 3.3** summarizes the statistics of the permeability distribution for each facies. The well location, completion architecture and instrumentation are the same for each of the realizations. **Fig. 3.17** shows the well along with the permeability field for each of the realizations (realization #1 corresponds to Case 2 above). In this example we did not attempt to assess the number of realizations required for reliable statistics. Our purpose here is simply to demonstrate that significant variability in well performance persists even when inflow control devices are applied and to illustrate the fact that instrumentation, in some cases, provides very little improvement in oil recovery.

We again ran the simulation model described above for each of the five realizations with

Table 3.3: Case 3 - Permeability Statistics

Facies	Average (md)	Standard Deviation (md)	Coefficient of Variation
Channel Sand	1534	635	0.4
Mudstone	4.9	1.5	0.3

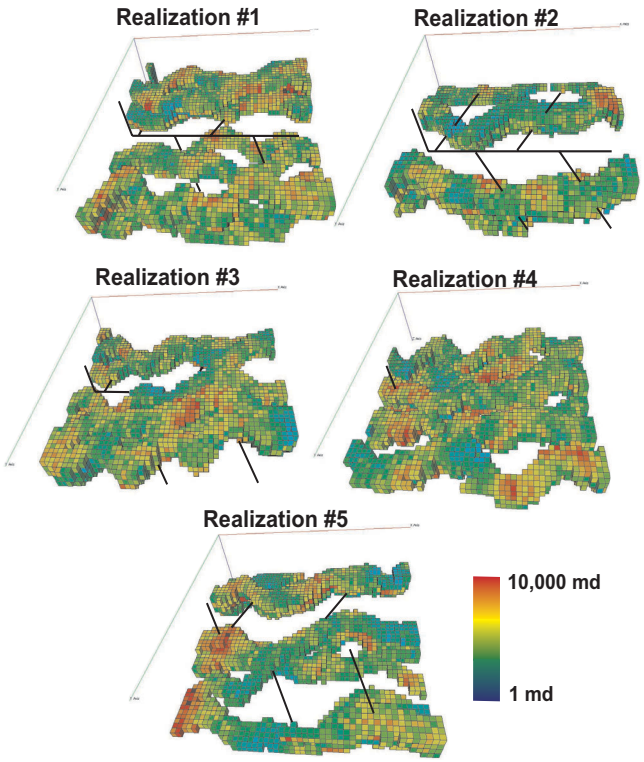

Figure 3.17: Case 3 - Geostatistical Realizations with the Fixed Multilateral Well

Table 3.4: Case 3 - Comparison of Cumulative Oil Production

Realization #	Uncontrolled Base Case (MMSTB)	Instrumented Case (MMSTB)	Additional Recovery %
1	2.61	3.83	46.7
2	2.22	2.26	1.8
3	3.80	4.13	8.7
4	2.59	4.27	64.9
5	2.18	2.48	13.8
Average	2.68	3.40	27.2
Std. Dev.	0.66	0.95	27.2

no well instrumentation. These simulations represent the base cases. Then we optimized the settings for each model to maximize the cumulative oil recovery for that particular realization. **Table 3.4** displays the cumulative production attained at the end of 900 days of simulation for the uncontrolled base cases and the optimized cases. The percentage increase in cumulative oil production due to optimized downhole inflow control (last column) varies from 1.8% to 64.9%. The average increase over the five realizations is 27.2%. This demonstrates the considerable level of improvement in oil production that can be achieved through the use of smart wells and also the considerable variation between realizations.

The variation in cumulative production between realizations, for both uncontrolled and controlled wells, is due to the high degree of geological variation between the realizations. These variations strongly impact the degree of connectivity of the well to the channels and to the gas cap and aquifer. For the realizations in which the well has more interaction with the sand channels but is to some degree isolated from the fluid contacts (realizations #1 and #4), the additional oil production using instrumentation is quite high. For the realization in which the sand channels are directly connected to either the gas cap or aquifer (realization #3), or for the realizations in which the well has less interaction with the channels (realizations #2 and #5), the additional production is lower.

Table 3.4 clearly shows how the uncertainty around the reservoir description could affect the decision on whether or not to instrument a well (it should be noted that in the case

considered here, however, the geostatistical realizations were not conditioned to any reservoir data). For the realizations with low additional recovery the instrumentation would not be economical. For other realizations, however, significant resources might be lost by not deploying the control devices.

In a practical setting, results such as those shown in Table 3.4 might lead one to proceed in several ways. One approach is to consider a number of relevant solution variables and their probability distributions and to introduce a utility function along with a risk aversion coefficient. This would then allow for the application of a decision analysis in the presence of uncertainty. Alternatively, one might attempt to better characterize the reservoir in order to narrow the geological uncertainty. This would require an assessment of the value of the additional geological information.

3.7 Comparison with Optimal Control Theory

In this section, we compare our defensive control strategy with a smart well optimization methodology based on optimal control theory. In this comparison, the optimal control theory solution is considered as the global optimum, and we test our algorithm to gauge how close it gets to this global optimum.

This methodology was developed by Brouwer and Jansen (2002) and Dolle *et al.* (2002). We use an example from Brouwer and Jansen (2002) (referred to as Type I, rate constrained example in Brouwer and Jansen (2002)) and implement the same parameters and essentially the same well configurations as in their example. The common reservoir model we use is a two-dimensional oil-water model discretized with 45×45 grid blocks. A producer is placed on the left flank of the model and a water injector is placed on the right flank. These wells are both horizontal and they fully penetrate the model along the $y-$axis. The background permeability and the wells are shown in **Fig. 3.18**.

During the optimization with the optimal control theory all the well completion blocks are treated as valves, so there are 45 valves on each of the wells. In our defensive control optimization case, only three valves are installed on each of the wells. The oil saturation map and the production profiles attained after each of the optimization methodologies are compared in **Fig. 3.19** and **Fig. 3.20**, respectively. In Fig. 3.20, the dashed lines show the

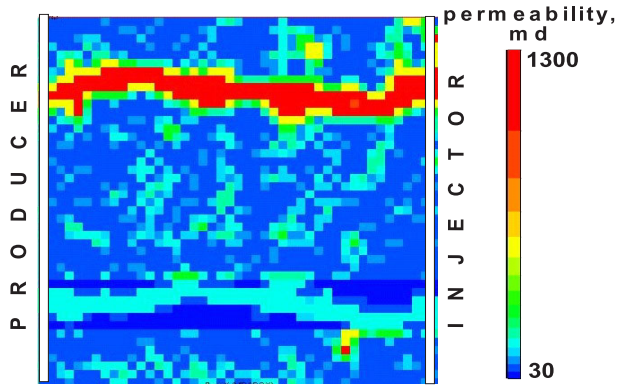

Figure 3.18: Permeability Distribution and Well Locations for Comparison Model (Brouwer and Jansen, 2002)

base cases (i.e., no optimization performed) and the solid lines show the optimized production profiles. The blue, red and black lines represent water, oil and total liquid, respectively. Note that the solution for the optimal control theory methodology is an updated version of what was presented in Brouwer and Jansen (2002). Brouwer (2002) provided this updated solution.

From these figures it can be concluded that there is not much difference in terms of the cumulative oil production, although the swept areas are slightly different. Based on this comparison the following conclusions can be drawn (Brouwer, 2002):

- Improvements obtained are quite similar for the example considered.
- The optimum strategies vary between the two methodologies. This might be due to the number of segments used and the possible existence of multiple solutions to the problem.
- The defensive control strategy is very flexible in terms of being able to handle any kind of well, reservoir type and geometry, since it drives a commercial reservoir simulator. On the other hand, the methodology based on optimal control theory requires its own simulator which restricts its applications.
- The defensive control methodology is more expensive in terms of number of function evaluations (simulations) than the optimal control methodology. Furthermore, the cost of the optimization scales with the number of valves in the defensive control

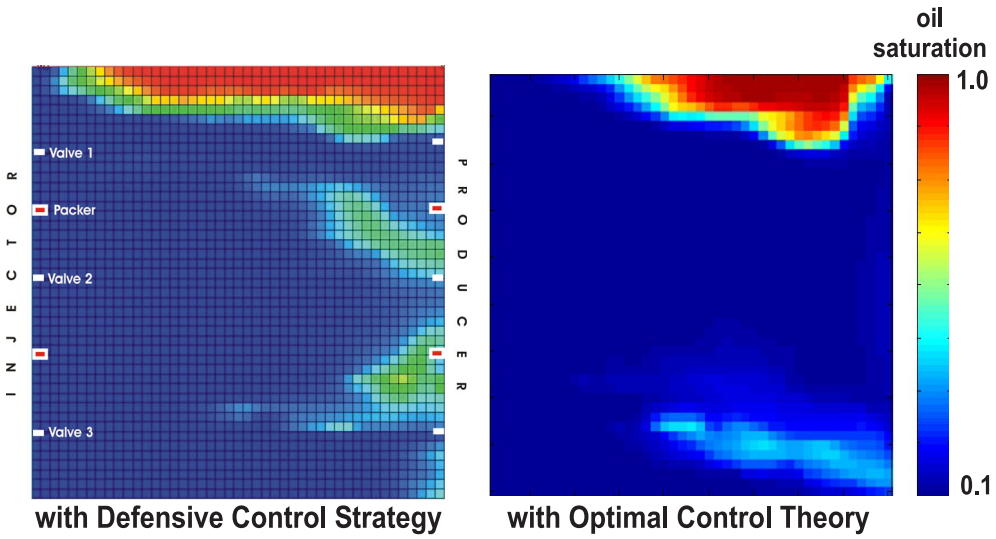

Figure 3.19: Comparison of Final Oil Saturation Maps

optimization, while this is essentially not an issue for the optimal control methodology.

- For both methods there is scope for improvement in efficiency.

3.8 Concluding Remarks

In this section we presented the development and implementation of an optimization algorithm that maximizes the recovery factor by utilizing optimum settings for the control devices in time. The framework presented here applies defensive control strategies, which can be used to screen reservoirs for the deployment of the smart well technology. We showed the possible benefits of this technology for different reservoir and well types. We also accounted for geological uncertainty and showed how the decision making process can be integrated with the field development design process. In the next chapter we will apply both reactive and defensive control strategies to a real field.

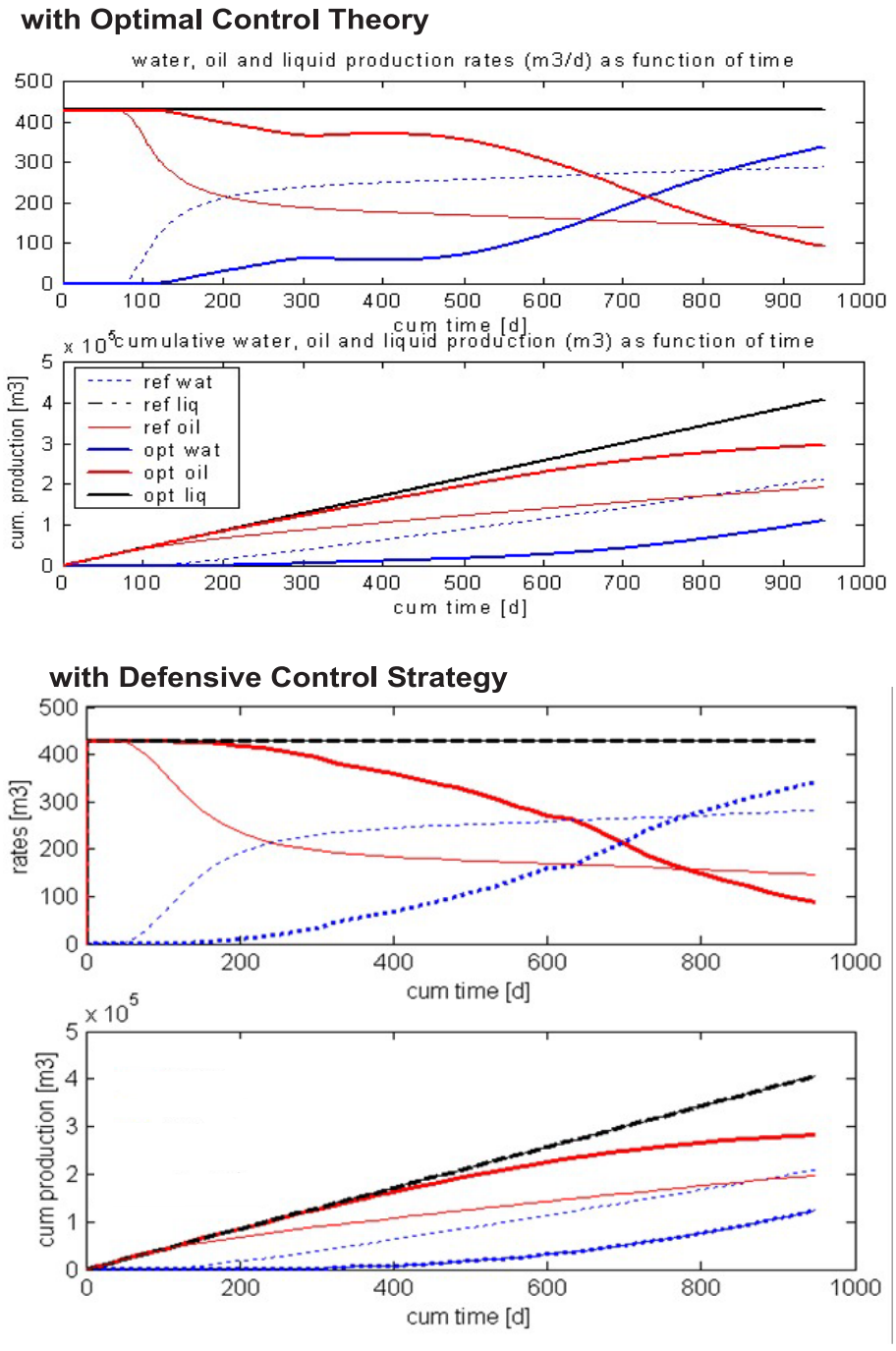

Figure 3.20: Comparison of Final Oil Saturation Maps

Chapter 4

Optimization in a Practical Setting

4.1 Screening for Nonconventional Wells

In this section we will show the benefits of smart completions in a highly heterogeneous reservoir through the use of an optimum defensive control strategy imposed on a tri-lateral well. This system is a conceptual representation of a portion of a huge Saudi oil field. The three-dimensional grid view of the model, populated with the initial oil distribution, is shown in **Fig. 4.1**. The red blocks indicate oil and blue blocks indicate the water, while the blocks in between indicate the transition zone. The reservoir model consists of $25\times33\times10$ cells with grid sizes in the x and y directions of 200 feet. The thickness of each layer varies. Average layer properties are presented in **Table 4.1**. The movable oil originally in place is around 18 MMSTB. The model has an aquifer support along the east flank. The other boundaries were modelled as no-flow.

This field is a naturally fractured carbonate reservoir. Fractures act as the fastest means of transporting fluids within the reservoir. The matrix also has good connectivity and contributes significantly to fluid flow. Two distinct fracture distributions are identified within the field. Here they will be referred to as fractures and stratiform "Super - K" layers. The fractures are explicitly modelled as vertical high permeability zones, oriented along the east-west plane, cutting all layers from the top to bottom. The stratiform Super - K layers are modelled as thin layers with high permeability. **Fig. 4.2** shows how the fractures and the stratiform Super - K layers are oriented. The permeabilities for the vertical and horizontal fractures were set by testing different values. The values that gave the behavior

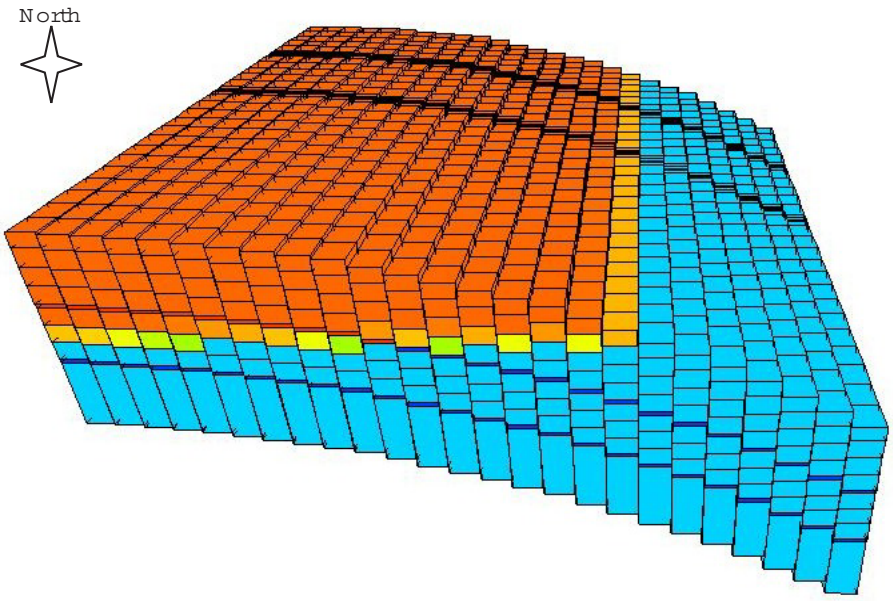

Figure 4.1: 3D View of the Simulation Model

closest to that observed in the field were chosen. Using this approach, permeabilities in the x and y directions were set to 2 and 30 Darcy for horizontal and vertical fractures, respectively. The vertical permeabilities were set to one tenth of these values. A transmissibility multiplier of 50 was also introduced in the x direction for the grid blocks that represent the vertical fractures. The refined grids in the y direction of the simulation model shown in Fig. 4.1 show the location of the fractures. In this model, simulation layers 5 and 9 were defined as the horizontal fractures and grids along $J = 8$ and $J = 18$ were defined as the vertical fracture regions. For the blocks in which horizontal and vertical fractures coincide, the properties of vertical fractures were applied, since these features are believed to belong to a more recent event in the reservoir. The matrix, horizontal and vertical fracture grids were defined as different regions within the simulation model, so that different relative permeability tables can be input. These data are tabulated in **Tables 4.2 - 4.4**.

Because the field is operated above the bubble point pressure, the simulation model only includes oil and water phases. Vertical flow performance tables, which honor some of the observed well performances, were generated and used during the simulations.

Next we proceed with implementing a multilateral well with three branches (tri-lateral) into the model, which is completed in the second layer. All laterals as well as the mainbore

Table 4.1: Properties of Simulation Layers

Layer	Average Horizontal Permeability (md)	Porosity (%)	Thickness (ft)
1	250	14.0	8.0
2	1400	27.0	10.0
3	1600	27.0	10.0
4	1000	23.0	10.0
5	2000	23.0	2.0
6	700	24.0	10.0
7	600	24.0	10.0
8	900	20.0	10.0
9	2000	20.0	2.0
10	600	15.0	38.0

Table 4.2: Rock Curves for Matrix Blocks

Water Saturation	Rel. Permeability to Water	Rel. Permeability to Oil	Capillary Pressure (psi)
0.10	0.0000	1.0000	2.000
0.15	0.0047	0.8948	1.400
0.20	0.0143	0.7936	0.660
0.25	0.0291	0.6965	0.540
0.30	0.0493	0.6037	0.400
0.35	0.0752	0.5154	0.100
0.40	0.1070	0.4320	0.070
0.45	0.1449	0.3536	0.050
0.50	0.1890	0.2806	0.035
0.55	0.2394	0.2134	0.029
0.60	0.2964	0.1527	0.024
0.65	0.3600	0.0992	0.020
0.70	0.4303	0.0540	0.004
0.75	0.5075	0.0191	0.002
0.80	0.5917	0.0000	0.000

Table 4.3: Rock Curves for Stratiform Super - K Layers

Water Saturation	Rel. Permeability to Water	Rel. Permeability to Oil	Capillary Pressure (psi)
0.05	0.0000	1.0000	0.0
0.10	0.0029	0.9178	0.0
0.15	0.0101	0.8381	0.0
0.20	0.0218	0.7607	0.0
0.25	0.0385	0.6859	0.0
0.30	0.0604	0.6138	0.0
0.35	0.0878	0.5443	0.0
0.40	0.1207	0.4777	0.0
0.45	0.1594	0.4141	0.0
0.50	0.2117	0.3536	0.0
0.55	0.2715	0.2963	0.0
0.60	0.3289	0.2425	0.0
0.65	0.3921	0.1925	0.0
0.70	0.4611	0.1464	0.0
0.75	0.5360	0.1048	0.0
0.80	0.6168	0.0680	0.0
0.85	0.7036	0.0370	0.0
0.90	0.7964	0.0131	0.0
0.95	0.8951	0.0000	0.0

Table 4.4: Rock Curves for Fracture Blocks

Water Saturation	Rel. Permeability to Water	Rel. Permeability to Oil	Capillary Pressure (psi)
0.00	0.0000	1.0000	0.0
0.10	0.1105	0.7895	0.0
0.15	0.1743	0.7257	0.0
0.20	0.2443	0.6557	0.0
0.25	0.3210	0.5790	0.0
0.30	0.4050	0.4950	0.0
0.35	0.4967	0.4033	0.0
0.40	0.5967	0.3033	0.0
0.45	0.7057	0.1943	0.0
0.50	0.8244	0.0756	0.0
1.00	1.0000	0.0000	0.0

are horizontal. The completions on the reservoir grid can be seen in **Fig. 4.3**. This trajectory was not optimized with the tools discussed before. The location and the trajectory of the well were intuitively selected, and do not necessarily represent the optimum ones. The heel of the mainbore is highlighted with a full white circle on this plot. The branch closest to the heel of the well will be referred to as Branch A, the one just below it will be referred to as Branch B, and the last one will be referred to as Branch C, as shown in Fig. 4.3. Note that the Branch B intersects a fracture and Branch A is very close to a fracture. Branches A and B are about 2000 ft long and Branch C is about 3000 ft long. The branches are spaced approximately 1400 ft apart from each other, and all have open hole completions. The laterals are fully perforated (no partial perforation) and the mainbore is not perforated.

The simulations were based on a period of 1800 days (~ 5 years). The production target was set to 6 MSTB/d of total liquid, and the constraint was defined as 250 psi tubing head pressure (THP). We first performed the simulations for this well configuration without applying any kind of control offered by the smart well technology. **Fig. 4.4** shows the oil production profiles for individual branches. Note how the 6 MSTB/d production target is distributed among them. The resulting production is unbalanced. Branch A, which is closest to the heel of the well tends to produce more than the other two branches due to pressure losses along the mainbore (accounted for by the multi-segment well model of

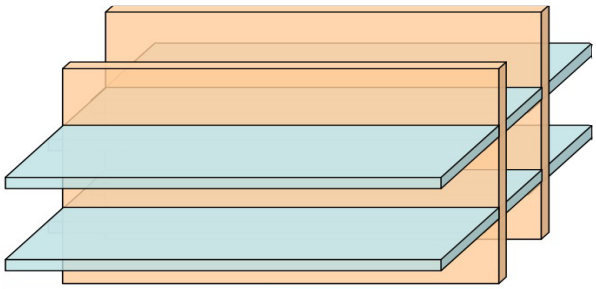

Figure 4.2: Orientation of Fractures on the Simulation Grid

ECLIPSE (GeoQuest, 2001b)). Branch B produces significantly more than Branch C, especially for the early times before the water breaks through, due to its proximity to the heel and its intersection with a fracture. **Fig. 4.5** presents the water cut for each branch. This plot also verifies the conclusions drawn from Fig. 4.4. Branch C does not reach even 10% water cut. The other branches, by contrast experience water earlier and water builds up quickly. This is detrimental to overall well performance.

Fig. 4.6 shows the oil production profiles after optimizing the valve settings with our defensive control optimization tool, described in the previous chapter. We used five optimization steps, each corresponding to 360 days (~ 1 year). Note that now more production is allocated to Branch C than the other branches. It can also be seen that Branch B has been allocated the least amount of production due to its direct connection to a fracture. **Fig. 4.7** shows the water cut profiles of the branches with the optimized valve settings. From Fig. 4.7 we see that water breaks through in Branch C earlier. This water comes from the matrix and it does not increase as quickly as in the other branches. Therefore the breakthrough in Branch C does not affect the overall performance as much as the breakthrough in other branches.

Fig. 4.8 shows the valve closure settings optimized for each year. The increase of the setting number on the y axis means that the valve is further closed. For the first three years (at 0, 360 and 720 days) these settings were optimized and then the settings optimized for the third year (settings at 720 days) were used for the rest of the simulation. This approach is valid because settings optimized for earlier time steps have more effect than the later ones in terms of overall performance. Note that the valve for Branch C was never used during

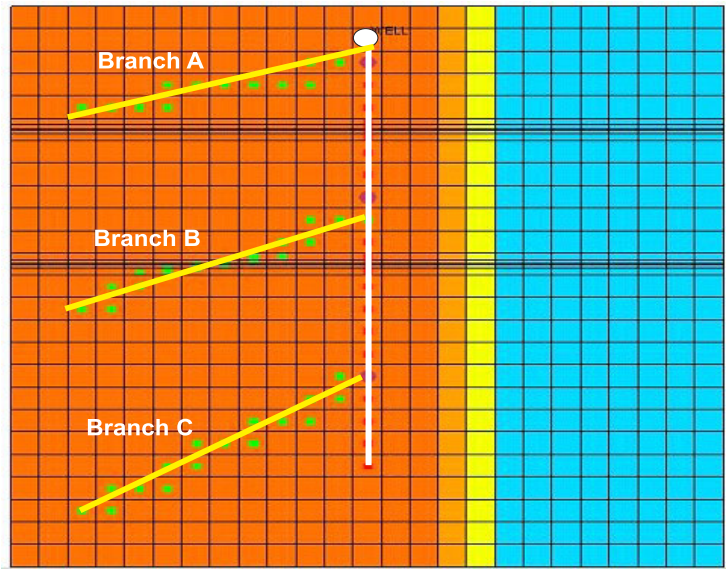

Figure 4.3: Areal View of the Completions of the Tri-lateral Well

the simulation (its setting is always 1, which means that the valve was always kept fully open). So, for this example, two valves were sufficient to achieve the optimum production allocation between the branches.

Fig. 4.9 and **Fig. 4.10** show the comparison of oil production and water cut profiles between the tri-lateral and the smart tri-lateral wells. The area lying between the two production profiles in Fig. 4.9 corresponds to an incremental recovery of about 1 MMSTB ($\sim 16\%$ increase). It is also worth noting that the water cut was reduced by almost 5% at the end of 5 years (see Fig. 4.10). This reduction was as high as nearly 20% during the earlier stages of the run. These plots clearly show how production can be accelerated by applying smart well technology. With time, however, incremental gains tend to decrease.

4.1.1 Comparison with Different Well Types

The benefits attained with the NCWs, both with and without smart completions, over conventional wells will now be addressed. To do this we also consider three vertical wells and a horizontal well. These wells were intuitively located in the reservoir model. The vertical wells were automatically put through workover processes after water breakthrough. The details of the implementation are given in Yeten and Sengul (2001). **Fig. 4.11** presents the

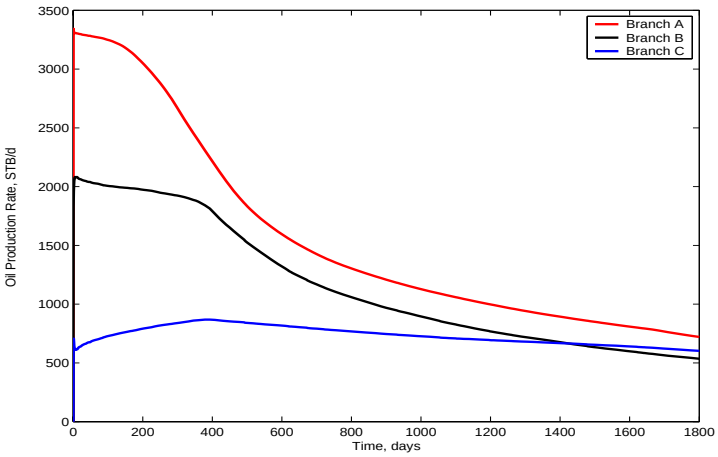

Figure 4.4: Production Profiles of Each Branch without Smart Completions

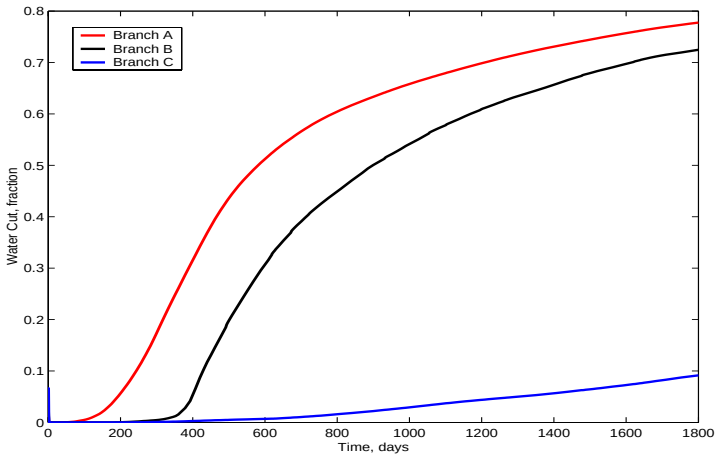

Figure 4.5: Water Cut Profiles of Each Branch without Smart Completions

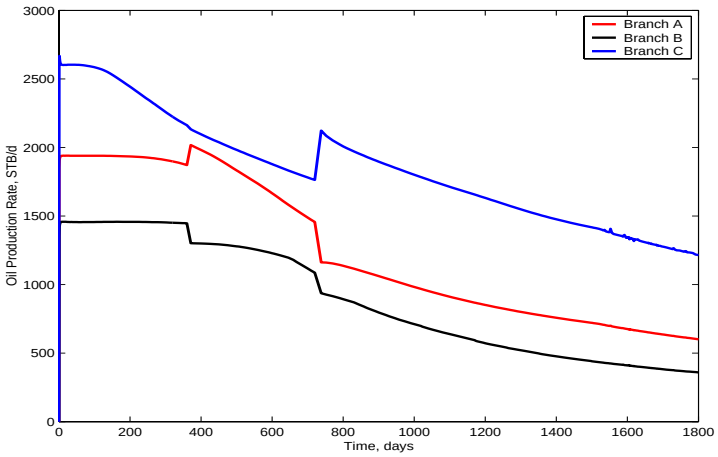

Figure 4.6: Production Profiles of Each Branch with Optimized Valve Controls

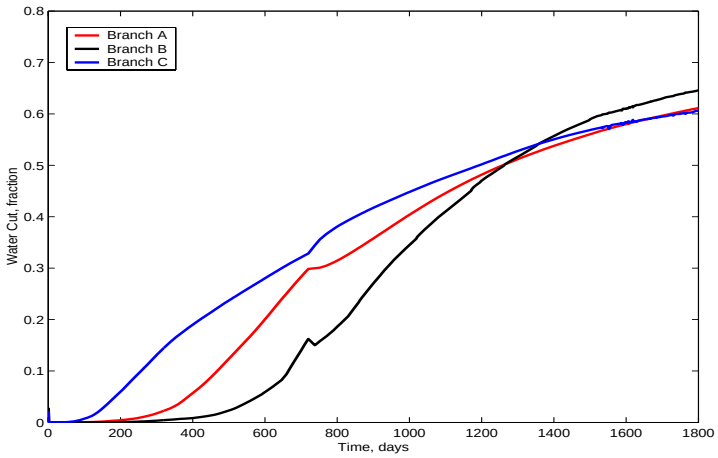

Figure 4.7: Water Cut Profiles of Each Branch with Optimized Valve Controls

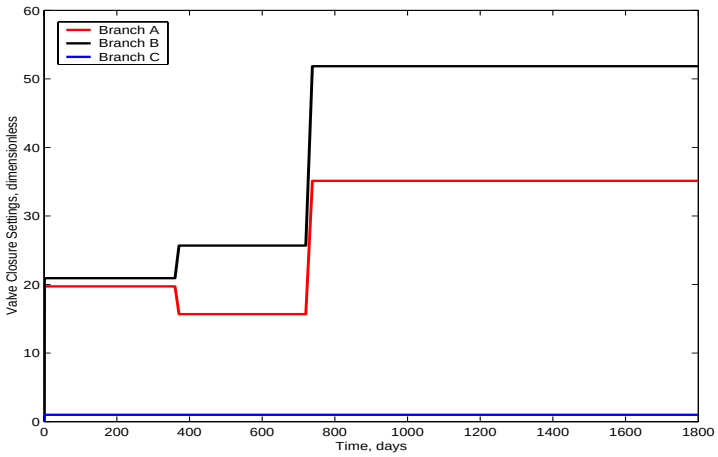

Figure 4.8: Closure Setting Profiles of Each Valve

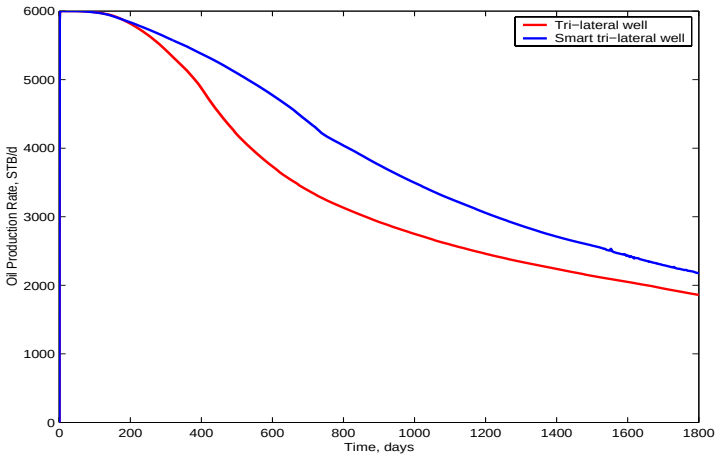

Figure 4.9: Oil Production Profiles for Tri-lateral and Smart Tri-lateral Wells

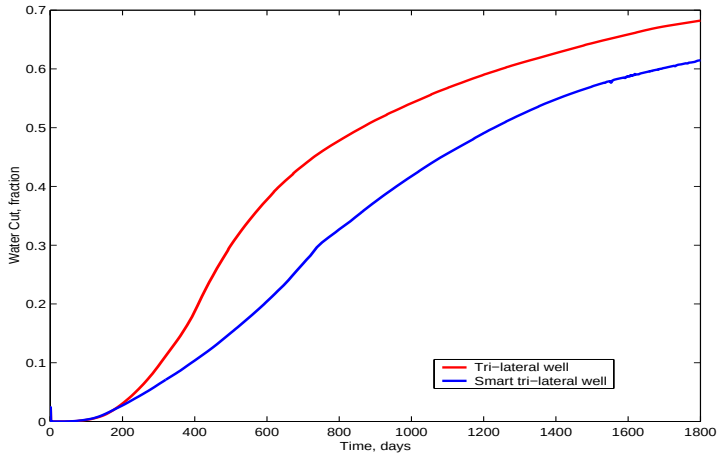

Figure 4.10: Water Cut Profiles for Tri-lateral and Smart Tri-lateral Wells

percentage of additional cumulative oil production attained by other well types over the three vertical wells and horizontal well cases. Fig. 4.11 shows that a horizontal well had 31% additional recovery, and the smart tri-lateral well had a 63% incremental recovery, compared to three vertical wells. An interesting point about the performance of a smart horizontal well for this reservoir is that it does not offer any significant benefits (around 1%) over a standard horizontal well as can be seen from Fig. 4.11. This shows the benefit of screening different options.

4.2 Optimum Nonconventional Well in SA-6 Area

In this section we apply our overall optimization methodology to find the optimum location, type, trajectory and control strategy for a smart well in a sector of a mature Saudi Arabian oil field (referred to here as SA-6). All the results reported here are for this sector model, which was provided by North Uthmaniyah Unit, URMD, Reservoir Management Department of Saudi Aramco.

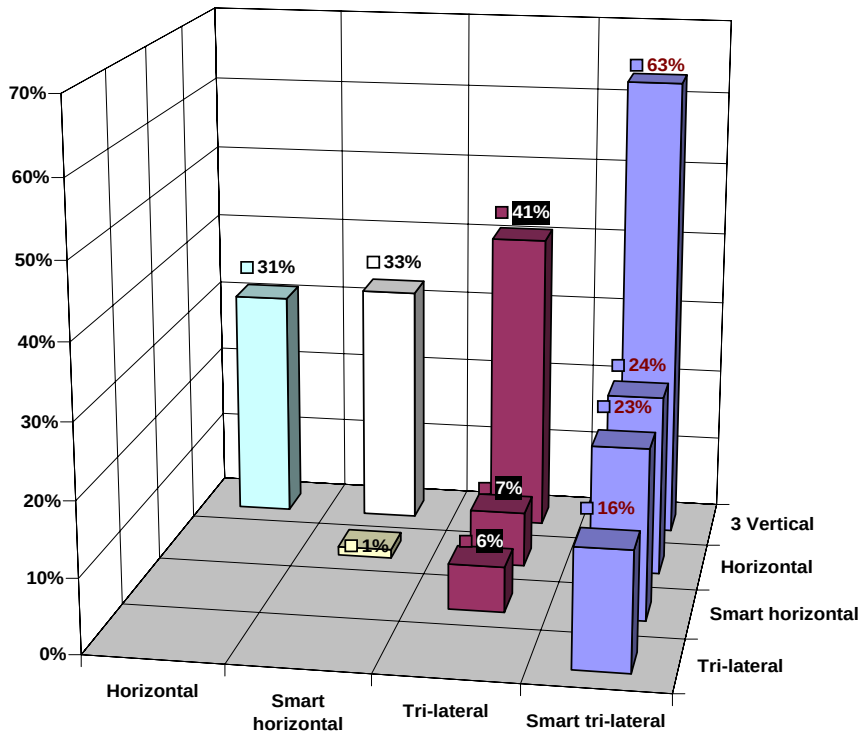

Figure 4.11: Incremental Recoveries Obtained for Various Well and Completion Alternatives

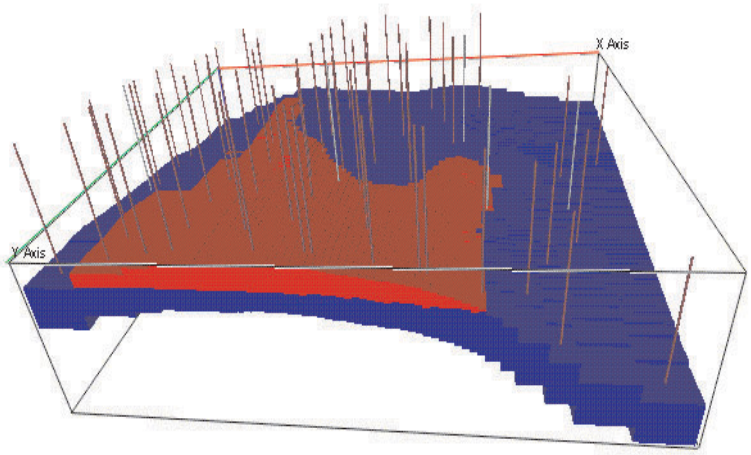

Figure 4.12: Initial Oil Saturation Distribution

Table 4.5: Fluid Properties

Phase	Formation Volume Factor (RB/STB)	Viscosity (cp)	Surface Density (lb/ft^3)	Compressibility (1/psi)
oil at $P = 1000$ psi	1.18805	1.027	53.66	1.16×10^{-5}
water at $P = 5900$ psi	1.02570	0.450	71.82	3.0×10^{-6}

4.3 Simulation Model

The simulation model extends 11.5 km from east to west and 9 km from north to south. This area is discretized with 48 blocks in the x direction and 61 blocks in the y direction. The model has 20 layers. The structure of the model with the oil saturation distribution and existing wells is shown in **Fig. 4.12**. Red indicates oil and water is shown in blue. This model was not history matched, and the initialization was performed explicitly by using the current water oil contact and pressure measurements obtained from the field. The reservoir pressure is known to be above the bubble point pressure and the injection rate is set to maintain pressure throughout the optimization runs. Therefore the simulation model only has oil and water phases. The fluid properties are given in **Table 4.5**. The rock compressibility is set to 2.0×10^{-6} psi^{-1} at a reference pressure of 3227 psi.

All the fractures and stratiform Super - K layers are modelled explicitly by using fine

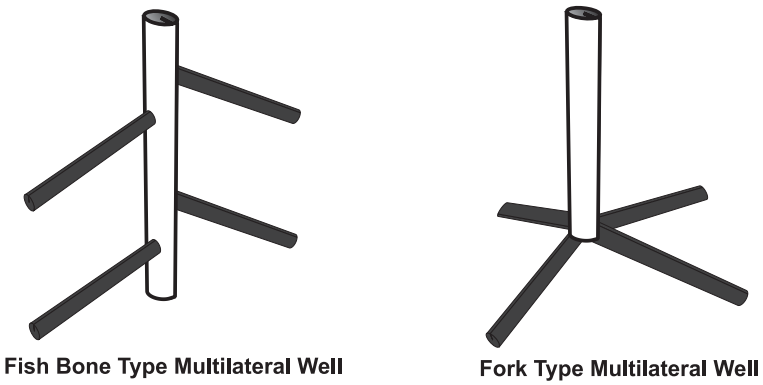

Figure 4.13: Well Templates Used for the Optimizations

grid representations, as was done in Section 4.1. Layers 5 and 13 are designated as stratiform Super - K layers with a constant permeability of 2 Darcy. The fractures are placed in the east-west direction penetrating all the layers vertically. There are three fractures which are located at $J = 11$, 29 and 47, with a constant permeability of 15 Darcy. No additional transmissibility multipliers were used. The relative permeability data for fractures, stratiform Super - K layers and matrix blocks are as in the previous example (Tables 4.2 to 4.4).

4.4 Smart Well Type Location and Trajectory Optimization

In this section we present the application of the previously developed algorithms to find the optimum location and trajectory of a smart well. Two well templates were considered: a fish-bone type and a fork type multi lateral well as shown in **Fig. 4.13**. Note that the well types were specified here rather than determined by the optimizations. This specification was requested by Saudi Aramco for practical reasons.

During our search for the optimum well, we also implemented a reactive control strategy for the laterals of the wells. That is to say, every well considered during the optimization was a smart well, with control devices deployed on each of the laterals to control production. This automatic control procedure was implemented via the `WSEGMULT` keyword of `ECLIPSE` (GeoQuest, 2001a) as described earlier (see Eq. 3.4). The parameters

of Eq. 3.4 were chosen as $A = -1$, $B = 6$ and $C = 2$ (note that the simulation model has only oil and water phases present). These values were determined by a trial-and-error procedure. The well and lateral diameters were fixed as 0.625 ft and 0.4 ft, respectively. The mainbore was not perforated, and therefore acted as a carrier pipe.

The objective function was to maximize the field oil production at the end of 10 years. All other existing wells were specified to produce or inject with their latest available target rates. Therefore by choosing the field oil production as our objective function, we could account for the interference between the smart well and other producers. Existing vertical production wells went through a workover process if their water cut exceeded 95%. The most offending completion and the completions below that were shut automatically during the simulation. The smart well was also subject to the same constraint, but it was not allowed to go through a workover process. Rather, it was completely shut if this constraint was violated. Thanks to the reactive smart well control strategy, this constraint was rarely hit during the optimizations. The smart well was assigned to have a target liquid rate of 25 MSTB/d subject to a 500 psi bottomhole pressure constraint. The mainbore and its laterals were allowed to dip at most ± 40 feet during the optimizations. So, the wells can be considered as almost horizontal.

In order to compare the performance of the optimized well, we ran a case without the smart well in place. This is our base case. We also introduced 4 new vertical wells at grid locations of (32,58), (10,43), (3,58) and (21,60). These locations were selected intuitively. All these wells penetrate layers 1 to 10, and are subject to the automatic workover procedure as applied for other producers in the model (although never triggered). Each well was assigned a daily liquid production of 6250 STB, to match the 25 MSTB/d target of the smart well. This case will be referred to as the Base Case 2, and will allow us to make a fair comparison between the optimized smart well configuration and drilling the new vertical wells. The base case produced 199.4 MMSTB of oil in 10 years, and the Base Case 2 resulted in 234.8 MMSTB of cumulative oil production.

The final oil saturation distribution of Layer 6 (which is chosen arbitrarily) at the end of 10 years of production for Base Case 2 is presented in **Fig. 4.14**. The legend for oil saturation for this and the following similar plots is given in **Fig. 4.15**.

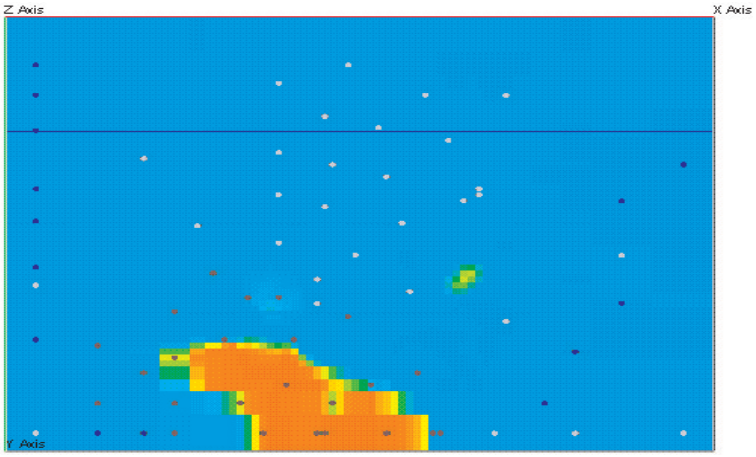

Figure 4.14: Final Oil Saturation Distribution of Layer 6 for Base Case 2

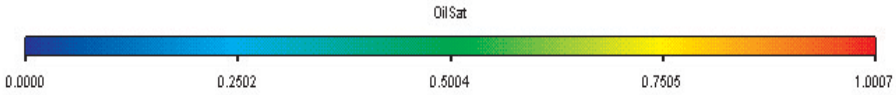

Figure 4.15: Oil Saturation Color Legend

Table 4.6: Fish Bone Type Smart Well Optimizations

Run #	Number of Laterals	Min. Lateral Length, (ft)	Max. Lateral Length, (ft)	Max. Possible Contact Length, (ft)
1	3	5000.0	5500.0	16500.0 (≈ 5030 m)
2	4	5000.0	5500.0	22000.0 (≈ 6705 m)
3	3	5000.0	8000.0	24000.0 (≈ 7315 m)

Table 4.7: Optimum Fish Bone Type Smart Wells

Run #	Optimized Total Contact Length, (ft)	Cumulative Oil Production, (MMSTB)
1	16000 (≈ 4875 m)	252.332
2	21000 (≈ 6400 m)	249.424
3	19000 (≈ 5800 m)	259.780

4.4.1 Optimization Runs - Fish Bone Type Smart Well

We first describe the run matrix for the fish bone type multilateral, which is presented in **Table 4.6**. We consider three different wells varying in length and in the number of junction points. A single lateral is allowed to emanate from a junction in our optimizations ($N_{lat} = 1$). Therefore, the total number of junction points corresponds to the total number of laterals. As can be seen from Table 4.6, the length of each lateral is also defined as a decision variable. The maximum possible length of the well open to flow is listed in the last column of Table 4.6.

The results of optimization with the templates given in Table 4.6 are shown in **Table 4.7**. As can be seen from Table 4.7, for Run #2, although it has the longest contact with the reservoir, the cumulative oil production is less than for the other cases. This is apparently due to interference with other producers and laterals.

The optimized well coordinates (in feet) and their corresponding grid indices are given in **Tables 4.8** to **4.10**. The origin of these coordinates coincides with the origin of the simulation axes (i.e., the upper left corner of the simulation grid).

Note that one of the laterals of the smart well optimized in run #1 intersects a fracture. The comparison of cumulative oil production in time and field water cut are shown in

Table 4.8: Optimized Fish Bone Type Smart Well Coordinates - Run #1

	Heel	Toe
Mainbore	(7381.9, 23170.7, 6053.4) - (3,56,3)	(15378.9, 23170.7, 6050.0) - (16,56,2)
Lateral 1	(10252.6, 23170.7, 6054.1) - (5,56,6)	(14148.6, 26246.5, 6047.6) - (13,60,6)
Lateral 2	(11072.8, 23170.7, 6058.0) - (6,56,6)	(13738.5, 18659.6, 6094.4) - (12,42,3)
Lateral 3	(12918.3, 23170.7, 6052.3) - (10,56,4)	(17429.4, 26246.5, 6053.1) - (21,60,5)

Table 4.9: Optimized Fish Bone Type Smart Well Coordinates - Run #2

	Heel	Toe
Mainbore	(7381.9, 23170.7, 6032.9) - (3,56,1)	(12508.2, 23170.7, 6028.2) - (9,56,2)
Lateral 1	(9022.3, 23170.7, 6028.1) - (4,56,3)	(11688.0, 28297.0, 6028.5) - (7,61,6)
Lateral 2	(10252.6, 23170.7, 6029.5) - (5,56,4)	(14968.8, 20710.1, 6066.2) - (15,50,1)
Lateral 3	(11072.8, 23170.7, 6033.7) - (6,56,4)	(13738.5, 28297.0, 6041.1) - (12,61,7)
Lateral 4	(12098.1, 23170.7, 6024.2) - (8,56,2)	(13328.4, 28297.0, 6024.7) - (11,61,6)

Table 4.10: Optimized Fish Bone Type Smart Well Coordinates - Run #3

	Heel	Toe
Mainbore	(12918.3, 22760.6, 6065.3) - (10,55,5)	(12918.3, 26246.5, 6061.6) - (10,60,7)
Lateral 1	(12918.3, 23580.8, 6068.7) - (10,57,6)	(7381.9, 26246.5, 6066.9) - (3,60,6)
Lateral 2	(12918.3, 24196.0, 6059.3) - (10,58,6)	(19069.8, 26246.5, 6064.2) - (25,60,2)
Lateral 3	(12918.3, 25016.2, 6068.2) - (10,59,7)	(17019.3, 28297.0, 6077.4) - (20,61,8)

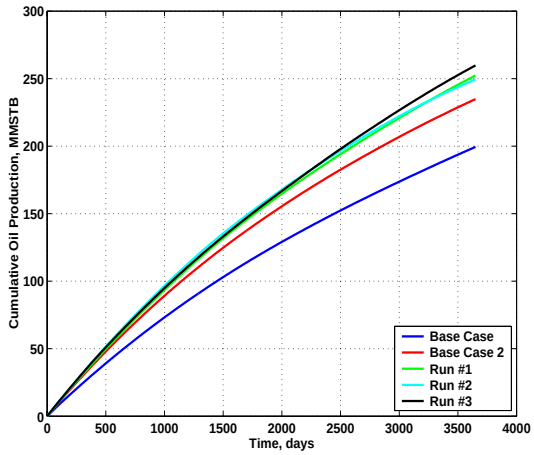

Figure 4.16: Comparison of Cumulative Oil Production for Optimized Fish Bone Type Smart Wells

Fig. 4.16 and **Fig. 4.17**, respectively, for all the optimized smart wells and the base cases described above. The final oil saturation maps of Layer 6 for each of the optimized smart wells are shown in **Fig. 4.18** to **Fig. 4.20**.

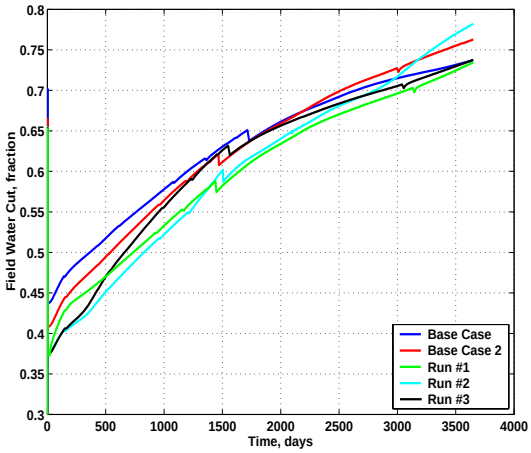

Figure 4.17: Comparison of Field Water Cut for Optimized Fish Bone Type Smart Wells

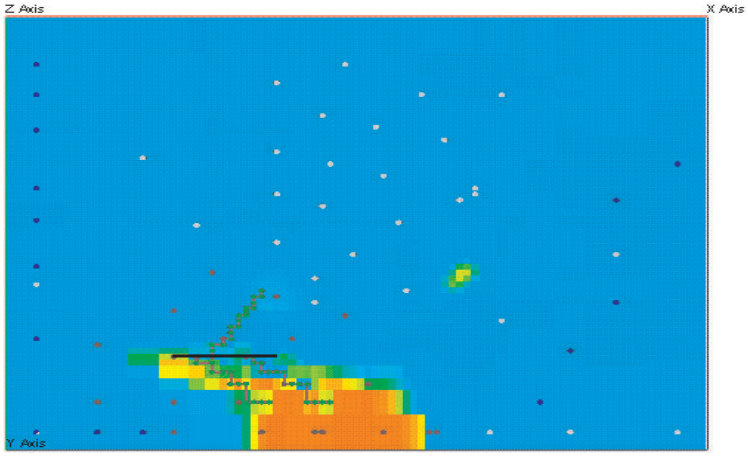

Figure 4.18: Final Oil Saturation Distribution of Layer 6 for Run #1

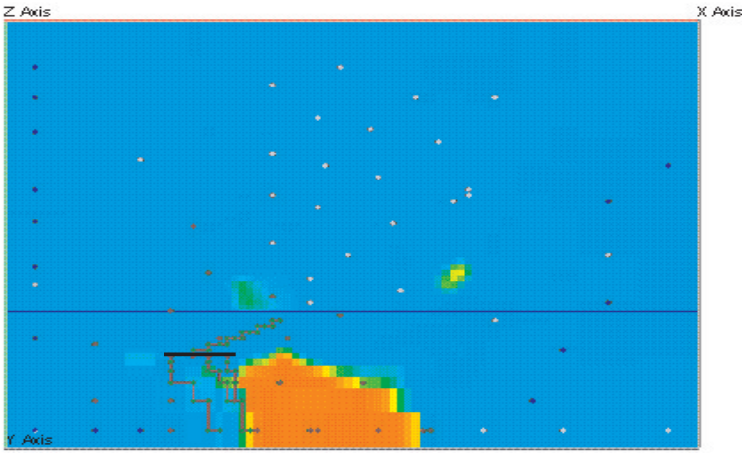

Figure 4.19: Final Oil Saturation Distribution of Layer 6 for Run #2

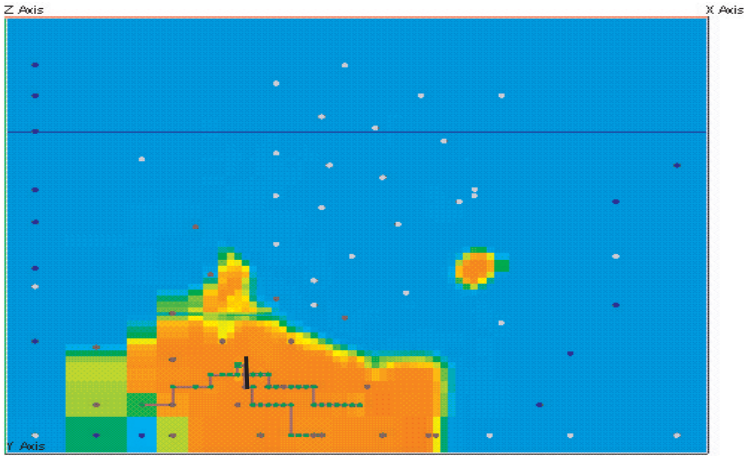

Figure 4.20: Final Oil Saturation Distribution of Layer 6 for Run #3

Table 4.11: Optimum Fork Type Smart Wells

Run #	Optimized Total Contact Length, (ft)	Cumulative Oil Production, (MMSTB)
1	15500 (≈ 4725 m)	259.126
2	21000 (≈ 6400 m)	243.639
3	17250 (≈ 5250 m)	247.626

Table 4.12: Optimized Fork Type Smart Well Coordinates - Run #1

	Heel	Toe
Mainbore	(15378.9, 25016.2, 6057.8) - (16,59,5)	(15378.9, 28297.0, 6058.2) - (16,61,8)
Lateral 1	(15378.9, 26246.5, 6054.7) - (16,60,6)	(15378.9, 21120.2, 6091.4) - (16,51,3)
Lateral 2	(15378.9, 26246.5, 6054.7) - (16,60,6)	(11072.8, 28297.0, 6052.6) - (6,61,7)
Lateral 3	(15378.9, 26246.5, 6054.7) - (16,60,6)	(19890.0, 28297.0, 6053.2) - (27,61,2)

4.4.2 Optimization Runs - Fork Type Smart Well

Now we switch to the fork type smart well template. We again perform three optimizations, and the run matrix is the same as presented in Table 4.6. The only difference is that now the laterals are emanating from the same junction point, instead of distinct junction points as for the fish bone type smart well.

The cumulative oil production attained for the optimum fork type smart wells are shown in **Table 4.11**. Note that one of the laterals of the smart well optimized in Runs #1 and #2 intersects a fracture. The comparison of cumulative oil production and field water cut are shown in **Fig. 4.21** and **Fig. 4.22**, respectively, for all the optimized smart wells and the base cases described before. The final oil saturation maps of Layer 6 for each of the optimized smart wells are shown in **Fig. 4.23** to **Fig. 4.25**.

When we compare the cumulative oil productions of these two well templates, we see that the fish bone type wells usually perform better than the fork type wells (see Tables 4.7 and 4.11), though the differences are slight. This is most probably due to interference between the laterals. As a result of its geometry, laterals of the fork type well have a higher chance of interfering with each other. Another possible reason is the wellbore hydraulics. Fork type wells produce from the same junction, which might result in higher frictional

Table 4.13: Optimized Fork Type Smart Well Coordinates - Run #2

	Heel	Toe
Mainbore	(11688.0, 21940.4, 6036.4) - (7,53,2)	(14558.7, 28297.0, 6038.4) - (14,61,7)
Lateral 1	(11688.0, 22350.5, 6040.6) - (7,54,3)	(17019.3, 22350.5, 6074.6) - (20,54,1)
Lateral 2	(11688.0, 22350.5, 6040.6) - (7,54,3)	(11688.0, 17429.3, 6077.8) - (7,39,3)
Lateral 3	(11688.0, 22350.5, 6040.6) - (7,54,3)	(4921.2, 22350.5, 6077.8) - (2,54,1)
Lateral 4	(11688.0, 22350.5, 6040.6) - (7,54,3)	(11688.0, 28297.0, 6051.7) - (7,61,7)

Table 4.14: Optimized Fork Type Smart Well Coordinates - Run #3

	Heel	Toe
Mainbore	(9022.3, 22350.5, 6075.0) - (4,54,6)	(12508.2, 28297.0, 6068.9) - (9,61,8)
Lateral 1	(10252.6, 23580.8, 6067.5) - (5,57,7)	(10252.6, 18659.6, 6067.9) - (5,42,2)
Lateral 2	(10252.6, 23580.8, 6067.5) - (5,57,7)	(4921.2, 26246.5, 6071.8) - (2,60,3)
Lateral 3	(10252.6, 23580.8, 6067.5) - (5,57,7)	(15789.0, 26246.5, 6074.0) - (17,60,7)

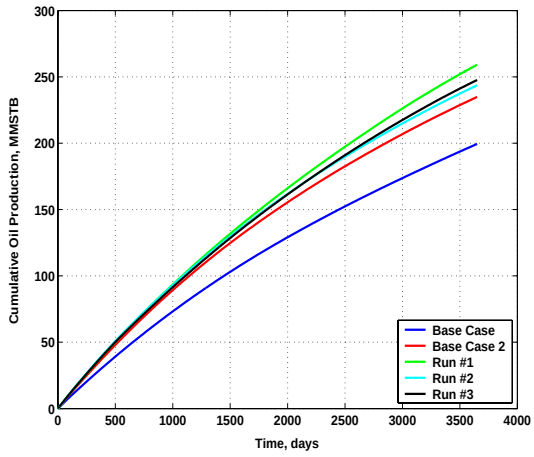

Figure 4.21: Comparison of Cumulative Oil Production for Optimized Fork Type Smart Wells

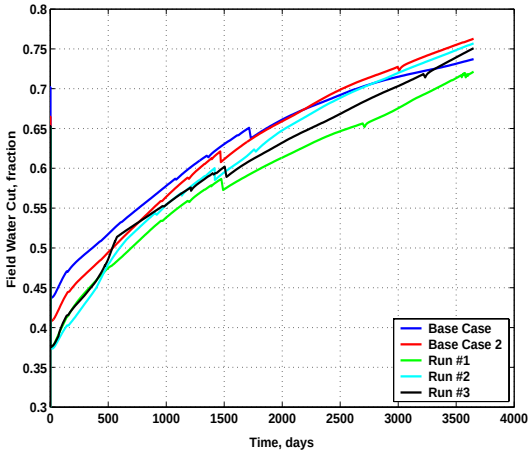

Figure 4.22: Comparison of Field Water Cut for Optimized Fork Type Smart Wells

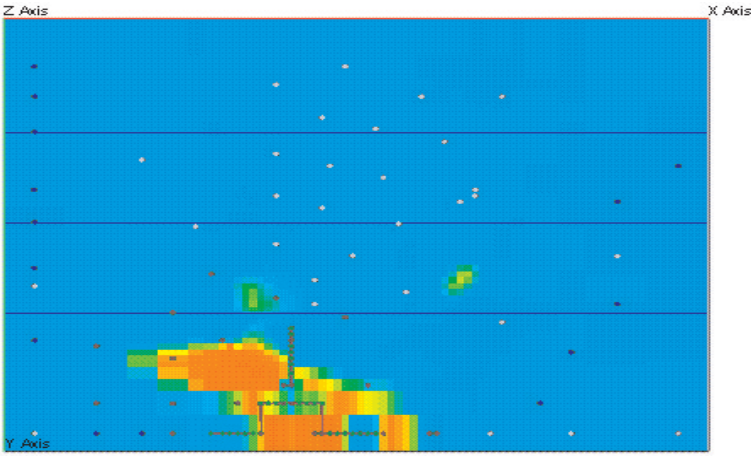

Figure 4.23: Final Oil Saturation Distribution of Layer 6 for Run #1

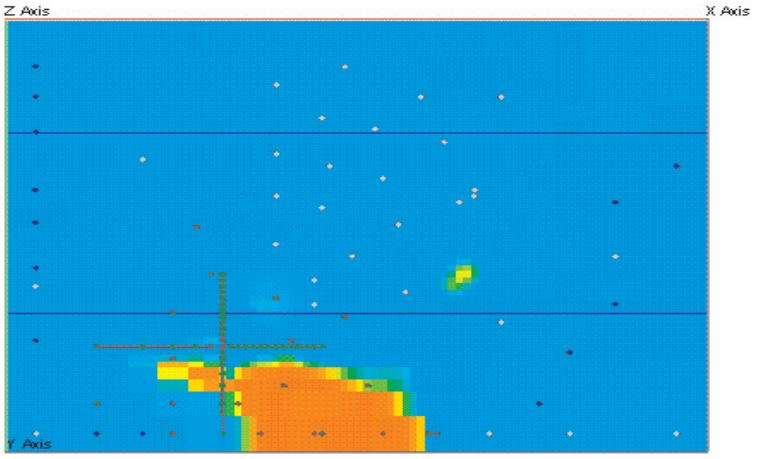

Figure 4.24: Final Oil Saturation Distribution of Layer 6 for Run #2

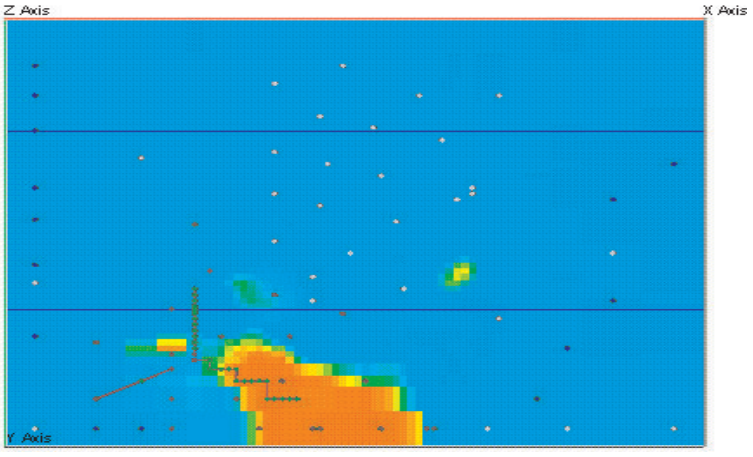

Figure 4.25: Final Oil Saturation Distribution of Layer 6 for Run #3

Table 4.15: Cumulative Oil Production (in MMSTB) for Optimum Fish Bone Type Smart Wells with Different Control Strategies

Run #	No Control	Reactive	Defensive
1	238.991	252.332	255.016
2	234.253	249.424	252.805
3	237.108	259.780	258.985

pressure drops along the mainbore.

4.5 Smart Well Control Optimization

In the previous section, the location and trajectory of the wells was optimized, and a simple and automatic control strategy ("reactive" control strategy) was implemented. In this section we will discuss the implementation of a "defensive" control strategy (see Chapter 3).

We divide the simulation period into 10 optimization steps; i.e., the valve settings are updated every year. This stepping can be further refined, but this level of control is adequate for our purposes. The objective function is to maximize the oil recovery for the optimum smart wells found in the previous sections. **Table 4.15** compares cumulative oil production (in MMSTB) attained for the optimized fish bone type well with reactive and defensive control strategies and without a control strategy. Similarly, **Table 4.16** compares the cumulative oil production (in MMSTB) attained for the optimum fork type wells. The cumulative oil production comparison plots in time are given in **Figs. 4.26** to **4.31**.

As can be seen from Tables 4.15 and 4.16, the smart well technology provides benefits in terms of cumulative oil production regardless of the control strategy. In this case, both of the control strategies give almost the same results. It is important to emphasize that the defensive control strategy might not be appropriate for a real life application, but it is a good tool in terms of screening options for well design and the use of control devices. For further discussion of this point see Section 3.3.

Table 4.16: Cumulative Oil Production (in MMSTB) for Optimum Fork Type Smart Wells with Different Control Strategies

Run #	No Control	Reactive	Defensive
1	251.549	259.126	261.781
2	224.603	243.639	246.686
3	219.886	247.626	240.258

4.5.1 Conclusions

In the example considered here we showed the benefits of smart well technology on a sector model of the SA6 Area of a huge mature oil field in Saudi Arabia. We found optimum wells for different well templates with various contact lengths. Then we optimized the control strategy on these wells. Almost all of the optimized wells perform better than four new vertical wells (Base Case 2).

We found that the shorter wells (Run #1 for both fish bone and fork type) perform better than the longer ones (except Run #3 of the fish bone type), showing that the interference between wells has a detrimental effect on the field performance. Another reason for the poor performance of longer wells (especially for the fork type wells) is their interaction with the fractures.

Although the fish bone type smart well optimized in Run #3 has the highest production in its class, we choose the well in Run #1 as the best one for this template, since it is simpler, shorter and therefore cheaper to drill. Similarly the fork type smart well optimized in Run #1 is chosen as the best well of its class. Now we compare the performances of these two wells in time in **Fig. 4.32** using a reactive control strategy. As can be seen the fork type well performs better than the fish bone type well. The fork type well production rate is $\sim 15\%$ higher than that of the fish bone type well at the end of 10 years, indicating good performance for the long term.

Both reactive and defensive control strategies produced similar results in terms of cumulative oil production. In some cases the reactive control strategy performed better than the defensive control strategy. The reason for this may be that the reactive strategy is more refined in time than the defensive strategy. The effect of the smart well technology is more apparent when the wells intersect a fracture (see Tables 4.15 and 4.16). The best well

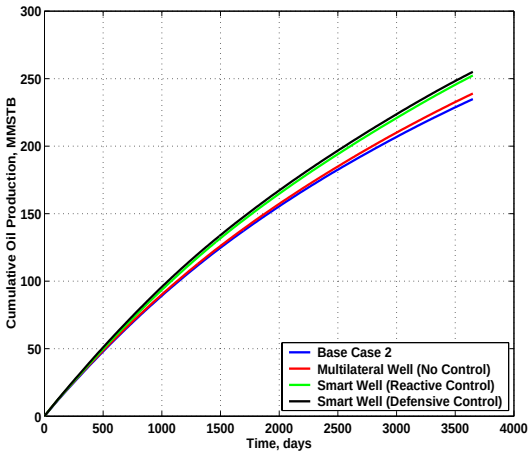

Figure 4.26: Comparison of Cumulative Field Oil Production for Fish Bone Type Smart Wells Optimized in Run #1

considered (well in Run #1) does not intersect any fractures. For this well, the increase in cumulative oil production with smart completions is less than that for the other wells considered.

4.6 Concluding Remarks

In this chapter we screened a conceptual reservoir model which is based on a real geological setting for deployment of NCWs. We showed the benefits of utilizing a NCW by comparing the performances of different well types. Defensive control optimization was performed on the NCW and we found that the smart well completions technology was beneficial for this reservoir model.

We then optimized different well templates with various numbers of laterals on a real model. We found that the NCW optimized in any of the cases almost always had a better performance than drilling vertical wells. We also showed the benefits of smart well technology for this model by considering both reactive and defensive control strategies.

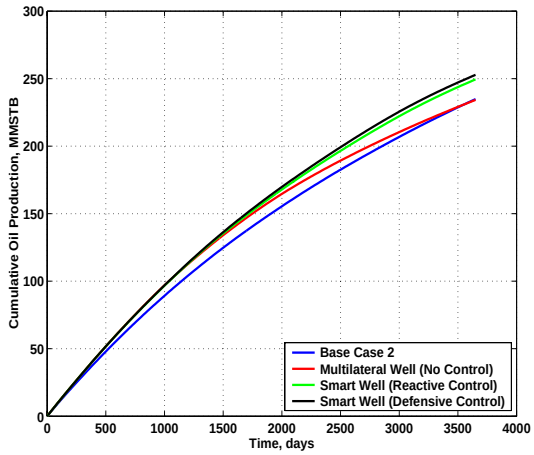

Figure 4.27: Comparison of Cumulative Field Oil Production for Fish Bone Type Smart Wells Optimized in Run #2

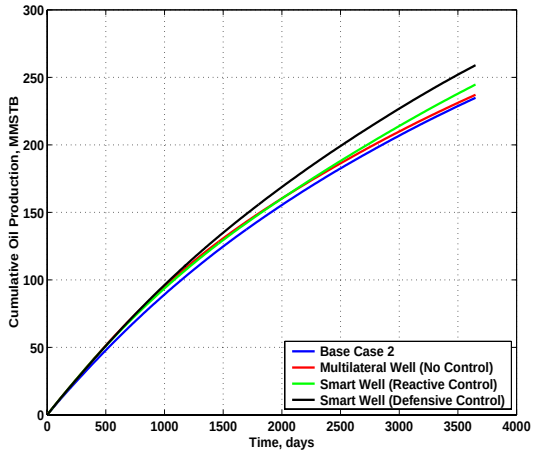

Figure 4.28: Comparison of Cumulative Field Oil Production for Fish Bone Type Smart Wells Optimized in Run #3

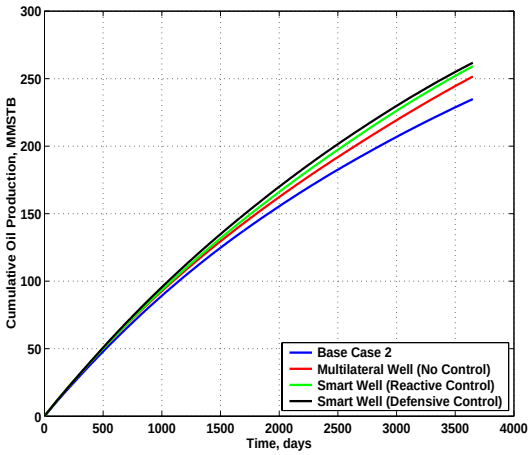

Figure 4.29: Comparison of Cumulative Field Oil Production for Fork Type Smart Wells Optimized in Run #1

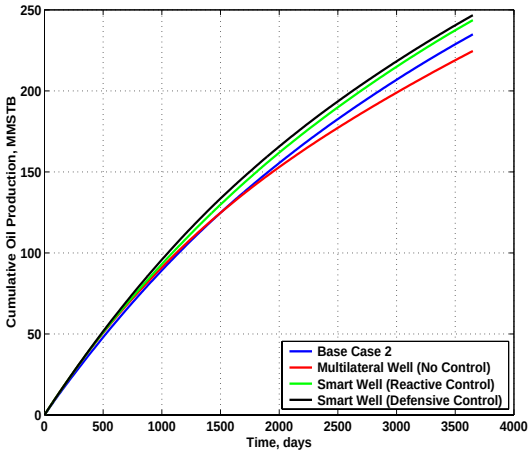

Figure 4.30: Comparison of Cumulative Field Oil Production for Fork Type Smart Wells Optimized in Run #2

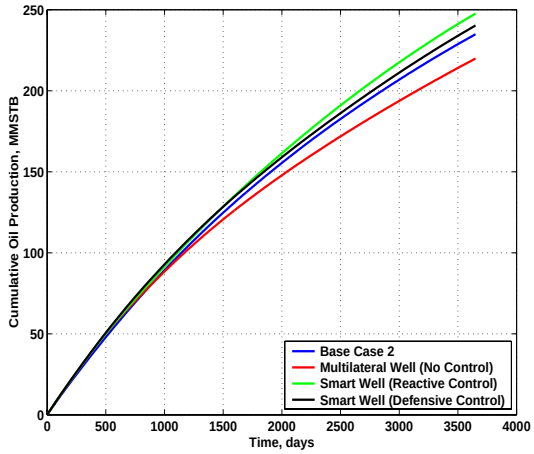

Figure 4.31: Comparison of Cumulative Field Oil Production for Fork Type Smart Wells Optimized in Run #3

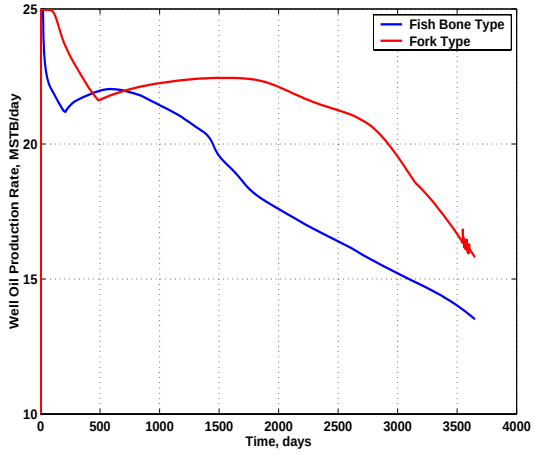

Figure 4.32: Comparison of Well Performances

Chapter 5

Conclusions and Future Work

5.1 Conclusions

The main contributions of this study can be summarized as follows:

- A general methodology for the optimization of nonconventional well type, trajectory and location was developed. The procedure is based on a genetic algorithm and is accompanied by a hill climber, artificial neural network and near-well scale up algorithms to accelerate the optimization.

- The optimization algorithm represents all types of wells with a chromosome of fixed length, which allows well types to appear in later generations that might not exist in earlier generations. As a result, the optimal type of well does not need to be specified a priori, but rather evolves as the optimization proceeds.

- The general algorithm was applied to a number of example cases. Optimized wells resulted in objective functions (cumulative oil or NPV) that exceeded that of the best well in the first generation by 15% to 34%. The optimum well type (i.e., number of laterals) was found to vary depending on the type of reservoir, the specific objective function, and the degree of reservoir uncertainty.

- Reactive and defensive control strategies which can be applied with downhole inflow control devices were defined. In this study we mainly focused on the defensive control strategy. For this purpose, a general method for the optimization of wells

with downhole inflow control devices was presented. The method entails the use of an optimization tool based on a nonlinear conjugate gradient algorithm. This tool is linked to a commercial reservoir simulator containing a wellbore flow model capable of modelling downhole inflow control devices. The optimization approach requires that the simulation be divided into a number of optimization time steps. The valve settings are then optimized for each of these time periods.

- The method was applied to examples involving vertical wells in a layer-cake reservoir and multilateral wells in a complex channelized reservoir. The use of optimized downhole inflow control devices was shown to improve cumulative oil recovery by as much as 65% over the uninstrumented base case.

- Multiple geostatistical realizations of the channelized reservoir case were considered. It was shown that the incremental recovery using downhole control varied significantly from realization to realization. This indicates that more data, or sophisticated decision-making procedures, will be required prior to the deployment of instrumented wells in cases with high degrees of uncertainty.

- The tools developed here were applied to a portion of a real reservoir located in Saudi Arabia. Different well types were optimized to maximize oil recovery. Both defensive and reactive control strategies were implemented. These were shown to produce similar results for the reservoir model considered. Smart well technology was shown to provide more than 10% incremental recovery over a case that involved drilling several vertical wells.

5.2 Future Work

We propose the following items to improve the well type, location and trajectory optimization:

- Additional search algorithms or proxies to increase the efficiency of the algorithm should be explored.

- In order to enable more reliable assessments when multiple sources of uncertainty are present, higher order designs, such as D-optimal or factorial designs should be

implemented. These techniques will provide better response surfaces that account for interactions between the uncertain parameters.

- Kriging should be explored as a means to construct the response surface of the experimental design methodology. This approach might add more nonlinearity to this proxy.
- The current implementation uses linear well trajectories. Curved trajectories or trajectories with multiple linear segments should also be implemented.

The following suggestions can enhance the smart well control optimization:

- The smart well control optimization can be extended to optimize the number of valves and their location on the production string (in the current implementation, these parameters are specified).
- The parameters of the reactive smart well control strategy (see Eq 3.4) should be further optimized to accelerate the overall algorithm.
- The optimization methodology can be modified to handle models that are updated in time (history matched), using real time data from sensors in smart wells. Then the valve settings for the future steps can be optimized using the history matched model. In this way the control strategy can be used in real time instead of just as a screening tool.

Nomenclature

A	cross-sectional area perpendicular to flow, ft^2
B	formation volume factor, volume/volume
c	mapping function between real and grid coordinates; rock compressibility, psi^{-1}
C	cost, $/bbl, $/MSCF or $/junction
C_u	unit conversion factor, 2.159×10^{-4} (field units)
C_v	valve flow coefficient, dimensionless
d	diameter, ft
$\mathbf{d}$	search direction
f	objective function (fitness of an individual), data units; Fanning friction factor
F	objective function for uncertainty assessment
G	grid space
GOR	gas oil ratio, MSCF/STB
h	heel coordinates, ft; step size in derivative evaluation, dimensionless
H	heel point
i	annual interest rate (APR), fraction
J	junction point
k	permeability, md
l	length, ft
n	number of optimization steps; number of realizations
N	number; population size
N_f	number of simulations
p	probability
$\mathbf{p}$	unknown matrix
P	pressure

q	production target, rate or pressure
Q	cumulative production during a period, MSTB or MMSCF
r	radius, ft; risk coefficient, dimensionless
$\mathbf{r}$	residual in CG formulation
R	correlation coefficient; real space
R_s	solution gas oil ratio, MSCF/STB
s	skin factor
t	toe coordinates, ft; time, days
T	toe point
v	velocity, ft/s
V	volume, STB or MSCF
WOR	water oil ratio, dimensionless
$\mathbf{x}$	scaled valve constriction areas, dimensionless
Y	total discounting period

Symbols

α	directional angle, radians; inclination of the well, fraction; step size in CG
β	Gram-Schmidt constant
ε	fractional convergence tolerance
Γ	normalizing factor in s-k approximation
γ	specific gravity, dimensionless
ϕ	porosity, fraction
μ	viscosity, cp; mean, data units
ρ	density, lb_m/ft^3
σ	standard deviation, data units
$\boldsymbol{\tau}$	trajectory vector
θ	angle between l_{xy} and x axis, radians
ω	permeability or rank weighting exponent, dimensionless
ζ	PI multiplier, dimensionless

Subscripts

a	near-well region
bub	bubble point
c	crossover; valve constriction
$comp$	completion
d	drilling and completion
f	friction; function evaluations
g	grid
gr	residual gas
h	horizontal
jun	junction
lat	lateral
m	mutation; fluid mixture
o	oil
or	residual oil
p	pipe
rg	relative to gas
ro	relative to oil
rw	relative to water
t	total
w	well; water
wc	connate water
xy	$x - y$ plane
v	vertical; valve

Superscripts

$*$	effective or equivalent
l	lower limit
m	multiplier
T	matrix transpose

u upper limit

Bibliography

Ababou, R. (1990). Identification of Effective Conductivity Tensor in Randomly Heterogeneous and Stratified Aquifers, presented at the Canadian-American Conference on Hydrogeology, Calgary, Canada, September 18-20.

Afilaka, J. O., Bahamaish, J., Bowen, G., Bratvedt, K., Holmes, J. A., Miller, T., Fjerstad, P., Grinestaff, G., Jalali, Y., Lucas, C., Jimenez, Z., Lolomari, T., May, E., and Randall, E. (2001). Improving the Virtual Reservoir. *Schlumberger Oilfield Review*, Spring, pp 29–36.

Antonsen, B., Olsen, G., and Høye, T. (1993). Opportunities and Pitfalls When Locating Horizontal Wells in a Geologically Uncertain Environment, paper SPE 26530 presented at the 68th Annual Technical Conference and Exhibition, Houston, Texas, 3-6 October.

Aubert, W. G. (1998). Variations in Multilateral Well Design and Execution in the Prudhoe Bay Unit, paper SPE 39388 presented at the IADC/SPE Drilling Conferenece, Dallas, Texas, 3-6 March.

Aziz, K., Arbabi, S., and Deutsch, C. V. (1999). Why is it so Difficult to Predict the Performance of Horizontal Wells? *Journal of Canadian Petroleum Technology*, October, pp 37–45.

Beckner, B. L. and Song, X. (1995). Field Development Planning Using Simulated Annealing - Optimal Economic Well Scheduling and Placement, paper SPE 30650 presented at the SPE Annual Technical Conference and Exhibition, Dallas, Texas, 22-25 October.

Beliveau, D. (1995). Heterogeneity, Geostatistics, Horizontal Wells, and Blackjack Poker. *Journal of Petroluem Technology*, December, pp 1068–1074.

Bittencourt, A. C. and Horne, R. N. (1997). Reservoir Development and Design Optimization, paper SPE 38895 presented at the SPE Annual Technical Conference and Exhibition, San Antonio, Texas, 5-8 October.

Boardman, D. W. (1997). Designing the Optimal Multi-Lateral Well Type for a Heavy Oil Reservoir in Lake Maracaibo, Venezuela, paper SPE 37554 presented at the SPE International Thermal Operations and Heavy Oil Symposium, Bakersfield, California, 10-12 February.

Bosworth, S., El-Sayed, H., Ismail, G., Ohmer, H., Stracke, M., West, C., and Retnanto, A. (1998). Key Issues in Multilateral Technology. *Schlumberger Oilfield Review*, Winter, pp 14–28.

Bowling, J. (2002). Personal Communication.

Brouwer, D. R. and Jansen, J. D. (2002). Dynamic Optimization of Water Flooding with Smart Wells Using Optimal Control Theory, paper SPE 78278 presented at the SPE European Petroleum Conference, Aberdeen, UNITED KINGDOM, 29-31 October.

Brouwer, D. R., Jansen, J. D., Van Der Starre, S., Van Kruijsdijk, C. P. J. W., and Berentsen, C. W. J. (2001). Recovery Increase through Water Flooding with Smart Well Technology, paper SPE 68979 presented at the SPE European Formation Damage Conference, The Hague, Netherlands, 21-22 May.

Brouwer, R. D. (2002). Personal Communication.

Cayeux, E., Genevois, J. M., Crepin, S., and Thibeau, S. (2001). Well Planning Quality Improved Using Cooperation between Drilling and Geosciences, paper SPE 71331 presented at the SPE Annual Technical Conference and Exhibition, New Orleans, Louisiana, 30 September-3 October.

Centilmen, A., Ertekin, T., and Grader, A. S. (1999). Applications of Neural Networks in Multiwell Field Development, paper SPE 56433 presented at the SPE Annual Technical Conference and Exhibition, Houston, Texas, 3-6 October.

ChevronTexaco (2001). *CHEARS - Initialization Data, 2001B.*

Chewaroungroaj, J., Varela, O., and Lake, L. W. (2000). An Evaluation of Procedures to Estimate Uncertainty in Hydrocarbon Recovery Process, paper SPE 59449 presented at the SPE Asia Pacific Conference on Integrated Modelling for Asset Management, Yokohoma, Japan, 25-26 April.

Chralez, P. A. and Bréant, P. (1999). The Multiple Role of Unconventional Drilling Technologies. From Well Design to Well Productivity, paper SPE 56405 presented at the SPE European Formation Damage Conference, The Hague, Netherlands, 31 May-1 June.

Corlay, P., Bossie-Codrenau, D., Sabathier, J. C., and Delamaide, E. R. (1997). Improving Reservoir Management with Complex Well Architectures. *World Oil*, January, pp 45–50.

Dejean, J.-P. and Blanc, G. (1999). Managing Uncertanties on Production Predictions Using Integrated Statistical Methods, paper SPE 56696 presented at the SPE Annual Technical Conference and Exhibition, Houston, Texas, 3-6 October.

Deutsch, C. V. and Journel, A. G. (1998). *GSLIB User's Manual*. Applied Geostatistics. Oxford University Press, New York, second edition.

Deutsch, C. V. and Tran, T. T. (2002). FLUVSIM: A Program for Object-based Stochastic Modeling of Fluvial Depositional Systems. *Computers and Geosciences*, May, pp 525–535.

Dolle, N., Brouwer, D. R., and Jansen, J. D. (2002). Dynamic Optimization of Water Flooding with Multiple Injectors and Producers Using Optimal Control Theory. paper presented at the XV International Conference on Computational Methods in Water Resources. Delft, Netherlands, 23-28 June.

Durlofsky, L. J. (2000). An Approximate Model for Well Productivity in Heterogeneous Porous Media. *Mathematical Geology*, May, pp 421–438.

Dykstra, H. and Parsons, R. L. (1950). The Prediction of Oil Recovery by Waterflood. *Secondary Recovery of Oil in the United States*.

Ehlig-Economodies, C. A., Mowat, G. R., and Corbett, C. (1996). Techniques for Multibranch Well Trajectory Design in the Context of a Three-Dimensional Reservoir Model,

paper SPE 35505 presented at the 3-D Reservoir Modeling Conference, Stavanger, Norway, 16-17 April.

Fang, K. (1980). Uniform Design: Application of Number Theory in Test Design. *ACTA Mathematicae Applicatae Sinica*.

Fernandez, B., Ehlig-Economidies, C. A., and Economidies, M. J. (1999). Multilevel Injector/Producer Wells in Thick Heavy Crude Reservoirs, paper SPE 53950 presented at the SPE Latin American and Caribbean Petroleum Engineering Conference, Caracas, Venezuela, 21-23 April.

Fichter, D. P. (2000). Application of Genetic Algorithms in Portfolio Optimization for the Oil and Gas Industry, paper SPE 62970 presented at the SPE Annual Technical Conference and Exhibition, Dallas, Texas, 1-4 October.

Freeman, A., Gronas, T., Berge, F., Durst, D., and Luke, M. (1998). First Successful Multilateral Well Installation From a Floating Rig: Development and Case History, paper SPE 39369 presented at the IADC/SPE Drilling Conference, Dallas, Texas, 3-6 March.

Friedmann, F. and Chawathé, A. (2001). Uncertainty Assessment of Reservoir Performance Using Experimental Designs. paper CIM 2001-170 presented at the 2001 Canadian International Petroleum Conference, Calgary, Canada, 29 September-2 October.

Fujii, H. and Horne, R. N. (1994). Multivariate Optimization of Networked Production Systems, paper SPE 27617 presented at the European Production Operations Conference and Exhibition, Aberdeen, UNITED KINGDOM, 15-17 March.

Gai, H. (2001). Downhole Flow Control Optimization in the World's 1st Extended Reach Multilateral Well at Wytch Farm, paper SPE 67728 presented at the SPE/IADC Drilling Conference, Amsterdam, Netherlands, 27 February-1 March.

Gai, H., Davies, J., Newberry, P., Vince, S., and Al-Mashgari, A. (2000). World's First Downhole Flow Control Completion of an Extended-Reach, Multilateral Well at Wytch Farm, paper SPE 59211 presented at the IADC/SPE Drilling Conference, New Orleans, Louisiana, 23-25 February.

Gallivan, J. D., Hewitt, N. R., Olsen, M., Peden, J. M., Tehrani, D., and Tweedie, A. A. P. (1995). Quantifying the Benefits of Multi-Lateral Producing Wells, paper SPE 30441 presented at the Offshore Europe Conference, Aberdeen, UNITED KINGDOM, 5-8 September.

GeoQuest (2001a). *ECLIPSE Reference Manual 2001A*. Schlumberger.

GeoQuest (2001b). *ECLIPSE Technical Description 2001A*. Schlumberger.

Gharbi, R. B. and Garrouch, A. A. (2001). The Performance of Miscible Enhanced Oil Recovery Displacements in Geostatistically Generated Permeable Media Using Horizontal Wells. *Journal of Porous Media*, pp 113–126.

Gill, P. E., Murray, W., and Wright, M. H. (1999). *Practical Optimization*. Academic Press Inc., San Diego, California, twelfth edition.

Goldberg, D. (1989). *Genetic Algorithms in Search, Optimization and Machine Learning*. Addison-Wesley, Reading, Massachusetts, second edition.

Greenberg, J. (1999). Intelligent Completions Migrating to Shallow Water, Low Cost Wells. *Offshore International*, February, pp 63–64, 66.

Guyaguler, B. (2002). *Optimization of Well Placement and Assessment of Uncertainty*. Phd dissertation, Department of Petroleum Engineering, Stanford University, California.

Guyaguler, B. and Horne, R. N. (2001). Uncertainty Assesment of Well Placement Optimization, paper SPE 71625 presented at the SPE Annual Technical Conference and Exhibition, New Orleans, Louisiana, 30 September-3 October.

Guyaguler, B., Horne, R. N., and Tauzin, E. (2001). Automated Reservoir Model Selection in Well Test Interpretation, paper SPE 71569 presented at the Annual Technical Conference and Exhibition, New Orleans, Lousiana, 30 September - 3 October.

Guyaguler, B., Horne, R. N., Rogers, L., and Rosenzweig, J. J. (2002). Optimization of Well Placement in a Gulf of Mexico Waterflooding Project. *SPE Reservoir Evaluation & Engineering*, June, pp 229–236.

Hamer, D. and Freeman, A. (1999). The Business Case for Multilateral Wells. *Petroleum Engineering International*, May, pp 25–29.

Harding, T. J., Radcliffe, N. J., and King, P. R. (1996). Optimization of Production Strategies Using Stochastic Search Methods, paper SPE 35505 presented at the 3-D Reservoir Modeling Conference, Stavanger, Norway, 16-17 April.

Harris, J. W. and Stocker, H. (1998). *Handbook of Mathematics and Computational Science*. Springer-Verlag, New York.

Hawkins, M. F. (1956). A Note on the Skin Effect. *Trans. AIME*, October, pp 356–57.

Holland, J. H. (1975). *Adaptation in Natural and Artificial Systems*. The University of Michigan Press, Ann Arbor, Michigan.

Holmes, J. A., Barkve, T., and Lund, Ø. (1998). Application of a Multisegment Well Model to Simulate Flow in Advanced Wells, paper SPE 50646 presented at the SPE European Petroleum Conference, The Hague, Netherlands, 20-22 October.

Horn, M. J., Plathey, D. P., and Ibrahim, O. (1997). Dual Horizontal Well Increases Liquids Recovery in the Gulf of Thailand, paper SPE 38065 presented at the SPE Asia Pacific Oil and Gas Conference, Kuala Lumpur, Malaysia, 14-16 April.

Hovda, S., Haugland, T., Waddel, K., and Lekness, R. (1996). World's First Application of a Multilateral System Combining a Cased and Cemented Junction with Fullbore Access to Both Laterals, paper SPE 36488 presented at the 71st SPE Annual Technical Conference, Denver, Colorado, 6-9 October.

Howard, R. A. (1998). The Foundations of Decision Analysis. Decison Analysis I, Course Reader, Department of Management Science and Engineering, Stanford University, California.

Isah, I. B., Steele, R. P., Macaulay, R. C., Stephenson, P. M., and Al Mantheri, S. M. (1995). Review of Horizontal Well Applications in Oman, paper SPE 29812 presented at the SPE Middle East Oil Show, Bahrain, 11-14 March.

Jalali, Y. and Charron, A. (1998). A Permanent System for Measurement of Downhole Flowrates - North Sea Examples, paper SPE 50670 presented at the SPE European Petroleum Conference, The Hague, Netherlands, 20-22 October.

Jalali, Y., Bussear, T., and Sharma, S. (1998). Intelligent Completions Systems - The Reservoir Rationale, paper SPE 50587 presented at the SPE European Petroleum Conference, The Hague, Netherlands, 20-22 October.

Jikich, S. A. and Popa, A. S. (2000). Hyperbolic Decline Parameter Identification Using Optimization Procedures, paper SPE 65634 presented at the SPE Eastern Regional Meeting, Morgantown, West Virginia, 17-19 October.

Joshi, S. D. (1988). Augmentation of Well Productivity with Slant and Horizontal Wells. *Journal of Petroluem Technology*, June, pp 729–739.

Kabir, C. S., Chawathé, A., Jenkins, S. D., Olayomi, A. J., Aigbe, C., and Faparusi, D. B. (2002). Developing New Fields Using Probabilistic Reservoir Forecasting, paper SPE 77564 presented at the SPE Annual Technical Conference and Exhibition, San Antonio, Texas, 29 September-2 October.

Karakas, M. and Ayan, C. (1991). Productivity and Coning Behavior of Phased Horizontal Completions, paper SPE 22928 presented at the SPE Annual Technical Conference and Exhibition, Dallas, Texas, 6-9 October.

Khargoria, A., Zhang, F., Li, R., and Jalali, Y. (2002). Application of Distributed Electrical Measurements and Inflow Control in Horizontal Wells under Bottom-Water Drive, paper SPE 78275 presented at the SPE European Petroleum Conference, Aberdeen, UNITED KINGDOM, 29-31 October.

Lie, O. H. and Wallace, W. (2000). Intelligent Recompletion Eliminates Need for Additional Well, paper SPE 59210 presented at the IADC/SPE Drilling Conference, New Orleans, Louisiana, 23-25 February.

Lucas, C., Duffy, P., Randall, E., and Jalali, Y. (2001). Near-Wellbore Modeling to Assist Operation of an Intelligent Multilateral Well in the Sherwood Formation, paper SPE 71828 presented at the SPE Annual Technical Conference and Exhibition, New Orleans, Louisiana, 30 September-3 October.

Manceau, E., Mezghani, M., Zabalza-Mezghani, I., and Roggero, F. (2001). Combination of Experimental Design and Joint Modeling Methods for Quantifying the Risk Associated with Deterministic and Stochastic Uncertainties - An Integrated Test Study, paper SPE 71620 presented at the SPE Annual Technical Conference and Exhibition, New Orleans, Louisiana, 30 September-3 October.

Martinez, E. R., Moreno, W. J., Corpoven, S. A., Moreno, J. A., and Maggiolo, R. (1994). Application of Genetic Algorithm on the Distribution of Gas Lift Injection, paper SPE 26993 presented at the SPE Latin American and Caribbean Petroleum Engineering Conference, Buenos Aires, Argentina, 27-29 April.

Masters, T. (1993). *Practical Neural Network Recipes in C++*. Academic Press.

Mohaghegh, S., Platon, V., and Ameri, S. (1998). Candidate Selection for Stimulation of Gas Storage Wells Using Available Data With Neural Networks and Genetic Algorithms, paper SPE 51080 presented at the SPE Eastern Regional Meeting, Pittsburgh, Pennsylvania, 9-11 November.

Montes, G., Bartolome, P., and Udias, A. L. (2001). The Use of Genetic Algorithms in Well Placement Optimization, paper SPE 69439 presented at the SPE Latin American and Caribbean Petroleum Engineering Conference, Buenos Aires, Argentina, 25-28 March.

Montgomery, D. C. (2001). *Design and Analysis of Experiments*. John Wiley and Sons, Inc., New York, fifth edition.

Montoya-O, S. J., Jovel-T, W. A., Hernandez-R, J. a., and Gonzalez-R, C. (2000). Genetic Algorithms Applied to the Optimum Design of Gas Transmission Networks, paper SPE 59030 presented at the SPE International Petroleum Conference and Exhibition, Villahermosa, Mexico, 1-3 February.

Nesvold, R. L., Herring, T. R., and Currie, J. C. (1996). Field Development Optimization using Linear Programming Coupled with Reservoir Simulation - Ekofisk Field, paper SPE 36874 presented at the SPE European Petroleum Conference, Milan, Italy, 22-24 October.

Nielsen, V. B. J., Piedras, J., Stimatz, G. P., and Webb, T. R. (2001). Aconcagua, Camden Hills, and King's Peak Fields, Gulf of Mexico Employ Intelligent Completion Technology in Unique Field Development Scenario, paper SPE 71675 presented at the SPE Annual Technical Conference and Exhibition, New Orleans, Louisiana, 30 September-3 October.

Palke, M. R. and Horne, R. N. (1997). Determining the Value of Reservoir Data by Using Nonlinear Optimization Techniques, paper SPE 38047 presented at the SPE Asia Pacific Oil and Gas Conference, Kuala Lumpur, Malaysia, 14-16 April.

Pan, Y. and Horne, R. N. (1998). Improved Methods for Multivariate Optimization of Field Development Scheduling and Well Placement Design, paper SPE 49055 presented at the SPE Annual Technical Conference and Exhibition, New Orleans, Lousiana, 27-30 September.

Paté-Cornell, M. E. (1996). Notes on Decision-Making Under Uncertainty. Department of Management Science and Engineering, Stanford University, California.

Plackett, R. L. and Burman, J. P. (1946). The Design of Optimum Multifactorial Experiments. *Biometrika*, June, pp 305–325.

Press, W. H., Teukolsky, S. A., Vetterling, W. T., and Flannery, B. P. (1999). *Numerical Recipes in C*. Cambridge University Press, Cambridge, UNITED KINGDOM, second edition.

Qiu, Y., Holtz, M. H., and Yang, A. (2001). Applying Curvature and Fracture Analysis to the Placement of Horizontal Wells: Example from the Mabee (San Andres) Reservoir, Texas, paper SPE 70010 presented at the SPE Permian Basin Oil and Gas Recovery Conference, Midland, Texas, 15-16 May.

Reed, R. R. and Marks II, R. J. (1999). *Neural Smithing, Supervised Learning in Feedforward Artificial Neural Networks*. The MIT Press, Cambridge, Massachusetts.

Rester, S., Thomas, J., Hilten, M. P., and Vidrine, W. L. (1999). Application of Intelligent Completion Technology to Optimize the Reservoir Management of a Deepwater Gulf of Mexico Field - A Reservoir Simulation Case Study, paper SPE 56670 presented at the SPE Annual Technical Conference and Exhibition, Houston, Texas, 3-6 October.

Robinson, C. E. (1997). Overcoming the Challenges Associated with the Life-Cycle Management of Multilateral Wells: Assessing Moves Towards the Intelligent Completion, paper SPE 38497 presented at the Offshore European Conference, Aberdeen, UNITED KINGDOM, 9-12 September.

Romero, C. E., Carter, J. N., Zimmerman, R. W., and Gringarten, A. C. (2000a). Improved Reservoir Characterization through Evolutionary Computation, paper SPE 62942 presented at the SPE Annual Technical Conference and Exhibition, Dallas, Texas, 1-4 October.

Romero, C. E., Gringarten, A. C., and Zimmerman, R. W. (2000b). A Modified Genetic Algorithm for Reservoir Characterisation, paper SPE 64765 presented at the SPE International Oil and Gas Conference and Exhibition, Beijing, China, 7-10 November.

Sadek, H., Williams, C. R., and Smith, M. (1998). Production Strategy Yields Unique Perforating, Cost-Efficient Multilateral Drilling Solution in the Beryl Field, paper SPE 50123 presented at the Asia Pacific Oil and Gas Conference and Exhibition, Perth, Australia, 12-14 October.

Santellani, G., Hansen, B., and Herring, T. (1998). "Survival of the Fittest" an Optimized Well Location Algorithm for Reservoir Simulation, paper SPE 39754 presented at the SPE Asia Pacific Conference on Integrated Modelling for Asset Management, Kuala Lumpur, Malaysia, 23-24 March.

Sarma, H. K. (1994). Horizontal Well Technology: A Research Perspective. In *Canadian SPE/CIM/CANMET International Conference on Recent Advances in Horizontal Well Applications, Calgary, Canada*, number HWC94-11, pp 1–8.

Seifert, D., Lewis, J. J. M., Hern, C. Y., and Steel, N. C. T. (1996). Well Placement Optimisation and Risking Using 3-D Stochastic Reservoir Modelling Techniques, paper SPE 35520 presented at the 3-D Reservoir Modeling Conference, Stavanger, Norway, 16-17 April.

Sen, M. K., Gupta, A. D., Stoffa, P. L., Lake, L. W., and Pope, G. A. (1993). Stochastic Reservoir Modeling Using Simualted Annealing and Genetic Algorithm, paper SPE

24754 presented at the Annual Technical Conference and Exhibition, Washington, DC, 4-7 October.

Shewuck, J. R. (1994). An Introduction to the Conjugate Gradient Method Without the Agonizing Pain. Internal Report. School of Computer Science, Carnegie Mellon University, Pittsburgh, Pennsylvania (available at http://www.cs.cmu.edu/ jrs/jrspapers.html).

Sinha, S., Vega, L., Kumar, R., and Jalali, Y. (2001). Flow Equilibration toward Horizontal Wells Using Downhole Valves, paper SPE 68635 presented at the Asia Pacific Oil and Gas Conference and Exhibition, Jakarta, Indonesia, 17-19 April.

Smith, J., Economides, M. J., and Frick, T. P. (1995). Reducing Economic Risk in Areally Anisotropic Formations with Multiple-Lateral Horizontal Wells, paper SPE 30647 presented at the SPE Annual Technical Conference and Exhibition, Dallas, Texas, 22-25 October.

Stoisits, R. F., Crawford, K. D., MacAllister, D. J., McCormack, M. D., Lawal, A. S., and Ogbe, D. O. (1999). Production Optimization at the Kuparuk River Field Utilizing Neural Networks and Genetic Algorithms, paper SPE 52117 presented at the Mid-Continent Operations Symposium, Oklahoma City, Oklahoma, 28-31 March.

Sudaryanto, B. and Yortsos, Y. C. (2000). Optimization of Fluid Front Dynamics in Porous Media Using Rate Control. I. Equal Mobility Fluids. *Physics of Fluids*, July, pp 1656–1670.

Sugiyama, H., Peden, J. M., and Nicoll, G. (1997). The Optimal Application of Multi-Lateral/Multi Branch Completions, paper SPE 38033 presented at the SPE Asia Pacific Oil and Gas Conference, Kuala Lumpur, Malaysia, 14-16 April.

TAML (1999). Technical Advancement of Multilateral Wells. Technical report, TAML. http://taml.altinex.no/.

Taylor, R. W. and Russel, R. (1997). Drilling and Completing Multilateral Horizontal Wells in the Middle East, paper SPE 38759 presented at the SPE Annual Technical Conference and Exhibition, San Antonio, Texas, 5-8 October.

Tubel, P. and Hopmann, M. (1996). Intelligent Completion for Oil and Gas Production Control in Subsea Multi-lateral Well Applications, paper SPE 36582 presented at the SPE Annual Technical Conference and Exhibition, Denver, Colorado, 6-9 October.

Valvatne, P. H. (2000). *A Framework for Modeling Complex Well Configurations*. Master's thesis, Petroleum Engineering Department, Stanford University, California.

Valvatne, P. H., Durlofsky, L. J., and Aziz, K. (2001). Semi-analytical Modeling of the Performance of Intelligent Well Completions, paper SPE 66368 presented at the SPE Reservoir Simulation Symposium, Houston, Texas, 11-14 February.

Vazquez, M., Suarez, A., Aponte, H., Ocanto, L., and Fernandes, J. (2001). Global Optimization of Oil Production Systems, A Unified Operational View, paper SPE 71561 presented at the SPE Annual Technical Conference and Exhibition, New Orleans, Louisiana, 30 September - 3 October.

Venkataraman, R. (2000). Application of the Method of Experimental Design to Quantify Uncertainty in Production Profiles, paper SPE 59422 presented at the SPE Asia Pacific Conference on Integrated Modelling for Asset Management, Yokohoma, Japan, 25-26 April.

Vij, S. K., Narasaiah, S. L., Walia, A., and Singh, G. (1998). Multilaterals: An Overview and Issues Involved in Adopting This Technology, paper SPE 39509 presented at the SPE India Oil and Gas Conference and Exhibition, New Delhi, India, 17-19 February.

Vo, D. T. and Madden, M. V. (1995). Performance Evaluation of Trilateral Wells: Field Examples. *SPE Reservoir Engineering*, February, pp 22–28.

Wolfsteiner, C., Durlofsky, L. J., and Aziz, K. (2000a). Approximate Model for Productivity of Nonconventional Wells in Heterogeneous Reservoirs. *SPE Journal*, June, pp 218–226.

Wolfsteiner, C., Durlofsky, L. J., and Aziz, K. (2000b). Efficient Estimation of the Effects of Wellbore Hydraulics and Reservoir Heterogeneity on the Productivity of Non-Conventional Wells, paper SPE 59399 presented at the SPE Asia Pacific Conference on Integrated Modeling for Asset Management, Yokohama, Japan, 25-26 April.

Wolfsteiner, C., Durlofsky, L. J., and Aziz, K. (2003). Calculation of Well Index for Non-conventional Wells on Arbitrary Grids. *Computational Geosciences*, (to appear).

Wong, S., Boon, W. S., Chia, R., and Chong, A. (1997). The Use of Multi-lateral Well Technology in an Infill Development Project, paper SPE 38030 presented at the SPE Asia Pacific Oil and Gas Conference, Kuala Lumpur, Malaysia, 14-16 April.

Xu, H. Y. and Vukovich, G. (1994). Fuzzy Evolutionary Algorithms and Automatic Robot Trajectory Generation. *IEEE*, April, pp 595 – 600.

Yamada, T. and Hewett, T. A. (1995). Production-Based Effective Vertical Permeability for a Horizontal Well. *SPE Reservoir Engineering*, August, pp 163–168.

Yeten, B. and Jalali, Y. (2001). Effectiveness of Intelligent Completions in a Multiwell Development Context, paper SPE 68077 presented at the SPE Middle East Oil Show, Bahrain, 17-20 March.

Yeten, B. and Sengul, M. (2001). Potential Applications of Smart Wells in SA Field: A Scoping Study. Internal report, North Uthmaniyah Unit, URMD, Reservoir Management Department, Saudi Aramco.

Yeten, B., Wolfsteiner, C., Durlofsky, L. J., and Aziz, K. (2000). Approximate Finite Difference Modeling of the Performance of Horizontal Wells in Heterogeneous Reservoirs, paper SPE 62555 presented at the SPE Western Regional Meeting, Long Beach, California, 19-23 June.

Yu, S., Davies, D. R., and Sherrard, D. W. (2000). The Modelling of Advanced “Intelligent” Well An Application, paper SPE 62950 presented at the SPE Annual Technical Conference and Exhibition, Dallas, Texas, 1-4 October.

Appendix A

Assessment of Multiple Sources of Uncertainty

When we have multiple sources of uncertainty, say a combination of engineering and geological parameters, it is not feasible to perform optimization considering every combination of the uncertain parameters, as we did in the previous section. As an alternative, we introduce experimental design methodology, which we now describe.

A.1 Experimental Design (ED)

When conducting laboratory experiments, there might be many parameters to consider and it might be infeasible to conduct an experiment for all combinations of parameters. Experimental design allows us to set up experiments such that the effects of the various parameters can be evaluated with a reasonable number of experiments (Montgomery, 2001). The basic principle is to get the maximum information at the lowest experimental cost by varying all uncertain parameters simultaneously. In our case the experiments to be conducted are the reservoir simulations and the parameters can be any uncertain geological or engineering data. The purpose of the experimental design is therefore to design simulations such that the individual effects and interactions of uncertain parameters on the objective function can be quantified.

Once the appropriate design is established and the corresponding simulations are performed, the next step is to investigate the results (Dejean and Blanc, 1999). This can be

done by introducing the response surface (RS) methodology. This methodology is a collection of mathematical and statistical techniques that can be used for the modelling and analysis of problems in which a response of interest is influenced by several variables and the objective is to optimize this response (Montgomery, 2001). Once this surface is generated, it can then be used as a proxy to the actual experiments (reservoir simulations in our case), since response surfaces are generally linear or polynomial models fit to the results of the experiments and as such are very fast to evaluate. They can therefore be used to quantify the uncertainties on the reservoir predictions. To do this a random function is first attached to each of the uncertain parameters and then these random functions are sampled by Monte Carlo simulations. The RS is used to estimate the response at each point of the sample. The final result is a density estimate of the response conditioned to RS and the random functions assigned to the parameters (Dejean and Blanc, 1999).

The overall approach is sketched in **Fig. A.1**. In this figure X_m represents one global source of uncertainty with m uncertain parameters, engineering data for example. Similarly Y_n represents another global source with n uncertain parameters, say geological data, and MC indicates the Monte-Carlo simulation. This sketch shows a Placket-Burman (Plackett and Burman, 1946) two level design (high and low) which is used in this study. The values -1 in the matrix designate the low value of the factors (X_j or Y_j), say the value corresponding to its 10^{th} percentile (P10 value) and $+1$ indicates the high value of the factor, which might correspond to the 90^{th} percentile (P90 value). The individual responses f_i are evaluated by considering combinations of high and low values of these factors. These combinations can not be chosen arbitrarily, since the Placket-Burman design requires this matrix to be orthogonal. The construction of these matrices is explained elsewhere (Plackett and Burman, 1946). The value of k in the index of the response of the last row of the design matrix (i.e., number of experiments) requires special attention. This value must be a multiple of 8 and should be greater than the number of factors for the Placket-Burman design. Therefore, for designs with up to 7 uncertain parameters, 8 experiments will be adequate to determine their effects. For designs with 12 factors, the design will require 16 experiments to be conducted.

Placket-Burman design can not estimate the interactions between the factors. Rather a linear RS is used to represent the experiments. A Placket-Burman two-level design matrix can be constructed for n factors, which requires k experiments to be conducted. Note again

that k should be a multiple of 8 such that $k > n$. The elements, e_{ij}, of this $k \times n$ matrix are either the high or the low values of a particular factor X_j; i.e., $+1$ and -1, respectively. The effect of each factor m_j can then be calculated as follows:

$$m_j = \frac{2}{k} \sum_{i=1}^{k} e_{ij} f_i \quad \text{where } j = 1 \ldots n, \tag{A.1}$$

where f_i is the outcome of experiment i of the design matrix. The linear RS equation is shown in Eq. A.2. In this equation a_j represents the coefficients of the RS, and x_j represents the value of the factor j. It is worth noting once again that x_j is bounded between -1 and $+1$ due to the scaling.

$$RS = a_0 + \sum_{j=1}^{n} a_j x_j. \tag{A.2}$$

From the least square analysis, the coefficients of Eq. A.2 can be calculated as follows:

$$\begin{aligned} a_0 &= \tfrac{1}{n} \sum_{j=1}^{n} m_j \\ a_j &= 2m_j, \end{aligned} \tag{A.3}$$

where m_j is the effect of the factor j as defined in Eq. A.1.

Kabir *et al.* (2002), Dejean and Blanc (1999), Friedmann and Chawathé (2001), Venkataraman (2000) and Chewaroungroaj *et al.* (2000) applied this technique to quantify the uncertainties for reservoir predictions.

A.2 Integrating ED to Optimization Algorithm

The optimization now proceeds as follows. The GA search engine proposes N random or intuitively selected wells (development plans), where N is the number of individuals during the first generation. Then the fitness of each individual is evaluated by using a Placket-Burman two-level experimental design. The development plan held by individual i is evaluated for each of the predetermined experiments (i.e., the design matrix is fixed a priori). Each experiment has its own ANN proxy, therefore training and testing is performed for each of the experiments. Once the training and testing is deemed to be successful, evaluation for the particular experiment will be done via ANN, otherwise simulation will be

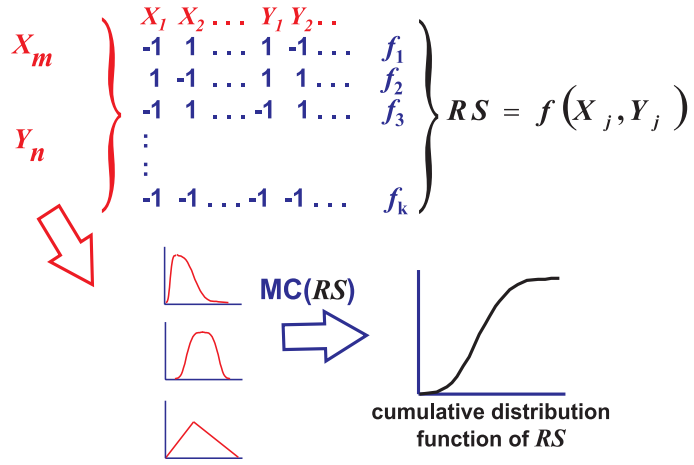

Figure A.1: Application of Experimental Design

performed.

For this particular development plan the corresponding linear RS is constructed and its coefficients are calculated using the outcomes of each experiment, as described through Eqs. A.1- A.3. Each factor is randomized by attaching it to a distribution function of type and parameters as specified a priori. Using these distributions, values are drawn between -1 and $+1$ for each of the factors x_j to evaluate the response of the constructed surface by using Eq. A.2. This Monte-Carlo simulation is performed 10,000 times to construct the cumulative distribution function of the RS (see Fig. A.1). The fitness of the individual F is then calculated from:

$$F = \langle \mathbf{RS} \rangle + r \cdot \sigma, \tag{A.4}$$

where $\mathbf{RS}$ is the vector of outcomes of the response surface from all the realizations, $\langle \mathbf{RS} \rangle$ is the expected value of all outcomes of RS; i.e., the mean or the P50 value of the distribution, σ is the standard deviation of $\mathbf{RS}$ and r is the risk attitude as defined previously.

A.3 Application

We now present an example application of the methodology described above to optimize locations and trajectories of multiple producers and injectors using a real geological model

considering several uncertain parameters.

A.3.1 Validation of the Coarse Model

We used a highly coarsened version of a real geological model to test our proposed method of solution. The initial fine grid model had $78 \times 59 \times 76$ grid blocks. This model was upscaled to $28 \times 21 \times 30$ grid blocks. The coarsened model was used during the optimization process in conjunction with the s-k near-well representation, discussed previously.

In order to test and validate the effectiveness of this upscaling, 40 different monobore wells were randomly generated. Simulation for each of these wells was run both on the fine grid and on the coarse grid with the s-k approximation. The rank correlation coefficient between the cumulative oil production values for these wells evaluated on the fine and on the coarse grid with the s-k approximation was found to be 0.95, which gave us confidence in the use of coarse models for the optimization process.

A.3.2 Selection of Uncertain Parameters

The following parameters were deemed to be uncertain: the depth of the water oil contact, WOC, the solution gas-oil ratio, R_s, initial water saturation, S_{wir}, oil formation volume factor, B_o and viscosity of oil, μ_o. These five factors require eight experiments; that is, for the evaluation of the fitness of an individual, eight simulations are required. The Placket-Burman design used in this study is shown in **Table A.1**.

For each of the factors, although our development allows us to attach different random functions such as lognormal, triangular and uniform, a Gaussian distribution is assumed. The P10 and P90 values of their corresponding distributions are selected as their low (-1) and high (1) values, respectively. The mean and the standard deviation of these distributions as well as the low and high values of each factor are given in **Table A.2**.

A.3.3 Optimization of the Field Development

Using the design shown in Table A.1 and the statistics in Table A.2, the optimization problem was set up to maximize the oil recovery at the end of 10 years by finding the location and trajectory of four producers and two water injectors with a risk neutral attitude ($r = 0$).

Table A.1: Placket-Burman Design

$Run\#$	WOC	S_{wir}	R_s	B_o	μ_o
1	$+1$	-1	-1	$+1$	-1
2	$+1$	$+1$	-1	-1	$+1$
3	$+1$	$+1$	$+1$	-1	-1
4	-1	$+1$	$+1$	$+1$	-1
5	$+1$	-1	$+1$	$+1$	$+1$
6	-1	$+1$	-1	$+1$	$+1$
7	-1	-1	$+1$	-1	$+1$
8	-1	-1	-1	-1	-1

Table A.2: Statistics of the Factor Distributions

Factor	mean	standard deviation	P10	P90
WOC, ft	5455	3.9	5450	5460
R_s, MSCF/STB	97	5.46	90	104
S_{wir}, fraction	0.225	0.05852	0.15	0.30
B_o, bbl/STB	1.35	0.117	1.20	1.50
μ_o, cp	2.2	0.156	2.0	2.4

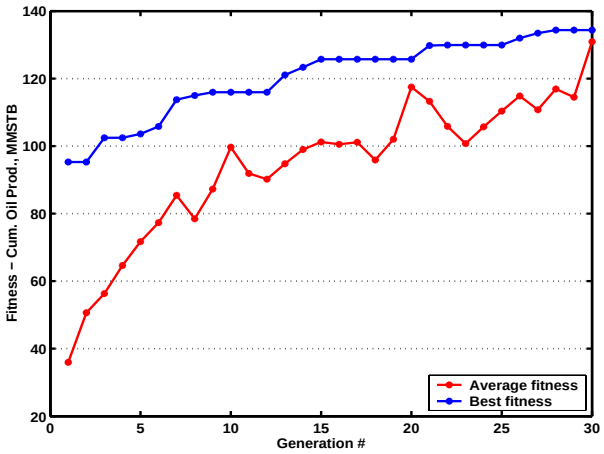

Figure A.2: Progress of Optimization

The number of wells was kept fixed during the optimization. The well type was limited to horizontal or slanted monobore wells. The production rate was fixed for all producers at 10 MSTB/d of total liquid with a minimum bottomhole pressure of 1500 psi. Injectors operated at 4000 psi of bottomhole pressure, with an upper limit of 10 MSTB/d. For the GA search engine, a population size of 50 was used. The maximum number of generations was limited to 30.

Fig. A.2 shows the progress of optimization for the risk neutral case. **Fig. A.3** shows the result of each experiment, as well as the equation of the linear RS and P10, P50 and P90 values sampled from this RS for the optimized plan. The RS of the development plan that maximized the average cumulative oil production attained from all realizations has a normal distribution as shown in this figure.

The optimum development plan found at the end of the optimization is shown in **Fig A.4**. On this plot the top depth is used as the grid property. Red blocks represent the highest part of the structure and blue blocks show the deepest portions. The map coordinates and the grid location of the heel and toe of the wells can also be seen in this figure. The wells tend to be located on the higher and thicker part of the structure, ignoring the low quality east flank. Note that the wells are all horizontal or slanted, with coordinates as indicated in the figure.

```
1   1 -1 -1   1 -1     1.27739e+08
2   1   1 -1 -1   1     1.44545e+08
3   1   1   1 -1 -1     1.44675e+08
4 -1   1   1   1 -1      1.2395e+08
5   1 -1   1   1   1     1.22592e+08
6 -1   1 -1   1   1     1.23669e+08
7 -1 -1   1 -1   1     1.41906e+08
8 -1 -1 -1 -1 -1     1.45065e+08
```

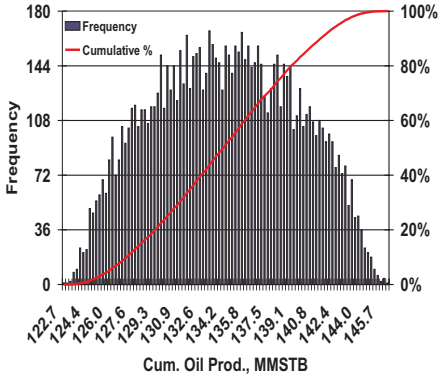


```
RSM = 1.34268e+08 + 620125 * WOC - 57875 * Rs - 986875
    * SWIR - 9.78012e+06 * Bo - 1.08962e+06 * visc

P10 = 1.2741e+08
P50 = 1.3448e+08
P90 = 1.41374e+08
```

Figure A.3: RS of the Optimized Development Plan

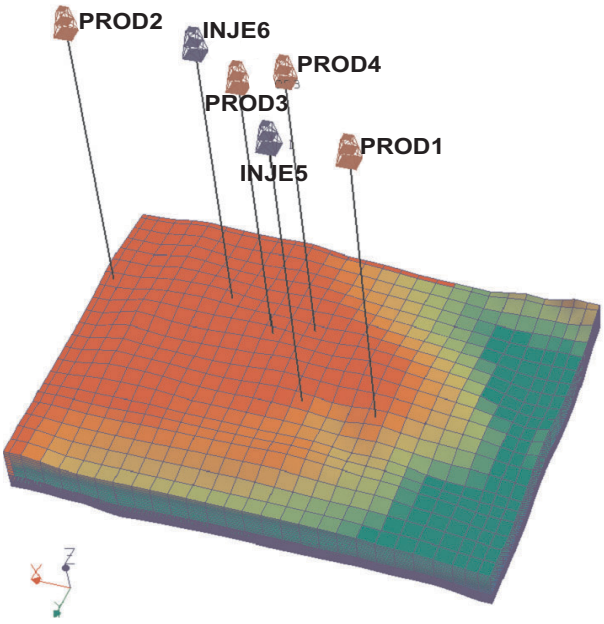

PROD1 **(10,9,**8**) – (7,12,**8**)**
(6270.78, 5723.22, 5151.44) - (4057.41, 7913.18, 5251.71)
PROD2 (27,**15,15) – (**25,**14,30)**
(18689.7, 10107.7, 5224.3) -(17336.8, 9374.6, 5311.79)
PROD3 (18,13,29**) – (16,13,24)**
(12172.8, 8649.5, 5353.89) - (10697.7, 8646.49, 5360.68)
PROD4 **(15,14,27)** – **(14**,13,**27)**
(9959.76, 9374.36, 5349.96) - (9221.65, 8646, 5352.36)
INJE5 (14,**9**,4**) – (**15,**8,15)**
(9221.69, 5724.95, 4971.27) - (9959.43, 4991.39, 5345.71)
INJE6 **(**20,15,**8) – (**23,18,**17)**
(13648.6, 10107.4, 5014.93) - (15861.7, 12297.9, 5202.14)

Figure A.4: Optimized Development Plan